Compositional characterization of iron gall inks in manuscripts using non-destructive techniques

Rita de Figueiredo Viegas

Thesis to obtain the Master of Science Degree in

Engineering Physics

Supervisors: Prof. Maria Teresa Haderer de la Peña Stadler
Dr. Victoria Corregidor Berdasco

Examination Committee

Chairperson: Prof. Horácio Fernandes
Supervisor: Dr. Victoria Corregidor Berdasco
Members of the Committee: Dr. Paula Cristina Vicente Teixeira Chaves
Dr. Luís Miguel Mota Ferreira
Prof. Luís Humberto Viseu Melo

June 2014

Acknowledges

In this thesis work there were many people that I would like to thank for helping me and believe in my capabilities.

First off all, I would like to thank my supervisors, Dra. Victoria Corregidor and Dra. Maria Teresa Peña, for the support given during my work and for never gave up on me. I would like to thank for the lessons and the advices, these are things that I will bring with me for the rest of my professional career.

I would like to thank to CTN the opportunity of letting realize my master thesis at the facilities.

I would like to give a special thanks to Dr. R. Winstanley for sharing with us his collection without which would not be possible to realize this work.

I also would like to give a special thanks to Dr. Luís Alves, for all the dedication and time spent with me in PIXE experiments. To Dr. Nuno Franco, for helping me in the XRD experiments and to Master Joana Lancastre for the time spent with me during the FTIR experiments. To Dr. Andrès for giving me highlights in the RBS software. Thanks to all for teaching me these techniques.

I would like to thank to technicians Rute and Filomena for helping me in the samples preparation.

I would like to thank all the people from the Laboratório de Feixe de Iões for receiving me so kindly and for always being willing to help. I felt really great during the days I spent in the laboratory.

I also would like to thank Arch. Sónia Francisco and Casa da Cerca for letting me visit the garden and bring the galls used to make the iron gall inks.

I would like to thank the organizers and teachers from the workshop “Conservação de Documentos com Tinta Ferrogálica – da Teoria à Prática”, lectured at Arquivo Histórico do Ultramar, for giving me the chance of learning more about iron gall inks and their history.

I would like to thank to Dr. Luís, for the company during lunch time and for all the conversations and jokes.

To Dr. Eduardo Alves, for always having a nice motivation word.

My great thanks goes to Victoria. I really have to thank you for all the patient and support you gave me along these months. I am aware I was not always a good learner but you never gave up on me and always did your best to pull me up and encourage me to do my best. I really can’t write how thankful I am. You taught me a lot. Thank you.

A special thanks to my friends for being there in all the moments and for making me laugh when I was too stressed.

A special thanks to my university colleagues, we are a great family and only we know the adventures we went through these years.

Finally, and the most important, a huge thanks to my parents, my sister and my grandmother, without whom I was not the person I am today.

Resumo

O objectivo deste trabalho experimental é a caracterização elemental e molecular de tintas ferrogálicas e papéis através de técnicas de análise não destructivas tais como: Raios-X induzidos por partículas carregadas(PIXE), espectrometria de retro-dispersão de Rutherford (RBS), técnica de difracção de raio-X (XRD) e espectroscopia de infravermelhos (FTIR). Fotografias com iluminação de luz ultravioleta (UV) e infravermelha (IR) permitiram detectar sobreposições de tintas e manchas nos papéis.

Diferentes documentos do início do século XX, pertencentes a uma colecção privada, foram analisados. Foram identificados vestígios de estrôncio e arsénio nos papéis, assim como celulose e calcite. A análise por FTIR complementou a identificação de compostos pertencentes aos papéis e tintas.

Os ingredientes base para produção de tintas ferrogálicas, para além da água, são: sulfato de ferro (vitriol), goma arábica e taninos. Através da análise PIXE aos ingredientes base identificaram-se como elementos comuns, entre outros, enxofre, cálcio e ferro. Usando a técnica de XRD identificámos ácido gálico e glucose nas fontes de taninos analisadas, assim como diferentes compostos de sulfato de ferro hidratados no vitriol.

Foram produzidas tintas ferrogálicas usando os ingredientes acima mencionados seguindo receitas antigas. Apenas uma das tintas apresenta vestígios de zinco, elemento identificado na goma arábica. Com RBS foi possível identificar elementos leves tais como carbono e oxigénio. A profundidade de penetração da tinta no papel foi estimada ser da ordem dos nanómetros. Através de XRD identificaram-se celulose e calcite nos papéis.

Palavras-chave: tintas ferrogálicas; PIXE; RBS; XRD; FTIR; fotografia.

Abstract

This work aims to characterize the elemental and molecular composition of iron gall inks and papers by means of several non-destructive techniques as: Particle Induced X-ray Emission (PIXE), Rutherford Backscattering spectrometry (RBS), X-ray diffraction technique (XRD), and Fourier Transformed Infrared spectroscopy (FTIR). Ultraviolet (UV) and Infrared (IR) photography were used for ink differentiation and detection of paper stains.

The basic ingredients of iron gall inks, besides water, are: iron sulphate (vitriol), Arabic gum and tannins. By means of PIXE analysis they were identified, among other elements, sulphur, calcium and iron. By XRD, gallic acid and glucose were identified in the tannin sources and different iron sulphate hydrate compounds in the vitriol.

Following old recipes we produced several iron gall inks. PIXE revealed traces of zinc in one of the inks, also identified in the Arabic gum.

In papers written with the prepared inks, by RBS technique it was possible to identify light elements as oxygen and carbon. An estimation of ink depth profiling revealed ink penetration in the paper of the nanometer order. By XRD it was possible to identify calcite and cellulose.

After the determination of the right experimental conditions which assure the pristine conditions of the documents, different documents date from the early XX century belonging to a private collection were studied. Besides the elements listed above, traces of strontium and arsenic were identified in the documents' papers. Papers are mainly composed of cellulose and calcite. The FTIR analysis could however discriminate between ink and paper compounds.

Keywords: iron gall ink; Particle Induced X-ray Emission; Rutherford Backscattering; X-ray Diffraction; Fourier Transformed Infrared; photography.

Contents

Acknowledges i

Resumo iii

Abstract v

List of Figures xi

List of Abbreviations xv

Chapter 1 - Introduction 1

Chapter 2 – State of the Art 5

Chapter 3 – Characterization of the applied techniques 11

3.1. Ion Beam Analytical (IBA) techniques 11

3.1.1. Particle Induced X-ray Emission 11

3.1.2. Rutherford Backscattering Spectrometry 16

3.2. Complementary Techniques 21

3.2.1. X-ray Diffraction technique 21

3.2.2. Infrared spectroscopy 24

3.2.3. Infrared and ultraviolet photography 27

Chapter 4 – Results and Discussions 29

4.1. Test to the methods 29

4.1.1. Ingredients 29

4.1.2. Manufactured inks following recipes 35

4.2. Analysis of old documents from the beginning of the XX century 43

Chapter 5 - Conclusions 59

References 61

Appendix A 67

Appendix B 69

Appendix C 75

Appendix D 79

List of Tables

Table 3. 1. Table of IR absorptions for several of the constituents compounds of paper and inks. 25

Table 4. 1. Elemental concentration ratios in iron gall inks main ingredients. ND: not detected. 31

Table 4. 2. Ratios of the identified elements for the six different iron gall ink recipes written in paper. The "≈ 0" value means that the result obtained for the correspondent ratios is of the order of three decimal places, yet the elements were detected by GUPIX in low concentrations. ND: not detected. 38

Table 4. 3. Cristallinity Index (*CrI*) for the papers written with the six ink recipes analyzed and the same papers unwritten. 40

Table 4. 4. Concentration (at.%) of the fitted elements in the two simulated layers for ink3 sample. .. 42

Table 4. 5. Estimation of the depth penetration of iron gall inks (considering only the $FeSO_4$ ingredient) in paper. Only the depth of the 1st layer was used for the calculations. 42

Table 4. 6. Summary of the identified compounds in the four documents analyzed. 54

Table 4. 7. Cristallinity Index (*CrI*) for the documents analyzed on inked and non-inked regions, considering the peaks from cellulose I. 55

List of Figures

Figure 3. 1. Atomic level diagram showing the main K and L X-ray transitions (a); dependency of the X-ray emitted energies with the atomic number Z of the elements (b) [29,30]. 12

Figure 3. 2. Photograph of the External beam set-up at CTN/IST: 1 - exit nozzle with a 100 nm thick Si_3N_4 window; 2 - X-ray detector; 3 – positioning laser beams; 4 – micro camera; 5 - particle detector with He flux. 15

Figure 3. 3. Photographs of a sample of modern papyrus (left side) and a document from the beginning of the XX century (right side) tested in four spots. 16

Figure 3. 4. Schematic RBS geometry with normal ion beam incidence [38]. 17

Figure 3. 5. Kinematic factor *K* at a scattering angle θ=165º as a function of target mass M_2 for incident protons and ^{4}He. 17

Figure 3. 6. Simulations of depth penetration of a 1940 keV proton beam in paper written with iron gall ink (left side) and bare paper (right side) targets. 20

Figure 3. 7. Simulations of depth penetration of a 2000 keV alpha particles in paper written with iron gall ink (left side) and bare paper (right side) targets. 20

Figure 3. 8. Principle of X-ray diffraction in a crystalline structure [42]. 21

Figure 3. 9. Photography of the experimental apparatus using the D8 Discover (left picture) and the Hotbird (right picture) diffractometers, both available at CTN/IST. 23

Figure 3. 10. Thermo Scientific Nicolet IS50 FT-IR setup: the chamber was used for the analysis of pellets (ingredients and manufactured inks) and the ATR module was used for manuscripts (as the one shown in the photograph). 26

Figure 3. 11. Preparation of the samples in pellets with KBr (a). Mechanical compressor to produce the pellets (b). 26

Figure 4. 1. Photographs of the main ingredients used in iron gall ink manufacturing. From the left to the right: iron sulphate, also called vitriol; Arabic gum; gallnuts from oak tree and nut tree. 30

Figure 4. 2. Pellets of commercial tannin (left side) and iron sulphate (right side) with some oxidized regions. 30

Figure 4. 3. X-ray energy spectra obtained from ingredients. The signals are normalized to the Fe-Kα line. 30

Figure 4. 4. X-ray diffraction patterns of oak gall (green line), nut gall (red line) and commercial tannin (blue line). 32

Figure 4. 5. X-ray diffraction patterns of iron sulphate pellets. One of the pellets had been exposed to air for approximately two weeks (blue line), while the other was produced minutes before the analysis through XRD (red line). 33

Figure 4. 6. Diffraction pattern of the Arabic gum. 33

Figure 4. 7. FTIR spectrum for Arabic gum. 34

Figure 4. 8. FTIR spectrum for the iron sulphate (pellet produced minutes before the measurement). 34

Figure 4. 9. FTIR spectrum for the commercial tannin. 35

Figure 4. 10. X-ray energy spectra of three papers used as support of the six made iron gall inks. The signal is normalized to the Fe-Kα line. 36

Figure 4. 11. X-ray energy spectra of three iron gall inks recipes using commercial tannins and for an ink drop. The signal is normalized to the Fe-Kα line. 37

Figure 4. 12. X-ray energy spectra of three iron gall inks recipes using natural tannins. The signal is normalized to the Fe-Kα line. 37

Figure 4. 13. X-ray diffraction patterns of six iron gall inks samples in paper. 39

Figure 4. 14. RBS spectrum of paper 3. The simulated curve (red line) was obtained with SIMNRA code assuming two layers. 41

Figure 4. 15. RBS spectrum of ink 3-nuts (recipe 3) in paper support. The simulated curve (red line) was obtained with SIMNRA code assuming two layers. 41

Figure 4. 16. FTIR spectra for the three types of ink 3 produced in laboratory. The marked peaks correspond to iron gall ink composition since it were produced KBr pellets of the inks for this analysis. 43

Figure 4. 17. X-ray energy spectra obtained from non-inked areas in documents A, B and C. The signal is normalized to the Fe-Kα line. 44

Figure 4. 18. X-ray energy spectra obtained from inked areas in documents A, B and C. The signal is normalized to the Fe-Kα line. 44

Figure 4. 19. UV photography of Document A (right side), Document B (left side) and Document C (down in the picture). 45

Figure 4. 20. S/Fe and Ca/Fe ratios obtained through PIXE analysis of document A. The amount of sulphur is much higher in non-inked areas while calcium does not differ that much from inked to non-inked areas. 46

Figure 4. 21. Detail of the IR and UV photography of Document A. 46

Figure 4. 22. Cu/Fe, Zn/Fe and Sr/Fe ratios for the spots analyzed in Document B (a); 2D elemental maps for Fe and Ca obtained for Document B. (800x800 μm^2) (b).. 47

Figure 4. 23. Ratios of some elements present in the ink spots analyzed in Document C (Cu/Fe, Zn/Fe and Mn/Fe ratios are multiplied by 100) (a). Elemental maps of ink spot C3 of Document C (800x800 μm^2) (b).. 48

Figure 4. 24. X-ray energy spectra of inked and non-inked areas in document D. 49

Figure 4. 25. Ratios of some elements present in the ink spots analyzed in Document D (Cu/Fe, Zn/Fe As/Fe and S/Fe ratios) (a). Elemental maps of ink spot D3 from the main text of Document D (800x800 μm^2) (b); a view from the micro-camera installed in the set-up is also showed. 50

Figure 4. 26. Detail of the IR and UV photography of Document D. 50

Figure 4. 27. X-ray energy spectra of inked and non-inked areas of document. 51

Figure 4. 28. Cu/Fe, Zn/Fe, Sr/Fe, Mn/ Fe and S/Fe ratios obtained (a). Detail of UV photography of the front page and back page (b) of the document. 52

Figure 4. 29. X-ray diffractogram of ink spots and paper of Document A. 53

Figure 4. 30. X-ray diffractogram of ink spots and paper of Document B. 53

Figure 4. 31. X-ray diffractogram of ink spots and paper of Document D. 54

Figure 4. 32. X-ray diffractogram of ink spots and paper of Document E. 54

Figure 4. 33. FTIR spectra of non-inked areas in the five documents. 56

Figure 4. 34. FTIR spectra of inked areas in the five documents. 56

List of Abbreviations

A.D. – Anno Domini
AGLAE - Accélérateur Grand Louvre d'Analyse Elémentaire
ATR - Attenuated Total Reflectance
B. C. - Before Christ
CTN/IST – Campus Tecnológico e Nuclear / Instituto Superior Técnico
CrI – Crystallinity Index
EDXRF - Energy Dispersive X-ray Fluorescence
FTIR – Fourier Transformed Infrared spectroscopy
IBA – Ion Beam Analysis
IR – Infrared
MS - Mössbauer spectroscopy
NIR – Near-infrared
PIXE – Particle Induced X-ray Emission
ppm - part-per-million
RBS – Rutherford Backscattering spectrometry
SEM-EDS - Scanning Electron Microscopy Energy Dispersive Spectrometry
XRD – X-ray diffraction
UV – Ultraviolet

Chapter 1

Introduction

How can we study the calculations about motion made by Galileu if he had not written his mathematical demonstrations? How can we know about Leonardo Da Vinci's studies on human anatomy if it wasn't from his sketches? How would we know about Vasco da Gama's adventures to India if we have not read "Os Lusíadas" by Luis de Camões? More obviously, how could people communicate to each other before the invention of telephone or internet? We could keep asking questions like those and the answer will be always the same: because the presence of manuscripts. History is mostly preserved thanks to the written thoughts of people. The existence of those manuscripts made possible the understanding and evolution of the knowledge we have nowadays.

Nowadays, and thanks to scientific investigations, it has been recognized that the rate of natural ageing and corrosion processes are accelerated by a polluted surrounding as well as by transport hazards and often high humidity and illumination levels. In the special case of documents written with iron gall inks, these degradation processes tend to be enhanced due to the delicacy of the paper and the chemical alterations in the inks, as it will be described later.

Iron gall inks, as the name suggests, are made of iron sulphate, together with tannin acid extracted from gall oaks and water [1]. Gum Arabic is also added as an ingredient and its function is to bind the ink to the paper. This type of ink had its origin in Antiquity (there are evidences of preparation methods since the IV century A.D. [1]) and it was used until the first decades of the 20th century, time it was replaced by other types of inks with non-corrosive properties. The main advantage of the iron gall ink is the fact that it is really hard to remove from the paper, making this ink the most preferred ink for writing official and important documents on those times.

The ingredients used for iron gall inks manufacturing could have many origins and usually they were local. In fact, depending on the source where the iron sulphate was extracted or on the quantity of tannin acid that the gall oaks had, the ink will present different composition which can alter its appearance and also its chemical behavior in paper.

The use of analytical techniques for the study of elemental composition of iron gall inks is of great importance to understand and study the origin of the inks and authenticity of the documents. Due to the already referred fragile conditions of documents, the use of nondestructive techniques is usually required to preserve their state. Several analytical techniques have been improved or modified along the latest years in order to be applied in the study of these ancient and valuable documents, most of the time unique. While some of them are used for the identification of the elemental composition of both, paper and ink, others are used for the detection of compounds existent in them.

Ion Beam Analysis (IBA) techniques have been applied to the study of elemental composition of iron gall inks. In fact, these techniques proved to be powerful tools to study these objects in a nondestructive way [2]. Furthermore, when using an external beam, which means that non-vacuum conditions are required, it enlarges the possibilities of studying the composition of manuscripts and inks [3] without the need of sampling or vacuum related problems as heating or dehydration phenomena.

The present work is focused on the application of IBA techniques, more specifically Particle Induced X-ray Emission (PIXE) and Rutherford Backscattering spectrometry (RBS), to study the elemental composition of iron gall inks on paper support using the external proton beam set-up installed in the nuclear microprobe available at the Campus Tecnológico e Nuclear-Instituto Superior Técnico (CTN/IST) from Universidade de Lisboa, Portugal. PIXE has been used in few laboratories around the world for the identification and quantification of elements present in iron gall inks and paper [4-6]. On the other hand, RBS was used to obtain complementary information on depth profiling composition and also to identify light elements that could not be detected by PIXE (elements with $Z<12$) which is of great significance to identify the elements that form cellulose and the other compounds present in paper.

Concerning to the investigation of the chemical composition, two complementary techniques, also available at CTN/IST, were used: X-ray Diffraction technique (XRD) and Fourier Transformed Infrared spectroscopy (FTIR), which are also considered noninvasive. In this work they will be performed in different documents for the purpose of identify the compounds belonging to iron gall inks and paper. Also the use of UV and IR photography helps on detecting foxing and stains in the documents and other signals which are not visible under normal light, that may help in determining the level of corrosion and degradation of the documents.

The complementary character of all of these techniques along with the cognition of the history of the iron gall inks and paper manufacturing techniques will allow a better analysis on documents.

The five documents that were studied during the present work, belonging to a private collection, were written with iron gall inks at the end of the 19th century and beginning of the 20th century and they are from Rio de Janeiro, Brazil. Some ancient iron gall ink recipes were reproduced and characterized with the objective of understanding the influence of the concentrations of each ingredient in the ink and the interaction inks in paper. It should be highlighted that the starting ingredients used to manufacture the iron gall inks were also characterized in order to understand the results obtained concerning the provenience of the elemental and molecular composition of these type of inks.

This Master thesis is divided in five chapters, including this one, the introduction. The second chapter describes a general overview of the application of non-destructive techniques to the study of cultural heritage objects. It will be also described some main aspects of the history of paper and iron gall inks production and the results obtained and already published for valuable manuscripts. Chapter three describes the techniques used in this Master thesis: PIXE, RBS, FTIR, XRD and UV and IR photography, also including the experimental procedures and details. Chapter four concerns to the results obtained and their discussion. At the end, chapter 5 is dedicated to the conclusions. Appendices are added at the end of this document with the recipes used to produce iron gall inks (Appendix A), photographs of the studied documents (Appendix B) and the X-ray powder diffraction charts for the compounds identified through XRD technique (Appendix C). Appendix D is a list of work published during this thesis.

Chapter 2

State of the Art

The application of analytical techniques in art and archaeological artifacts provides results and crucial information for historians, art experts, curators, etc., in a way that gives information about the composition, structure and physical behavior of objects under study. This knowledge is necessary for example to perform restorations, to establish the better conservation conditions or to test the authenticity of the artifacts [7].

Until the 1960s, techniques for chemical composition analysis were the only ones available for studying artifacts [3]. Since then, other techniques such as electron beam microscopes and microprobes or mass spectrometry techniques have been modified in order to adapt them to the specific analysis conditions that these type of artifacts need. More recently, techniques based on ion beam analysis have been applied to the study of these kind of objects. Recalling the sentence from Schreiner and Grasserbauer [8]: *"(…) a work of art has more faces than those which can be examined by scientific methods. Therefore, not only the applicability of an analytical method should govern the work of chemists in the field of archaeology, art, history or restoration and conservation, but the respect and careful treatment of the future of the work of art. (…)"*; it is essential to have in mind that the quality of the results obtained when analyzing a piece of art depends on the interdisciplinary collaboration between the scientists, art historians and archaeologists.

Concerning to ancient manuscripts, plenty of historical information on the human cultural development can be obtained through the study of manufacturing techniques of the support (i.e. parchment or paper), inks, dyes, pigments, etc. Different scriptoria or geographical areas as well as different periods were, probably, characterized by the use of specific materials and preparation techniques for these items. The main concern to have when analyzing the manuscripts is related to the fact that they are composed mainly by organic components. Organic materials are always subject to ageing processes through effects of the environmental conditions [8].

Writing supports have experienced important advances in the manufacturing techniques and materials along the centuries, and it still continues. Papyrus in Ancient Egypt (3150 B.C.) was well known for its easy and cheap production. In Ancient Greek, the scribes used wax tabulas which could be recycled. The parchment started to substitute the papyrus during the first century before Christ. It revealed to be more resistant than papyrus and adapted to handwriting although its production was expensive [9]. The manufacture of paper in Europe was first established in Islamic Spain in the middle of the 11th century, and in the second half of the 14th century the use of paper had become well accepted in Western Europe. In the beginning of the 19th century paper was made from cellulose and water by using hemp, flax and cotton fibers [10]. Originally, animal glue was used for sizing, but it was substituted by rosin and alum in the 19th century and nowadays other synthetic products are used [11].

There are many external and internal agents which causes deterioration of paper. The internal agents concern mostly to the purity of the components and the type of cellulose used to manufacture the paper, since durability and life expectancy increases with the use of good quality raw materials. Unfortunately, the appearance of wood pulp in the 19th century led to a reduction in the quality of paper due to the chemical and physical processes that it suffers during its manufacturing. The use of an acidic medium during the sizing process and the presence of transition metals (iron and manganese mainly) in paper catalyzes oxidation processes. These oxidation factors react directly on the chemical groups of cellulose and so the paper rapidly loses durability. On the other hand, the external factors are derived from air pollution, unfavorable climate conditions, biological agents or storage and lighting conditions [10].

Inks have also evolved in their recipes and main ingredients. Carbon ink was the first documented ink, its first use is reported to circa 2500 B.C.. This ink consists of carbon pigments, soot or lampblack, and a weak gum or animal glue acting as a binder. Good quality carbon inks had a blue-black appearance and they were considered permanent inks, even though there were found documents and drawings with signs of detrition due to the ink [1]. Iron gall inks emerged has an alternative for carbon inks and there are evidences of different preparation methods since IV A.D. where it was used has a hair dye in India [9]. In the 5th century an early recipe for iron gall ink can be found in the Encyclopedia of Seven Free Arts by Martianus Capella who describes *"Gallarum gummeosque commixtio*" as a writing ink [12]. There is not exact date for the transition from carbon ink to iron gall ink and in Middle Age period they were even mixed along with vegetable inks [9]. Nevertheless, it can be safely stated that by the end of the late Middle Age iron gall ink was the primary ink chosen for writing in manuscripts [1]. Iron gall ink has some advantages compared to carbon inks, as for example it is easier to manufacture and it is hard to remove from the surface of the support in which it is applied, being a valued characteristic for official record keeping.

A basic iron gall ink is created from four ingredients: tannin acid, vitriol (iron sulphate), gum Arabic and water. The tannin acid is extracted from gall nuts containing Gallo tannins. The gall nuts are created as a result of certain insects stinging and laying eggs on the leaf steams of oaks trees, then, a nut-like swelling will be formed. When these galls are collected and immersed in water, tannin and gallic acids may be soaked out [13]. The iron sulphate ($FeSO_4$), also known as vitriol or copperas, is obtained from minerals which contain many other metals as contaminants such as copper, aluminum, magnesium or zinc, which in really small concentrations do not contribute to color of the ink solution. The third ingredient, gum Arabic, is a natural gum obtained from the Acacia tree. The gum seeps out of the tree forming globules, sometimes as large as walnuts. It has an amber like appearance and it has golden orange color. Gum Arabic is soluble in water (the fourth element), being its main purpose to bind the ink at the paper surface, producing a great brilliance and deep color [1].

When solutions of gallotannic acid and iron sulphate are mixed, the oxidation takes place immediately and a violet-black solution is formed with eventually a violet-black deposits [12]. Therefore, it is necessary to expose the starting solution to the air for some time to obtain the appropriated level of blackness. The earliest method of preparing iron gall ink, described by Mitchell and Hepworth [12], is the Elizabethan domestic ink which consists in rain water (or claret wine or red vinegar); 5 oz. galls; 4 oz. ferrous sulphate, and 3 oz. gum Arabic, then, after five days soaking, the extract from the galls is heated just to the boiling point with the ferrous sulphate [12].

Historical recipes contain an excess of iron sulfate over gallic acid. Iron gall inks are known to influence the structure of cellulose fibers, causing deterioration of the paper. The presence of iron ions in the ink, even after a long period of time, combined with ambient moisture (in the presence of moisture the sulfate ions are converted into sulfuric acid), explains the corrosion process of the ink that leads to paper degradation through the acid hydrolysis of cellulose caused by sulfuric acid present in inks [9]. This motivates the quantitative investigation of the elemental and molecular composition of inks by the application of atomic and molecular techniques in order to predict and mitigate further degradation.

Ion Beam Analysis (IBA) techniques rely on the interaction of light ions of energy in the MeV range with the constituent atoms of materials and the detection of secondary products which can be either ions or photons with characteristic energy of the target atom [14]. The main qualities of IBA techniques are:

- the nondestructive character for most materials (in the case of materials constituted by organic compounds, such as the documents studied in this work, an external beam can be used);
- quantitative and standardless techniques, with an accuracy generally better than 5%, and they are very sensitive;
- multi-elemental, including light elements, and complementary. Usually they can be implemented simultaneously;
- short time measurements of a measurement (typically 10-15 minutes);
- they can provide spatial information via depth profiling and micro-mapping (when using a nuclear microprobe).

However, there are some limitations in a way that it is not possible to obtain information on the chemical state of elements, and also these techniques are considered as “superficial” since it is the near-surface of materials (10-20 μm) which is analyzed and thus the bulk composition can be smeared by surface alteration [14]. Particle Induced X-ray Emission (PIXE) and Rutherford Backscattering spectrometry (RBS) are two of the IBA techniques which can be used for elemental characterization in the field of cultural heritage.

Particle Induced X-ray Emission (PIXE) technique was developed in 70ths and it was mainly concerned with feasibility tests. Long proven as an analytical tool of uncommon accuracy and utility, PIXE soon has enjoyed a solid reputation in the areas of chemical and physical analysis. Through the years it started to be applied as a technique to study analytical problems in many different fields, such as biomedical, mineralogy, geology, art or archaeology [15]. The pioneering works of PIXE using an external beam in documents belong to Davis´ group, where the iron gall inks on the Gutenberg Bible and on the Vinland map were studied [5,16]. They used an external proton beam to identify the elemental composition of the inks present in the two mentioned manuscripts so they can prove their authenticity and also their origin. In the case of the Gutenberg Bible, they discovered that the composition of Gutenberg's first typographical ink was exceptionally rich in copper and lead, and that he made new mixtures during the production of the Bible with different elemental composition. The comparison between the Cu/Pb ratio along the pages of the Bible allowed to conclude that the two folio volumes were produced in six sections, being printed simultaneously. Additionally, this investigation provided the connection to other important manuscripts printed by Gutenberg, as for example the 31-line Papal Letter of Indulgence, dated from 1455 [17].

The possibility of beam focusing and beam scanning adds spatial resolution and imaging capabilities to the IBA techniques. In this sense, by 2D PIXE elemental maps it is possible to identify the element´s migration around the inscriptions when inks are under study. An investigation performed with the external beam at the microprobe set-up in the AGLAE facility of documents belonging to the 18^{th} century concluded, through PIXE elemental mapping, that the elemental contents were not uniform in inked areas [18]. PIXE mapping is used as a complementary technique of spot PIXE analysis for the study of ink corrosion and paper degradation.

As it was mentioned above, PIXE technique can identify and quantify the elements of a sample, providing reliable information for helping in dating and authentication of documents through the study of elemental composition of the inks and paper. However, PIXE cannot give any information about depth profiling of inks in paper, that could help to understand more about ink corrosion processes. Rutherford Backscattering Spectrometry (RBS) is an ideal technique to study the elemental depth distribution and to study superficial layers containing heavy elements [3]. Furthermore, this technique also makes possible the identification of light elements that PIXE cannot detect (those with $Z<11$), which is very important when paper is characterized since it is mostly constituted by cellulose and other organic compounds with carbon and oxygen in its composition [10]. The possibility of employing the two techniques simultaneously promotes the interest in using RBS for the analysis of documents.

The referred IBA techniques provide the identification and quantification of the elements present in manuscripts, together with the study of depth profiling of ink in paper, giving the possibility not only to investigate the elemental composition of paper and ink but also to differentiate between paper and ink recipes and also to understand the interaction between inks and papers.

Likewise, the study of the influence of iron gall ink in paper documents can be done with the use of photographic and visual techniques. Charred, dirty, faded or very deteriorated documents often reveal their secrets through recording their near-infrared (NIR) reflectance or ultraviolet (UV) signals. NIR often can differentiate between dyes and pigments that look indistinguishable to the human visual system [19]. Foxing, which is usually undetectable under visible light at an early stage, exhibit fluorescence signal under UV excitation. UV photography also allow the perception of ink migrations and water stains in the manuscripts since the legibility is enhanced by the contrast between the background luminescence of the paper and the absorption of the UV light by the ink [20]. These two techniques have been used to investigate corrosion and degradation marks in the documents.

XRD technique is a valuable technique for studying paper composition. Paper is composed of a matrix of cellulose and a variety of inorganic and organic fillers added to confer the desired physical-mechanical properties. The quantity and nature of the ingredients is characteristic of each producer. Thus, XRD allows to study both polymeric matrix and inorganic formulation of paper composition. On one hand, regarding some restraints, it is possible to assess the crystallinity degree attained by the cellulose as a consequence of the nature of the raw materials adopted in its manufacturing and ageing processes. This calculation gives an idea of the quality level of paper, providing better conclusions about the age of the document or on the environmental conditions in which it was kept. A recent study on old and modern papers using energy dispersive X-ray diffraction [21] allowed the differentiation between documents through the identification of different types of cellulose existent in papers, leading to the conclusion that they had suffered different manufacturing processes.

XRD technique is also a complementary technique associated to Mössbauer spectroscopy (MS), Energy Dispersive X-ray Fluorescence (EDXRF) and Scanning Electron Microscopy Energy Dispersive Spectrometry (SEM-EDS) [22].

A molecular technique that is one of the most important methods for the identification and characterization of chemical structures is Infrared spectroscopy [23]. Its greatest use lies in its unique application to the identification of chemical functional groups from vibrational spectra. It relies on the analysis of chemical bonds existent in the molecules that constitute the sample, allowing the identification of its compounds. FTIR is usually used for paper characterization, since it allows the identification of the fibers existent in papers and the determination of the chemical composition of additives used in papermaking. The identification of the chemical composition of inks is also possible and so this technique is useful in the analysis of manuscripts [24]. Gorassini et al. [25] studied the composition of many ancient paper documents by means of FTIR in order to identify their components. It were found differences in paper composition between documents from the 11th century until nowadays. It was possible to identify the presence of cellulose in all documents and in the specific case of documents from the 19th and 20th century it was referred the presence of calcium carbonate and some inorganic fillers such as gypsum. In the study of a 19th century document from the archives in the Palazzo Ducale (Venice, Italy) [26], the use of Attenuated Total Reflectance (ATR) method enable the identification of Arabic gum and metal-gall complex from the position of the peaks found in the spectra.

In Portugal there are some studies dealing with the characterization of the illuminated manuscripts using nondestructive analytical techniques or with micro-sampling [27,28]. A recent study on the Manueline foral charter of Sintra using EDXRF spectroscopy, Raman and Infrared micro-spectroscopies allowed the identification of pigments, such as malachite, azurite and gold in the illuminations and letterings.

Despite IBA techniques, several other analytical techniques are used in the analysis of manuscripts, such as X-Ray Diffraction (XRD) technique and Fourier Transform Infrared (FTIR) spectroscopy. These techniques, along with the already referred IBA techniques, can be considered complementary: some of them give information at an elemental level (PIXE and RBS), while others detect the presence of compounds or molecular structure (XRD and FTIR respectively).

Chapter 3

Characterization of the applied techniques

3.1. Ion Beam Analytical (IBA) techniques

3.1.1. Particle Induced X-ray Emission

Particle Induced X-ray Emission (PIXE) method was first proposed by Johansson and Johansson in 1970 [15]. When a material is exposed to a high energetic ion beam particle, the ionization of the inner shells of the atoms that constitute the material may occur. As a result of the reorganization of the electronic shells, the emission of X-rays characteristic of the ionized atoms may happen. This phenomenon is the basis of PIXE technique.

The excited atoms lose their energy when these inner-shell vacancies are filled by electrons from the outer shells with the subsequent emission of either X-ray or Auger electrons. Figure 3.1a shows schematically the generation of various X-ray lines caused by de-excitation of electrons falling from higher shells. In this sense, if an L-shell electron fills a K-shell vacancy, a K_α X-ray is emitted. In the same way, if the electron transition to the K-shell is from M shell, more energetic X-rays (K_β) are emitted. L_α, L_β and L_γ X-rays are emitted when L-shell vacancies are filled by electrons from M and higher shells. Figure 3.1b shows the energies of the main X-ray line groups as a function of the atomic number, Z. An approximate estimation of the emitted X-ray energy (in keV) can be obtained using the relationship between the atomic number and the relative intensities of the shell series [29] (equations 3.1):

$$E_{K_\propto} \sim \frac{Z^2}{100}\ ; E_{L_\propto} \sim \frac{Z^2}{750}\ ;\ E_{M_\propto} \sim \frac{Z^2}{3000} \qquad (3.1)$$

From these equations, it can be used the approximation that the K, L and M shell energies vary with the square of the atomic number Z and so they are distinct for every element. Since the energy of the emitted X-ray is unique to the originating element, the measured X-ray energy spectrum will allow the identification of the elements present in the sample.

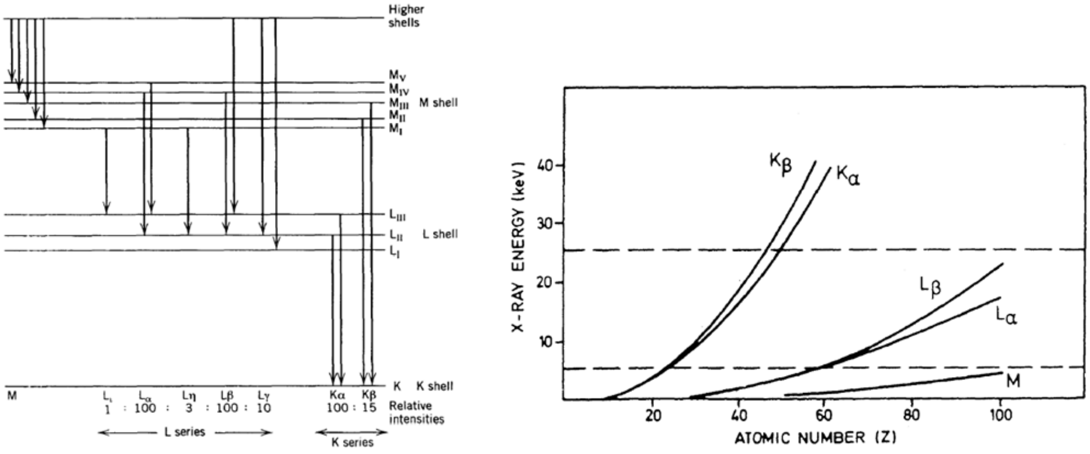

a **b**

Figure 3. 1. Atomic level diagram showing the main K and L X-ray transitions (a); dependency of the X-ray emitted energies with the atomic number Z of the elements (b) [29,30].

The most important contributions for a X-ray spectrum are given by the X-rays characteristic of the elements present in the sample and the background radiation. The dominant source of background in a X-ray energy spectrum measured using a semiconductor detector is the bremsstrahlung radiation. This radiation occurs due to the fact that any charged particle emits electromagnetic radiation when subjected to acceleration. In this sense, whether the incident beam particles or the bound atomic electrons are accelerated, will contribute to the background radiation due to interactions with the target material. Note that although the contribution of electrons to the background radiation is much higher than that due to protons or other heavy particle, this only affects initial region of the spectrum. In fact, the maximum possible energy transfer in a frontal collision between a free electron and a much larger particle mass is given by the classical expression in equation 3.2 [30],

$$E_T = 4\frac{m_e}{m_p}E_p \qquad (3.2)$$

where E_T is the maximum energy transferred, m_e is the electron mass, m_p is the proton mass and E_p is the energy of the incident particle. For example, a proton with 2MeV energy can transfer to an electron a maximum of 4keV which will be the maximum limit expected from the electrons bremsstrahlung contribution.

Due to the characteristics of the X-ray detector used in the experiment, other contributions, such as escape peaks and sum peaks, will also appear in the spectrum. The escape peaks are the result of the partial loss of energy due to fluorescence in matrix detector. Regarding the sum peaks, these arise from the fact that the detector can detect two or more photons at the same time. When this happens, it will appear in the spectrum one peak with energy equal to the sum of the energies of the detected photons.

The X-ray production cross section of each element increases with the increase of the energy of the incident particles. In other words, the higher the beam energy the better the detection limits of PIXE technique. However, this assumption is not completely true since the detection limits are function of the background intensity. On the other hand, the increase of the energy of the incident particles leads to the increase of the braking radiation of the ripped electrons and of the incident particles. By combining the behavior of the X-ray production cross section with the intensity of the background radiation, it is possible to verify that the best detection limits are found for protons with beam energies between 1 and 3 MeV [30]. Therefore, the sensibility of this technique is strongly affected by the overlapping of the energy of the detected X-rays and consequently strongly dependent of the resolution of the detector and the sample composition.

During the interaction between the incident ion beam and the target, the incident charged particles suffers numerous inelastic collisions with the sample atoms, losing energy. This energy loss occurs mainly due to inelastic Coulomb encounters with bound electrons thus, the trajectory of the ion beam is altered during the slowing-down process. The specific energy loss of an ion with energy *E*, also known as stopping power, *S(E)*, gives the decrease of the ion energy along its trajectory and it is defined as the energy loss per unit mass thickness crossed, following the equation 3.3:

$$S(E) = -\frac{1}{\rho}\frac{dE}{dx} \qquad (3.3)$$

with ρ being the density of the stopping material (g.cm^{-3}) and x the distance (cm). The stopping power is typically expressed in keV.g^{-1}.cm^{-2}.

Quantitative determination of elements using PIXE, even in trace concentration, relies on an accurate knowledge of the electron-shell ionization cross section. To describe the ionization process it has to be taken into account the phenomena involved. For instance, from the projectile point of view, it is necessary to consider the velocity loss and deflection in the columbic nuclear field, as well as the loss of energy transferred to the electron. GUPIX software [31], which is the software used during this Master Thesis to determine the elemental concentrations from the areas of X-ray peaks in the spectra, has the capability of calculating the production and ionization cross sections as well as to subtract the background. Since these calculations are not in the scope of this thesis, more detailed information about the software algorithms can be found on [31].

In the specific case of valuable and fragile artifacts, the use of an external beam is mandatory to guaranty their safety. The major benefits using an external ion beam are: it allows the analysis of artifacts of any size and shape without any sample preparation or sampling; since the measurements are done under atmospheric conditions, the dehydration problems related with local heating and consequent damage are reduced [32]. These features enable the use of PIXE technique for the study of small amount of material and delicate objects [33].

3.1.1.2 Experimental setup

The PIXE measurements were performed using the external beam set-up which is installed at the nuclear microprobe end-station, at the CTN/IST. The proton beam is generated by a 2.5 MeV single ended Van de Graaff accelerator and directed to the microprobe beam line.

The external beam set-up photograph is shown in figure 3.2. The exit nozzle assembly (figure 3.2, number 1) has at its end a vacuum tight extraction window made of 100 nm thick Si_3N_4 membrane held in a 200 µm thick Si frame, allowing nearly 100% transmission with negligible energy loss. The size of this window (1x1 mm^2) sets the limit of the maximum beam scanning area. The micro-beam has a final dimension of 70x70 μm^2. An X-ray Si-SDD detector (figure 3.2, number 2) is placed at 2.8 cm from the sample at an angle of 45º to the beam direction. It has an active area of 30 mm^2 and 145 eV resolution at 5.9 keV (Mn $K\alpha$ line). During measurements a 50 µm Mylar foil was placed in front of the detector to avoid the entrance of protons into the detector crystal, reducing the damage. Documents (or sample to be analyzed) have to be placed at 3 mm distance from the exit window and the distance is controlled with the guidance of two laser beams intersection (figure 3.2, number 3) and a micro camera (figure 3.2, number 4). It is also available a particle detector to perform RBS measurements (figure 3.2, number 5). In order to reduce air interference during the measurements, a helium rich atmosphere is set by insufflating He gas towards the analyzed region by means of a nylon chamber, placed around the particle detector and connected to a He flow controller (figure 3.2, number 5). More details about the set-up can be found on [33].

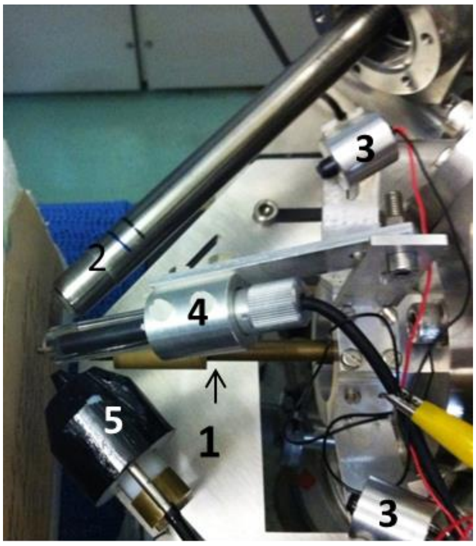

Figure 3. 2. Photograph of the External beam set-up at CTN/IST: 1 - exit nozzle with a 100 nm thick Si_3N_4 window; 2 - X-ray detector; 3 – positioning laser beams; 4 – micro camera; 5 - particle detector with He flux.

Another very interesting capability of the external microprobe available at CTN is the possibility to perform scan analysis as large as 800x800 μm^2, to study the elemental distribution in the analyzed area.

Data acquisition and beam control is performed with the OMDAQ V5.2 software package [34]. PIXE spectra evaluation and quantification was done with the GUPIX [35] software. During the analysis the samples were assumed as thick homogeneous target.

Since this is a novel study in the lab, the experimental conditions had to be established in a preliminary stage of this thesis work [36], to assure the pristine conditions of the documents. For this purpose, modern papyrus was firstly used to study the damage produced by the deposited charge and to adapt the current beam intensity and time of measurements. To compare the effects of the deposited charge in different paper supports and since this thesis is focused in the analysis of documents with paper support the same experimental conditions were also tested in a piece of document sample from the beginning of the XX century without any historical value.

Figure 3.3 shows photographs of the papyrus and the document samples irradiated with four different current beam intensities for different acquisitions times. We set at first the current beam intensity at 3 nA for a period of 8 minutes but it was found to be prejudicial for the samples as it produced a permanent mark in both. We chose to diminish the current beam intensity and increase the time of acquisition and, as it can be seen by the photographs, although a current beam intensity of 300 pA left a mark in the papyrus, it is not visible in the document sample. The observed residual stains in the document disappeared in approximately a week. Therefore, for the characterization of the documents, the beam intensity was set at 300 pA and the acquisition time was ~ 15 minutes for each measurement. Measurements were performed in both, bare paper areas and inked regions.

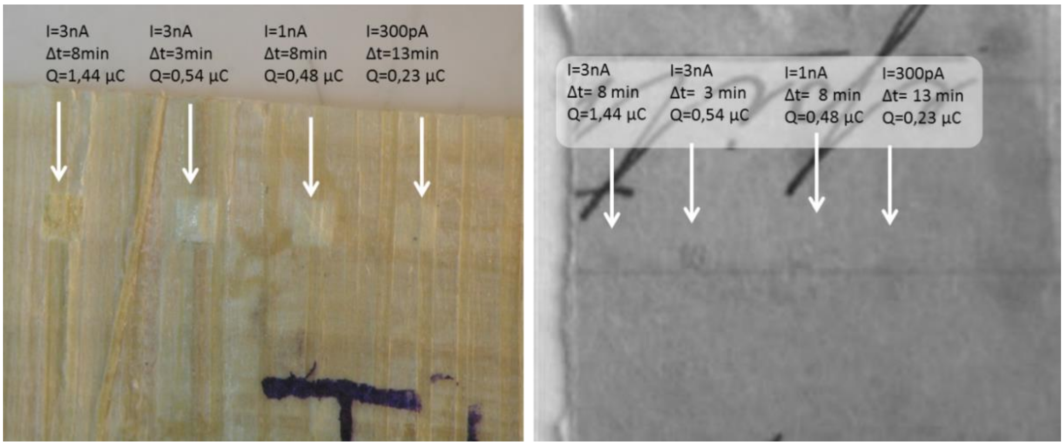

Figure 3. 3. Photographs of a sample of modern papyrus (left side) and a document from the beginning of the XX century (right side) tested in four spots.

3.1.2. Rutherford Backscattering Spectrometry

Rutherford Backscattering Spectrometry (RBS) is a widely used nuclear method for the near surface layer analysis of solid materials.

RBS method in materials analysis was firstly described in 1957 by Rubin *et al*. [37]. It relies on the Coulomb (electrostatic) interaction between the incident ions and the nucleus of the target atom. This technique has a good depth resolution, of the order of several nm from the surface, and a very good sensitivity for heavy elements especially if they are in light matrix. Therefore, RBS provides quantitative determination of the composition of materials as well as the depth profiling of the individual elements. Backscattering spectrometry is confined to detection of elements that are heavier than the incident ions, for instance in the case of ^{4}He ions as beam, this limitation only applies for hydrogen and helium.

Figure 3.4 exemplifies a schematic RBS geometry. The incident ions with a defined energy E_0, atomic number Z_1 and mass M_1, collide with a target with an areal density $N_i.t$. The scattered ions have an energy E_1, atomic number Z_2 and mass M_2, with θ being the backscattering angle measured with respect to the direction of the incident beam to a detector. Ω is the solid angle and R is the distance of the detector from the sample.

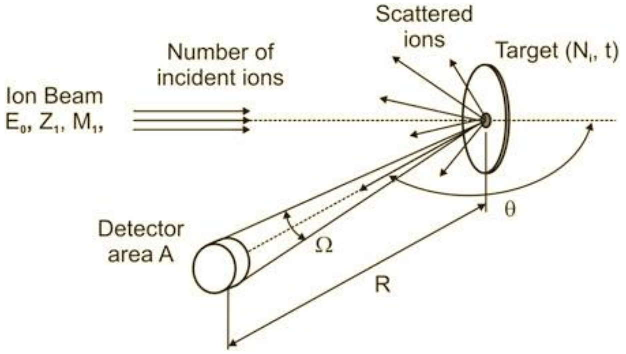

Figure 3. 4. Schematic RBS geometry with normal ion beam incidence [38].

Three main aspects have to be considered during RBS experiments: the mass identification and mass resolution; the sensitivity limits for the compositional analysis and the depth resolution. The accuracy of an RBS analysis depends essentially on these factors.

The element identification of a target atom requires the knowledge of the kinematic factor, *K,* which is defined as the ratio of the projectile energies after and before elastic collision according to equation 3.6 [39]:

$$K = \frac{E_1}{E_0} = \left\{ \frac{M_1 cos\theta + \sqrt{M_2^2 - M_1^2 \sin\theta^2}}{M_1 + M_2} \right\}^2 \qquad (3.6)$$

As it can be seen from equation 3.6, the kinematic factor is independent of the incident ion energy E_0 and it only depends on the mass ratio M_1/M_2 and on the angle θ [29]. Figure 3.5 shows the dependence of the kinematic factor with the mass of the target atom for both cases, a proton beam and an alpha particle beam. One can conclude that the mass resolution diminishes for heavy elements, becoming difficult to distinguish atoms with neighboring masses since the kinematic factors are very close.

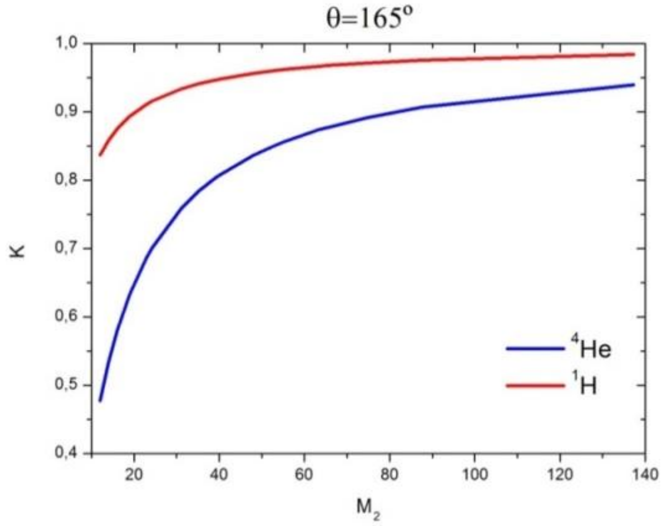

Figure 3. 5. Kinematic factor *K* at a scattering angle θ=165° as a function of target mass M_2 for incident protons and ^{4}He.

The specific energy loss or stopping power *dE/dx* represents the mean energy loss <*δE*> of a large number of ions travelling through an infinitesimal thickness *dx*. Due to the atomic character of energy loss, an indication of thickness in length units without consideration of the atomic density N_i (cm^{-3}) in the analyzed layer is not reasonable. Therefore, in ion beam analysis, the stopping cross-section *ε(x)* is used, which is given in units of $eV.cm^2$. Thus (equation 3.7),

$$\varepsilon(x) = -\frac{1}{N_i}\frac{dE}{dx} \qquad (3.7)$$

which represents the mean energy loss <*δE*> per crossed atomic areal density $N_i.\Delta t$.

Only a small portion of ion beam is backscattered and detected. The relative number of particles backscattered from a target atom into a given solid angle for a given number of incident particles is related to the differential scattering cross section as (equation 3.7):

$$\frac{d\sigma}{d\Omega} = \left(\frac{Z_1.Z_2.e^2}{16\pi.\varepsilon_0.E_0}\right).\left(\frac{1}{\sin^4\left(\frac{\theta}{2}\right)}\right) \qquad (3.7)$$

where $d\Omega$ is the solid angle subtended by the detector, Z_1 is the atomic number of the incidence particles, Z_2 is the atomic number of the elastically scattered particles, ε_0 is the vacuum permittivity and *e* the electric charge. One can also correlate the cross section (*σ*) to the yield Y_i of backscattered ions from a thin layer Δt containing atoms N_i through (equation 3.8) [38],

$$Y_i(t) = N.\,\Omega.N_i.\Delta t.\sigma \qquad (3.8)$$

that depends on the number of incident particles *N*, the solid angle *Ω* of the particle detector, the atomic areal density $N_i.\Delta t$ (which gives the number of scattering atoms) and finally on the probability of scattering (backscatter cross section *σ*).

The knowledge of the differential backscatter cross section allows the standardless quantification of elements M_i in a thin layer Δt with an areal density of $N_i.\Delta t$ from the measured yield $Y_i(t)$ in equation 3.8. The energy values of the lines are identified by the kinematic factors of the atom masses $M_{i,}$ and their intensity (yield) ΔY_i by the differential cross section and the number *N* of incidence primary ions. Therefore, it is possible to calculate the areal densities of target atoms using equation 3.9,

$$Ni.\Delta t = \frac{\Delta Yi}{N.\Omega.\left(\frac{d\sigma}{d\Omega}\right)_i} \qquad (3.9)$$

From figure 3.4 it can be seen that the solid angle is the ratio between the detector area and the square root of distance of the detector from the sample, $\Omega = A/R^2$. The expression for the yield ΔY_i can be then be written as

$$\Delta Y_i = \left(\frac{Z_1.Z_2.e^2}{16\pi.\varepsilon_0.E_0}\right).\frac{N.N_i.\Delta t}{\sin^4\left(\frac{\theta}{2}\right)}.\frac{A}{R^2} \tag{3.10}$$

From equation 3.10 follows that the Rutherford scatter yield is very forward directed, going as $1/\sin^4(\theta/2)$. The scatter yield increases with decreasing incident ion energy E_0 (proportional to $1/E_0^2$). Furthermore, (equation 3.7) shows that since $d\sigma/d\Omega$ and therefore Y_i are proportional to $Z_1^2.Z_2^2/E_0^2$, the sensitivity increases with increasing Z_1 and Z_2 and decreases with E_0 [38].

Considering the case of compound layers containing more than one element, for example, elements *A* and *B* with the chemical formula A_xB_y, to determine the stoichiometry of layers A_xB_y with thickness *t* it is necessary to calculate, from the RBS spectrum, the ratio of A and B areal densities. From equations 3.8 and 3.10 it follows that

$$\frac{N_A.t}{N_B.t} = \frac{Y_A}{Y_B}.\left(\frac{Z_A}{Z_B}\right)^2 \tag{3.11}$$

where Z_1, E_0 and the scattering angle θ are the same for the two elements.

3.1.2.1. Experimental setup

When the RBS experiments were performed under vacuum conditions only samples with no historical value were characterized, because the destructive effect of the beam in these conditions. The samples were positioned at an incident angle of α=10º with the beam direction and the data analyzed were collected by means of a PIPS particle detector (passivated implanted planar silicon) placed at θ=165º. The detector solid angle is 11,7 msr. Considering the elements to be analyzed (mostly Fe from the ink and Ca from the paper support which have a close atomic number), in order to increase the mass resolution of the technique, an alpha particle beam (2 MeV) was chosen to perform these measurements (see figure 3.5). The collected charges were 1μC and 0.5μC according to the sample.

Figure 3.6 shows two simulations of beam depth penetration made with SRIM software [40] for a 1940 keV proton beam interacting with bare paper and inked paper with iron gall ink. In the case of bare paper, the beam penetrates about 70 μm depth inside the target while for the case of paper+ink it only goes about 60 μm depth. Comparing figure 3.6 with figure 3.7 which shows the same simulations using a 2000 keV alpha particles beam instead of a proton beam, it can be seen that in this case the beam almost does not penetrate into the target as it only goes at around 9 μm into the inked target and about 10 μm in the case of bare paper.

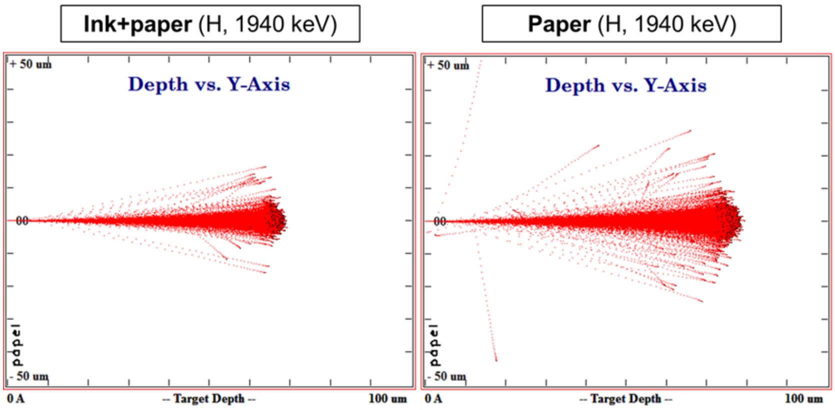

Figure 3. 6. Simulations with SRIM software of depth penetration of a 1940 keV proton beam in paper written with iron gall ink (left side) and bare paper (right side) targets.

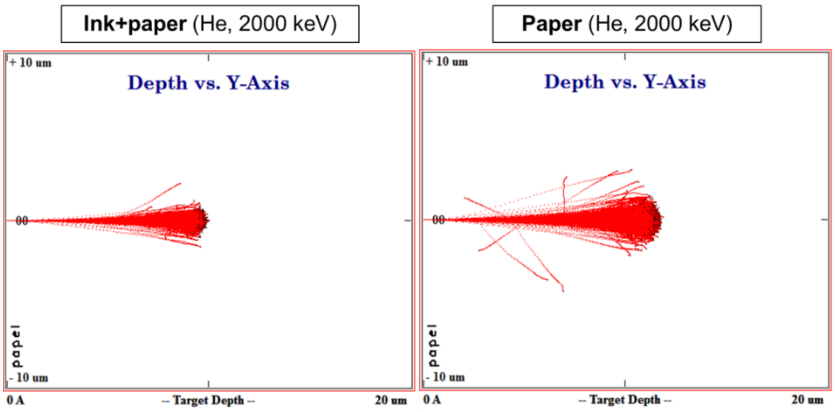

Figure 3. 7. Simulations with SRIM software of depth penetration of a 2000 keV alpha particles in paper written with iron gall ink (left side) and bare paper (right side) targets.

The SIMNRA software (version 6.06) was used to fit and to calculate the depth profiling of the experimental RBS spectra [41].

3.2. Complementary Techniques

3.2.1. X-ray Diffraction technique

An ideal crystal consists in a repetition of high number of unitary structures, which are composed of atoms of the same or either different elements, according to a well-defined order.

Miller indices *hkl* are a set of three integers that specify the orientation of a plane in the crystal. The reason why X-ray diffraction is so commonly used in crystal structural analysis arrives from the fact that the interplanar distance of the majority of the materials is of the same order of magnitude as the wavelength λ ($\sim\dot{A}$) of the X radiation used.

When a photon interacts with the electrons present in the nodes of a crystalline lattice it originates an isotropic dispersion from each node. The resulting interference of all dispersed photons creates the X-ray diffraction phenomena. The diffraction has maximum of intensity in specific directions, called reflections, due to the constructive interference of the scattered waves [42]. The conditions for constructive interference are easily derived from the simple geometrical picture for the scattering of an X-ray beam by planes of atoms in a crystal, shown in figure 3.8.

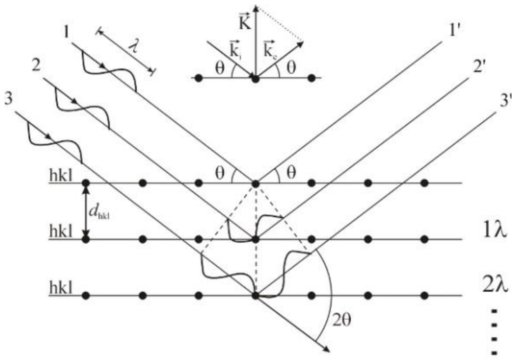

Figure 3. 8. Principle of X-ray diffraction in a crystalline structure [42].

Considering an X-ray beam with a certain wavelength which is focused in a set of parallel planes, reflection only occurs if the waves dispersed from the planes are in phase with each other. This means that if an incident X-ray is specularly reflected by a set of crystal planes, constructive interference occurs when the difference in path length is an integral number (*n*) of wavelength λ [43]. Bragg's Law, equation 3.12, relates the incidence angle, θ, and the beam wavelength with the distance between atomic planes d_{hkl},

$$2.d_{hkl}.sin\theta = n.\lambda \qquad (3.12)$$

X-ray diffraction (XRD) in *θ-2θ* geometry method is the most used when studying polycrystalline samples and it provides the identification and quantification of the compounds present. Generally speaking, all substances have a characteristic diffraction pattern. When a polycrystalline substance is submitted to a monochromatic X-ray beam in a define direction, it produces diffraction cones as a result of the random orientation of the crystals that constitutes the sample. A symmetric *θ-2θ* scan is used to determine the interplanar distance of the planes parallel to the sample surface. In this type of scan, the angle *θ* of the incoming beam with respect to the sample surface is varied, while simultaneous keeping the detector at an angle of *2θ*. The angle *θ* at which a diffraction peak is observed can be inserted into equation 3.12 to obtain the interplanar distance (d_{hkl}).

The intensity of the peaks in a XRD spectrum depend on some factors, namely the Lorentz factor, the polarization factor, the multiplicity factor, atomic scattering factor, the structure factor and the temperature factor [43]. In the XRD experiments performed during this thesis work, the only factors to have in consideration are the multiplicity factor, the atomic scattering factor and the structure factor since considering the experimental conditions used the others factors can be negligible.

The multiplicity factor has to be taken into account since when diffraction occurs in a polycrystalline material, the reflection in a given plane will be equal to the reflection in its family planes if the interplanar spacing is the same.

Since the electrons are distributed around the atom, not all of them are going to scatter the X-rays with the same phase. The difference in the phases causes a partial interference that produces a decrease of the intensity of the diffracted beam. Thus, the intensity is a function of the Bragg angle and decreases with $\sin\theta/\lambda$. The atomic scattering factor, f_0, is given by the ratio between the dispersion of an atom and the dispersion of a single electron of that atom:

$$f_0 = \int_0^{\infty} U(r).\frac{\sin(kr)}{kr}.dr \qquad (3.13)$$

where $k = 4\pi sin\theta/\lambda$ and $U(r).dr$ is the probability of finding and electron between *r* and *r+dr*.

Only a few numbers of crystalline structures are composed of only one element. Therefore, once it is necessary to take into account the atomic scattering factor for each element, the structure factor, F_{hkl}, is no more than the sum of the atomic scattering factors of the atoms in the sample, accounting with the different phases corresponding to the *hkl* planes of the different elements. The structure factor is given by

$$F_{hkl} = \sum_{n=1}^{N} f_n e^{2\pi i(hu_n+kv_n+lw_n)} \qquad (3.14)$$

where u_n, v_n and w_n are the coordinates of each element *n* in the unitary cell.

3.2.1.2. Experimental Setup

In this work, the experiments were performed in two different difractometers, the Hotbird [44] and the D8 Discover [42], both of them available at the CTN/IST.

The Hotbird is a high resolution diffractrometer, projected and constructed at the Unit of Physics and Accelerators of the CTN, with considerable large dimensions and very versatile which turned to be the best option for the study of the XX century documents because of their sizes. Also, this set-up provides much higher intensity than the D8 diffractometer. The D8 Discover from Bruker has smaller dimensions and so it was used for the study of small samples of paper and inks and also to characterize the ingredients. In both diffractometers the θ-2θ geometry was used to acquire the X-ray diffraction spectra, determine the interplanar distance of the planes parallel to the sample surface, and then identify the compounds.

Both systems use the Cu-$K_{\alpha1}$ monochromated radiation (1.540597 Å) as excited radiation beam, and a divergence slit (0.6mm) was used to collimate the beam before traveling towards the sample. The samples are mounted on a 6-axes Eulerian cradle, making possible translation (x, y, z) and rotation (ω,χ,φ) independent movements. The movement of the detector introduces another additional axis (2θ). The (χ,φ) angles are normally used for the alignment of the samples, but they are not taking part in the XRD measurement. The θ angle covers the whole 360º range while 2θ can be varied from -4º to 170º. The $\theta/2\theta$ reproducibility is ±0.0001º.

To reduce the divergence in the detector, the diffracted beam is passing through another slit (detector slit) of 0.32 mm. An scintillation NaI(Tl) detector (D8 Discover) or gas detector (Hotbird) receives the diffracted X-rays from the sample.

Usually, each diffractogram takes around 4 - 5 hours to scan each sample and it were used two different softwares, Match! and PhasanX, to identify the compounds, together with the help of the Pearson's Database for crystalline compounds. Figure 3.9 shows photographs of the experimental setup used for the analysis of two of the documents under study in the D8 Discover and the Hotbird diffractometers. As it was already mentioned, the size of the documents determines the use of the diffractometer as it can be seen through the photographs. Since the documents have to be carefully handled it were used tweezers and magnets to fix the documents in the experimental support.

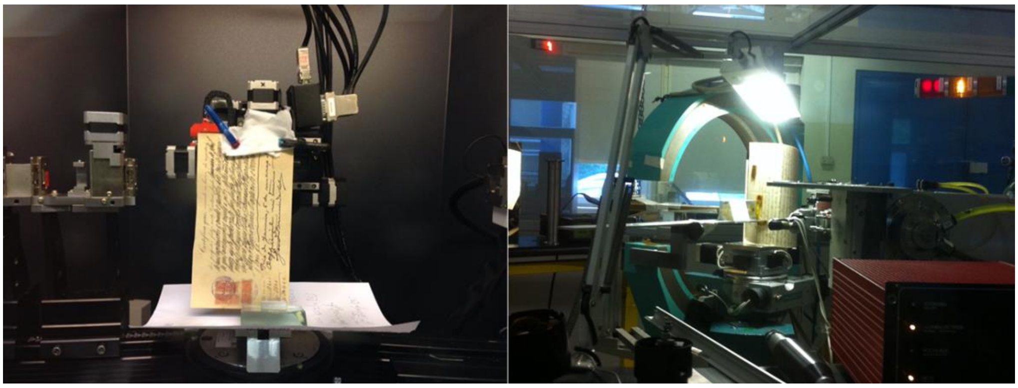

Figure 3. 9. Photography of the experimental apparatus using the D8 Discover (left picture) and the Hotbird (right picture) diffractometers, both available at CTN/IST.

3.2.2. Infrared spectroscopy

The infrared (IR) spectroscopy is a nondestructive technique that exploits the fact that molecules absorb specific frequencies in the infrared part of the electromagnetic spectrum which are characteristic of their structure. When the radiant energy matches the energy of a specific molecular vibration, absorption occurs. This absorption is called resonant frequency and it is related to the strength of the bond and the mass of the atoms (equation 3.14) and also with a particular normal mode of motion, which is associated to a change in dipole moment [45],

$$\nu = \frac{1}{2\pi c}\sqrt{\frac{k}{\mu}} \qquad (3.14)$$

where k is the spring constant for the bond, c is the speed of light, and μ is the reduced mass of a given A–B system.

There are five modes of molecular vibrations: symmetrical and antisymmetrical stretching, scissoring, rocking and bending. For a molecule consisting of N atoms, it has 3N-5 degrees of vibrational modes if it is a linear molecule and 3N-6 degrees of vibrational modes if it is a nonlinear molecule. As an example, the nonlinear molecule H_2O has 3x3-6=3 degrees of vibrational modes.

For the analysis of the IR spectra the scan-range normally employed is 4000-400 cm^{-1} since the organic compounds show spectra in which many peaks are spread over this range. Each peak is associated with a particular vibration and the complexity of the spectra reflects the large number of fundamental vibrations, which depend on the complexity of the molecule, i.e. its number and type of bonds and neighborhood. Fortunately, certain absorptions are related with stretching or bending vibrations of typical functional groups present in an organic molecule, enabling the identification of certain absorption peaks in the spectra. Other absorptions observed are characteristic of the molecule as a whole. Although these will add complexity to the analysis of the spectra, they provide the equivalent of an unambiguous fingerprint for any particular molecule [46].

Table 3.1 presents the characteristic absorptions peaks and bands for the main compounds usually found in paper and inks. Concerning to paper composition, it is mainly constituted of cellulose ($C_6H_{10}O_5$), which characteristic absorptions peaks due to the C-O bonds and C-OH and C-O-C groups are shown in table 3.1 [47,48]. The spectrum of paper may also show the evidence of inorganic compounds such as calcium carbonate, gypsum and barite. Calcium carbonate ($CaCO_3$), also known as calcite, shows strong absorption bands at about 1414 and 874 cm^{-1} [26] and a weak peak centered at 1085 cm^{-1} [10]. Pure gypsum ($CaSO_4.H_2O$) and barite ($BaSO_4$) have their characteristic absorption peaks tabulated in table 3.1 [10,25,49].

Regarding to iron gall inks, iron oxide ($Fe_2O_3.xH_2O$) shows peaks at 397 and 300 cm^{-1} [10], which are out of the analyzed absorption band. However, once there occur various chemical reactions between the different ingredients of the inks and even with the paper, different chemical bonds may appear and one may consider the absorptions bands related to sulphur to investigate the peaks in the spectra associated to iron gall ink.

Table 3. 1. Table of IR absorptions for several of the constituents compounds of paper and inks.

Name	Compound	Characteristic absorption(s) cm^{-1}	References
Cellulose	$C_6H_{10}O_5$	3450	[47,48]
		1200	
		1150-980	
Calcite	$CaCO_3$	1414	[25]
		1085 (weak)	[10]
		874	[25]
Barite	$BaSO_4$	1186	[49]
		54	
		1082	
		983	
		638	
		610	
Pure Gypsum	$CaSO_4.H_2O$	1146	[10,25]
		1116	
		669	
		602	
	(due to vibrations of H_2O molecules)	3700-3000	
		1620	
Compounds containing sulphur	O-H group	3500-3200	[50]
	chemical bond $S(=O)_2$	1440-1350	[48]
		1230-1150	
	thiols	2590-2540	
		1435-1410	
		1330-1290	
	sulphite ions (SO_3^{2-})	980	
		652	
	SO_4^{2-}	1101	[50]
		989	
		536	
Iron oxide hydrate	$Fe_2O_3.xH_2O$	397	[10]
		300	

3.2.2.1. Experimental Setup

The experiments were performed using a Thermo Scientific Nicolet IS50 FT-IR model with the ATR (Attenuation Total Reflectance) module with a slide diamond crystal, available at the CTN/IST. The experiments were performed at room temperature. Figure 3.10 shows a photography of the two possible setups used to perform FTIR analysis depending on the sample under study. The data were acquired in the 4000-400 cm^{-1} range (4 cm^{-1} of resolution) during 64 scans each round, and a total acquisition time of approximately one minute.

For the study of the ingredients and the manufactured inks it were prepared samples in the form of pellets potassium bromide (KBr), which is transparent from the near ultraviolet to long-wave infrared wavelengths and it has no significant optical absorption lines in this transmission region. Figure 3.11 shows photographs of the process used for the pellets manufacturing. First, very low quantity of material (few micrograms) has to be mixed with grade dried KBr to create an homogeneous powder (figure 3.11a) and then it is compressed using a Specac squeezer to create the pellets (figure 3.11b). For the study of the documents, since they have large dimensions and don't fit in the chamber it was used the ATR module. A criteria for successful FTIR-ATR measurement is to apply sufficient pressure to obtain intimate contact between the sample and the ATR crystal.

The spectra obtained are plots of transmittance of energy at a given wavelength, rather than absorption of energy. The OMNIC software was used for spectra acquisition and data manipulation [51].

Figure 3. 10. Thermo Scientific Nicolet IS50 FT-IR setup: the chamber was used for the analysis of pellets (ingredients and manufactured inks) and the ATR module was used for manuscripts (as the one shown in the photograph).

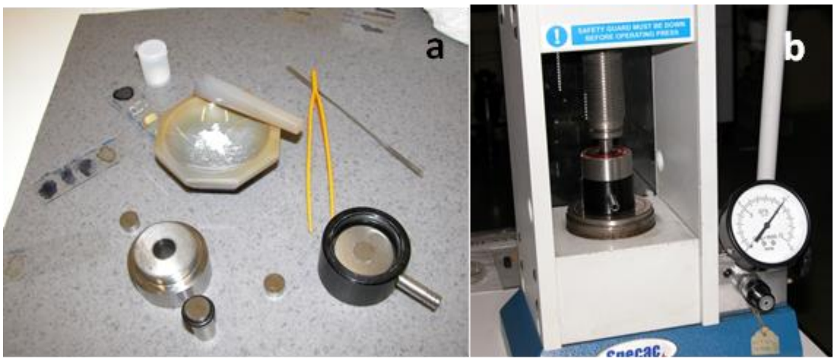

Figure 3. 11. Preparation of the samples in pellets with KBr (a). Mechanical compressor to produce the pellets (b).

3.2.3. Infrared and ultraviolet photography

Infrared (IR) radiation has been used in the scientific and technical examination of multiple works of art. In the specific case of documents or paintings, the IR radiation has been used to detect for example, the presence of under drawings [52].

The aforementioned IR portion of the electromagnetic spectrum comprises wavelengths between 750 nm and 1mm, hence spanning three orders of magnitude. By far the most applied, the photography using reflected/transmitted portion of the incident IR radiation consists in the fact that every object exposed to NIR radiation will absorb, reflect and transmit these incident photons to some extent [19]. The process of recording these amounts is generally termed reflected NIR photography.

In studying under drawings with infrared photography first of all it should be remembered that mostly only part of the drawing is being revealed. Thus, conclusions based on such evidence alone should be treated with wariness. In some cases infrared photography can show various stages in the creative process in a single document precisely because it shows under drawing and overlying paint layers at the same time [19].

Infrared photography is usually combined with ultraviolet photography since it provides additional and complementary information about the state of the paper and inks.

The ultraviolet lamp is a common tool for the examination of painted surfaces of art objects. Ultraviolet light excites fluorescence of certain materials on the surface. When electromagnetic radiation, such as UV light, impinges upon the material, part of it can be absorbed, causing electronic transitions in some of the molecules of the material. These molecules rapidly lose their excess electronic energy, or it may be partly emitted as radiation. Different materials may exhibit different colors and intensities of fluorescence which can provide information on the condition of the paint surface [52].

Most fluorescent compounds are organic compounds while fluorescence is a rare phenomenon in inorganic compounds. Inorganic crystalline compounds may show fluorescence although it is very often associated with irregularities in the crystal structure, such as vacancies and impurities [52].

For images taken under UV illumination, the non-degraded ink strongly absorbs the incident light, while parchment is luminescent in the visible range [18]. Studies of paper documents [20] found that the more the paper is degraded, the more it becomes UV absorbent. UV illumination also provides the differentiation between paper and ink in documents. Observation under ultraviolet light should be interpreted with care, preferably with complementary information obtained through other examinations techniques, such as IR photography.

3.2.3.1. Experimental Setup

A high resolution Nikon camera with a digital sensor was used to record images under visible and UV illumination. The UV source is composed by 4 lamps of long wave UV light at 350 nm and they were oriented at 45º with the documents. NIR images were recorded with a Sony camera with Carl Zeiss® Vario-Tessar lens.

Chapter 4

Results and Discussions

4.1. Test to the methods

4.1.1. Ingredients

As it was mentioned in Chapter 2, the main ingredients used to make iron gall inks are iron sulphate, Arabic gum, tannins (extracted from oak galls) and water. Figure 4.1 shows photographs of them. In this work, two types of galls as tannin sources were used. The more commonly used in recipes were galls from oak tree, but since nut galls are also a source of gallotannic acid we found it interesting to use them and thus, to analyze. It has to be remarked that commercial powder tannin was also used during this work.

Figure 4. 1. Photographs of the main ingredients used in iron gall ink manufacturing. From the left to the right: iron sulphate, also called vitriol; Arabic gum; gallnuts from oak tree and nut tree.

Elemental composition analysis by PIXE was the first to be performed in the ingredients and in the manufactured inks. Except for the Arabic gum, which was polished to create a flat area for analysis, pellets were used for the analysis of the rest of the ingredients. Figure 4.2 shows the photography of two pellets used during the analyses using PIXE and XRD (commercial tannin and iron sulphate).

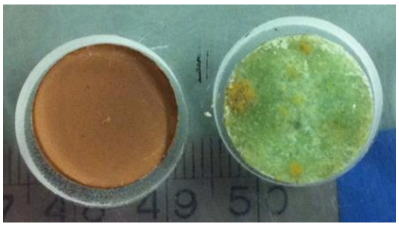

Figure 4. 2. Pellets of commercial tannin (left side) and iron sulphate (right side) with some oxidized regions.

As expected, the analyses revealed differences in the elemental composition of the ingredients. Figure 4.3 shows the PIXE spectra obtained for the three ingredients.

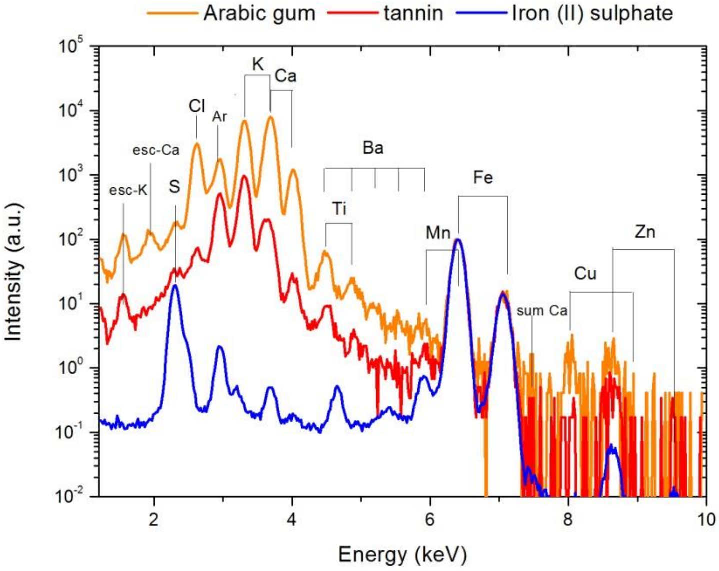

Figure 4. 3. X-ray energy spectra obtained from ingredients. The signals are normalized to the Fe-Kα line.

In all X-ray energy spectra there were identified sulphur, chlorine, calcium and iron. Additionally, there were identified potassium, titanium, copper, zinc and barium in the Arabic gum. In iron sulphate pellet there were also identified manganese and zinc while the commercial tannin pellet has traces of potassium and titanium.

Table 4.1 shows the ratios of the identified elements in the ingredients to get a better perception of the relative amount of each element. The errors for the elemental concentration were assumed to be 10% in all calculations.

Table 4. 1. Elemental concentration ratios in iron gall inks main ingredients. ND: not detected.

	S/Fe	Cl/Fe	K/Fe	Ca/Fe	Ti/Fe	Mn/Fe	Cu/Fe	Zn/Fe	Ba/Fe
Arabic gum	2,00	33,43	45,86	54,10	0,27	ND	0,03	0,04	0,58
Iron sulphate	1,00	0,01	ND	0,01	ND	0,01	ND	0,01	ND
Commercial tannin	0,47	0,53	6,45	1,14	0,05	ND	ND	ND	ND

From table 4.1, we can determine that Cl, K and Ca are the major constituents of the Arabic gum.

In the case of iron sulphate, manganese and zinc may be considered contaminants since the ratios are low, in the order of 10^{-3}. If we consider the result for the S/Fe ratio we can conclude that it has an excess of S, which is not in accordance with the chemical stoichiometry formula ($FeSO_4$) and the atomic weight of these elements (32.07 and 55.85 for S and Fe, respectively). These inconsistencies may be related to be lever of purity of the ingredients used. However, since the analyzed ingredients are commercial and we did not have access to their purity degrees, it is not possible to make considerations about this.

The high value for the ratio K/Fe in the tannin pellet, approximately 6, suggests that potassium is the major constituents of this ingredient, traces of titanium were also found.

XRD analysis were also performed in the ingredients. Figure 4.4 shows the diffractograms for the three sources of gallotannic acid used in this work: oak galls, nut galls and commercial tannin. To produce iron gall ink, the gallotannic acid is mixed with water that breaks the ester links of the gallotannic acid, forming gallic acid and glucose [53]. The pellets analyzed were not mixed with water although by XRD it was possible to identify them (gallic acid and glucose) on the pellets (see peaks position on Appendix C), suggesting that the moisture from the atmosphere is able to promote these ester links breaks. It has to be emphasized that the natural sources of gallotannin acid (oak and nut galls) exhibit quite similar diffractograms while the commercial tannin shows a broader band centered a 25º and more intense peaks of glucose and gallic acid at higher angles.

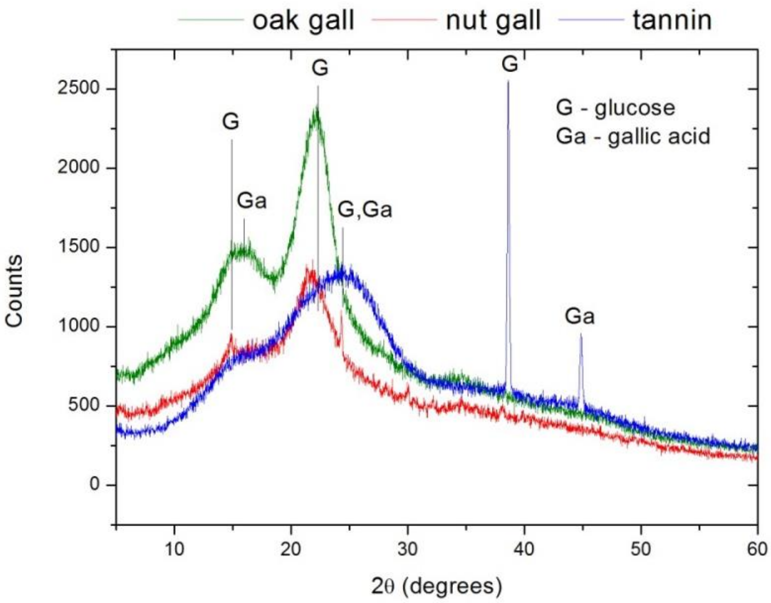

Figure 4. 4. X-ray diffraction patterns of oak gall (green line), nut gall (red line) and commercial tannin (blue line).

The diffractograms obtained for the iron sulphate pellets are shown in figure 4.5. To understand if the exposure to the atmosphere could change the composition of this ingredient, we analyzed two pellets of iron sulphate, one having already two weeks and the other was produced minutes before the XRD analysis. As it can be observed from the figure, there are slightly differences between them, referring to the compounds identified in the two pellets. In the case of the iron sulphate pellet produced two weeks before the measurements, which was in contact with the atmosphere, copiapite ($Fe_{14}O_3(SO_4)_{18}.63H_2O$) and rozenite ($FeSO_4.4H_2O$) were identified. The other pellet also evidences copiapite but melanterite ($FeSO_4.7H_2O$) was identified instead of rozenite. The main difference in these molecules is the level of hydration they present. Therefore, the exposure to the atmosphere influences the chemical composition of this ingredient too, which can also influence the behavior of the iron gall inks.

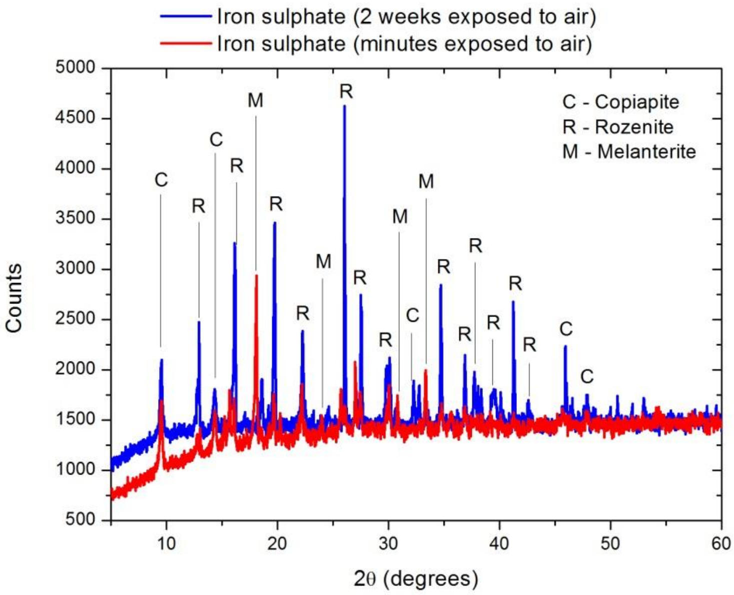

Figure 4. 5. X-ray diffraction patterns of iron sulphate pellets. One of the pellets had been exposed to air for approximately two weeks (blue line), while the other was produced minutes before the analysis through XRD (red line).

The XRD results obtained for the Arabic gum (figure 4.6) are similar to the ones found in the literature [54], where the diffraction pattern shows the amorphous nature of the gum with wide bands centered at 18º and 35º.

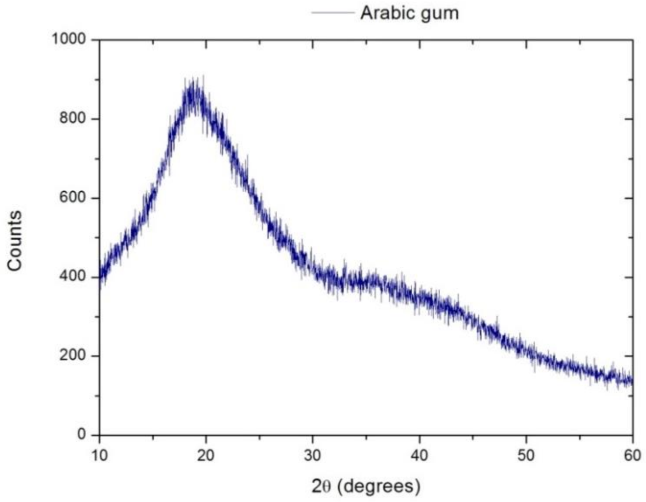

Figure 4. 6. Diffraction pattern of the Arabic gum.

Regarding the FTIR analysis, measurements were performed for three ingredients: Arabic gum, iron sulphate and commercial tannin. Figures 4.7 – 4.9 shows the transmittance spectra obtained for the ingredients.

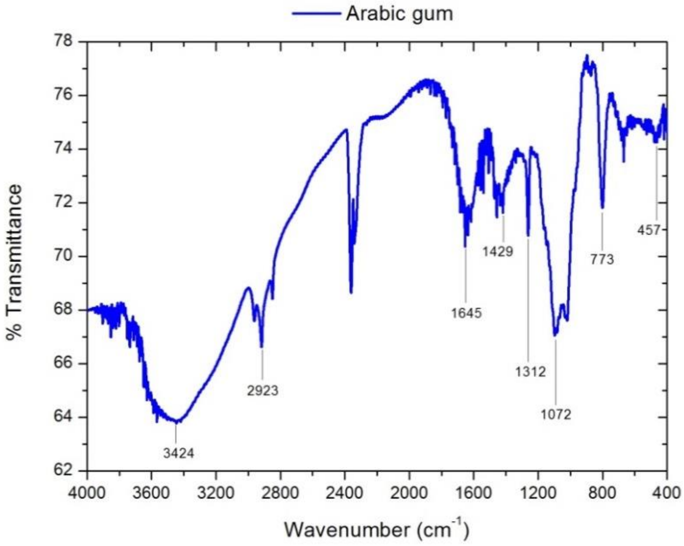

Figure 4. 7. FTIR spectrum for Arabic gum.

The identified peaks in the Arabic gum spectrum (fig. 4.7) are in accordance with the results found in the literature [50]. The broad band at around 3424 cm^{-1} is assigned to the OH functional groups for the alcohols in polysaccharides and to the N-H vibration in the amines, while the peak at 2923 cm^{-1} reflects the C-H absorption [55]. The peak at 1072 cm^{-1} may be assigned to the C-O and C-C deformation vibrations and C-O vibrations in alcoholic groups. The peak at 773 cm^{-1} is one of the peaks that may reflect the 5- and 6- member rings in monosaccharide [50].

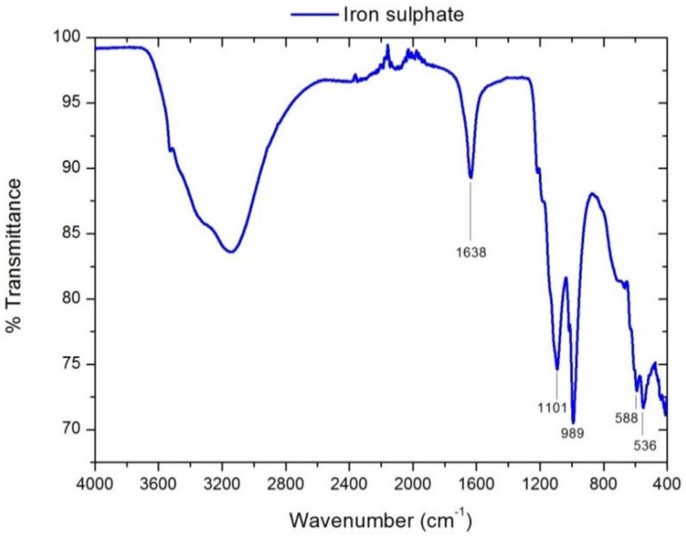

Figure 4. 8. FTIR spectrum for the iron sulphate (pellet produced minutes before the measurement).

Concerning to the iron sulphate spectrum (fig. 4.8), the broad absorption band in the range 3500-3200 cm^{-1} correspond to the OH group present in the sulphate. The bending vibrations of the absorbed molecules of water correspond to the peak at 1638 cm^{-1}. Comparing to the results obtained in [50] we see that peaks 1101 cm^{-1} and 536 cm^{-1} are indicative for the SO_4^{2-} ions, along with the peak at 989 cm^{-1} [50].

Finally, some peaks where possible to identify in the commercial tannin FTIR spectrum (fig. 4.9). It was already verified the identification of gallic acid the XRD analysis of this ingredient (figure 4.4) and the peaks observed in the transmittance spectrum in figure 4.9 are correspondent to this compound [50].

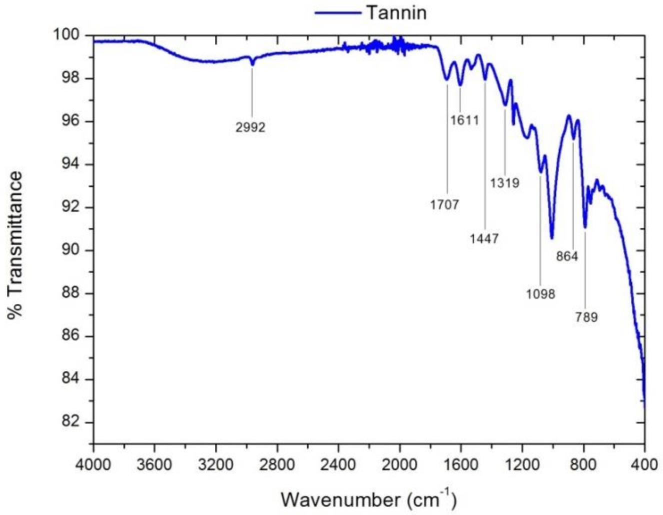

Figure 4. 9. FTIR spectrum for the commercial tannin.

4.1.2. Manufactured inks following recipes

The process of fabricating iron gall inks is not complicated. By mixing tannin with iron sulphate, a water soluble ferrous tannate complex is formed. The ink is able to penetrate the paper surface, making it difficult to erase. When exposed to oxygen a ferric tannate pigment is formed and this complex is not water soluble, contributing to its indelibility as a writing ink. In general, the color of a freshly made iron gall ink solution is rather pale. By exposing the ink to the air atmosphere for a long period of time before use, the ink usually gets a dark blue color but with the aging it becomes brown.

The oxidation of iron (II) to iron (III) in air forms complexes with gallic acid, phenomenon that leads to the degradation of tannins and the oxidation of the Arabic gum [9]. The process of degradation of the tannins provides the retention of the complexed iron (III), without which there would be no ink. On the other hand, in the presence of moisture sulphate ions are converted into sulfuric acid, which is then also present in the ink residue [56]. This phenomenon is the one largely responsible for the ink degradation in paper and the degradation of the organic acids in the Arabic gum.

Due to the corrosion and degradation processes explained above, it is necessary to investigate the elemental and chemical composition of iron gall inks in their primordial state, i.e. immediately after their production and application in paper, when the oxidation and hydrolysis reactions are minimized. Therefore, six different iron gall ink recipes were used to produce new inks (the recipes can be found in Appendix A). The inks were applied to modern paper just after their production, and then analyzed. Different papers were used in order to study also the influence of the paper in the behavior of the inks. Inks from recipes 1, 2 and 3 were written in paper 1; inks from recipes 3nut and 3oak were written in paper 3 and the ink from recipe 4 was written in paper 4. As referred above, all the liquid inks have a pale color when applied to the paper since they were not in contact with air atmosphere for the necessary period of time.

In order to discriminate the contribution of the ink from the paper in the results, it was needed to do measurements in both, bare and inked papers, in all the experimental techniques used.

Figure 4.10 shows the X-ray spectra recorded for the different papers, being the main difference the absence of Cl in paper 1, which have traces of titanium according with GUPIX. Slightly differences between paper 3 and paper 4 are found.

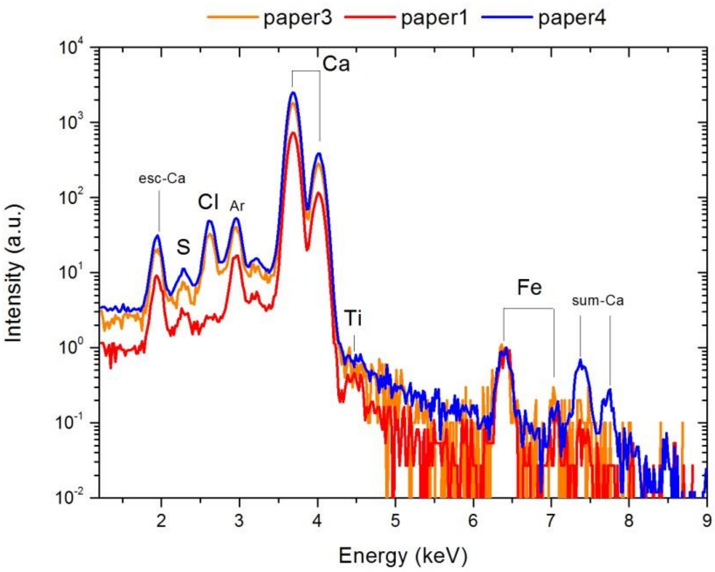

Figure 4. 10. X-ray energy spectra of three papers used as support of the six made iron gall inks. The signal is normalized to the Fe-Kα line.

X-ray energy spectra of the three iron gall ink recipes using commercial tannin (inks 1,2 and 3) are shown in figure 4.11, where it is also shown the PIXE spectrum recorded for an ink-drop (ink 1) analyzed by PIXE. X-ray spectra for recipes 4, 3oak and 3nuts are presented in Figure 4.12 while in the Table 4.2 are shown the ratios of elements with Fe obtained.

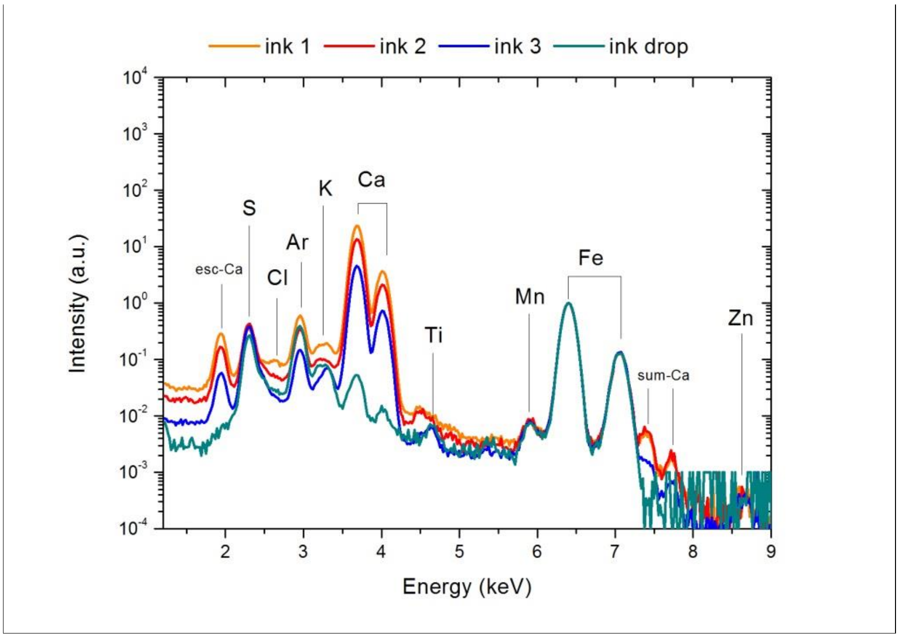

Figure 4. 11. X-ray energy spectra of three iron gall inks recipes using commercial tannins and for an ink drop. The signal is normalized to the Fe-Kα line.

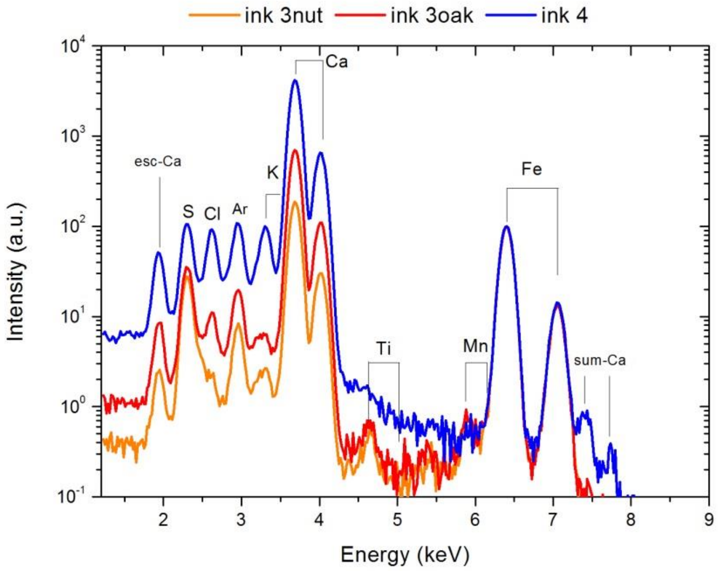

Figure 4. 12. X-ray energy spectra of three iron gall inks recipes using natural tannins. The signal is normalized to the Fe-Kα line.

Table 4. 2. Ratios of the identified elements for the six different iron gall ink recipes written in paper. The "≈ 0" value means that the result obtained for the correspondent ratios is of the order of three decimal places, yet the elements were detected by GUPIX in low concentrations. ND: not detected.

Recipes	S/Fe	Cl/Fe	K/Fe	Ca/Fe	Ti/Fe	Mn/Fe	Zn/Fe
1	0,75	0,04	0,04	7,43	0,01	≈ 0	ND
2	1,12	0,03	0,02	5,01	0,01	0,01	ND
3	1,22	0,03	0,03	2,24	≈ 0	≈ 0	≈ 0
3oak	1,04	0,16	0,02	3,11	ND	≈ 0	ND
3nuts	1,03	0,05	0,01	1,12	ND	≈ 0	ND
4	2,36	0,99	0,35	14,93	≈ 0	≈ 0	ND
Ink drop	1,01	0,07	0,08	0,04	ND	0,01	ND

Since these can be considered "new" inks and they were manufactured using the ingredients analyzed through PIXE technique (section 4.1.1.), it is relevant to discuss the results obtained having in mind the elemental composition of the ingredients. Sulphur, chlorine, potassium, calcium and iron were identified in all inks in figure 4.11. Only potassium and manganese were not identified in bare paper and so it is correct to assume that these elements belong to the inks.

Despite the different tannin sources, it is clear from table 4.2 that the elemental composition of the different inks does not vary except for the case of "ink3" which was the only one where zinc was identified, although in low concentration. This fact is not well understandable since inks "3oak" and "3nuts" were also manufactured with the same recipe as "ink3" and so it was expected that these inks also show evidences of zinc. This element was identified in both Arabic gum and iron sulphate , figure 4.3, (and so does not depend on the tannin source) but since the quantity of the iron sulphur used in this recipe is higher than the quantity of Arabic gum (almost the double), it is more plausible to think that the iron sulphate is more likely to cause meaningful changes in the elemental composition of the ink.

Concerning to the ink drop, it was manufactured with the three ingredients following the Recipe no.1 (Appendix A). Recipe no.1 has more quantity of iron sulphate (15 g) than Arabic gum (5 g) and tannins (11,7 g). If one look at figure 4.11 and table 4.2, we see that the same elements where identified in the two samples. The only difference is concerned to the fact that the ink drop has no contribution of elemental composition of the paper and so its Ca/Fe ratio is very low compared to the value of "ink1" recipe.

Apart from recipe 1 and 4, the other inks have a S/Fe ratio of approximately one which again indicates that the stoichiometry of the iron sulphate is not respected, having always an excess of S. However, in these analyses we have to considerer the fact that papers also have iron and sulphur in their composition which may influences the results.

In order to characterize the manufactured iron gall inks and paper in terms of compound composition we choose to do XRD analysis. Figure 4.13 shows the X-ray diffraction patterns of the six samples of iron gall inks on the paper support.

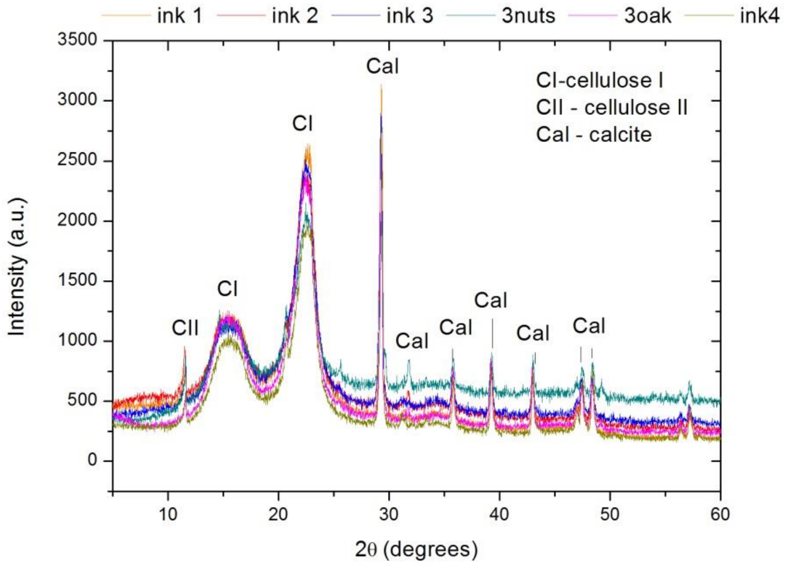

Figure 4. 13. X-ray diffraction patterns of six iron gall inks samples in paper.

All spectra show similar peaks identified as compounds belonging to paper support. Unfortunately, it was not possible to find any differences between the diffractograms recorded on inked and bared paper support. This could be due to the small quantity of ink deposited on the paper, which is not enough to be detected by XRD. It has to be highlighted that even doing the experiments at raising angles (to obtain information from the very near surface of the sample) the results were not positive. In the papers, two types of cellulose, I and II, were identified and it was also possible to identify calcite, the most stable polymorph of calcium carbonate ($CaCO_3$), which is used as filler in paper manufacturing process [57].

Paper is generally composed of cellulose fibers. Cellulose I is the common variety found in nature (and hence in paper) and cellulose II is the variety found in chemically regenerated celluloses, e.g. rayon [58]. High quality papers are often made of cotton linters whilst cheaper ones are based on wood pulps, which is the case of most papers manufactured after the 19th century.

The wood-based papers themselves are made from pulps processed in a number of ways involving different mechanical and chemical processes which degrade the cellulose fibers and modify their crystallinity. The crystallinity of the cellulose, or cristallinity Index (CrI), is a function of its source and the degree of degradation of the fibers due to grinding, beating or other treatments [59,60] and it can be calculated considering the XRD patterns following the method suggested by Segal and co-workers [60]. They calculate the CrI from the ratio of the intensities of the crystalline and amorphous contributions of the cellulose, as follow:

$$CrI = \frac{(I_{002} - I_{am})}{I_{002}} \times 100 \qquad (4.1)$$

where I_{002} is the intensity of the crystalline peak at 2θ between 22º and 23º for cellulose I and I_{am} is the intensity of the amorphous reflection at 2θ between 18º and 19º for cellulose I. Values of CrI lower than those typical of cellulose (more than 80%) indicate a degraded material or a paper made of low-quality cellulose fibers, i.e. those coming from woods [61].

In table 4.3 are presented the correspondent Crystallinity Index for each of the six samples analyzed through XRD and also the values for the papers without inks.

Table 4. 3. Cristallinity Index (*CrI*) for the papers written with the six ink recipes analyzed and the same papers unwritten.

	CrI (%)	
Sample	*ink+paper*	*paper*
1	75,88	81,43
2	71,65	
3	74,80	
3oak	77,01	74,32
3nuts	67,81	
4	75,09	82,34

Despite the approximated results between the Crystallinity Index for ink+paper and bare paper, we see that the percentages are lower in the case of paper written with iron gall inks. This fact is direct consequence of the ink interaction with the paper cellulose fibers, even after short time interaction. Moreover, from the results of *CrI* obtained for bare paper we may only assume that paper used has support for inks “3oak” and “3nuts” (paper 3) is probably made of low quality raw materials.

To have a better perception of the behavior of the ink in paper, it may be helpful to have an idea of its spread inside the paper, for example to study the penetration depth of the ink: if it passes to the back page or it remains only at the surface of the paper. Rutherford Backscattering Spectrometry (RBS) measurements allow the analysis of depth profiling of inks and also the identification of light elements with Z<11, such as carbon and oxygen, present both in iron gall inks and paper.

RBS was performed in the six samples (bared and inked papers) in vacuum conditions using an 2MeV alpha beam, as refereed in the experimental chapter. Figure 4.14 shows the RBS experimental spectrum and the best simulated curve obtained for paper 3. Figure 4.15 shows the RBS experimental spectrum for ink 3nuts and the best simulated curve obtained using SIMNRA code.

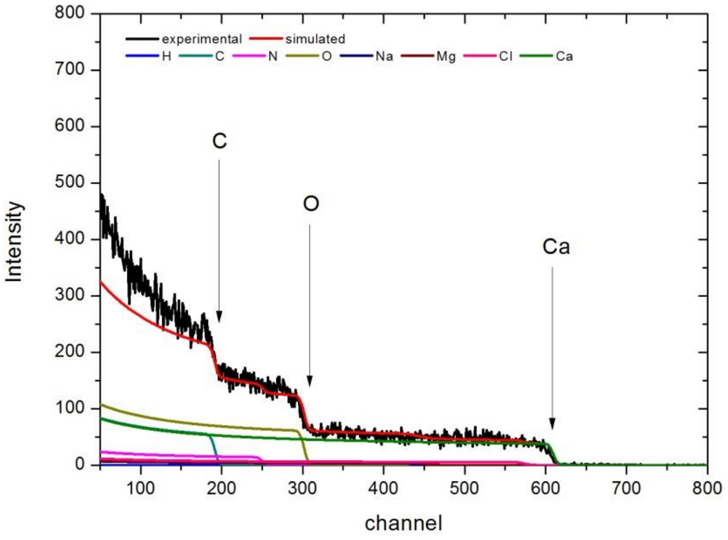

Figure 4. 14. RBS spectrum of paper 3. The simulated curve (red line) was obtained with SIMNRA code assuming two layers.

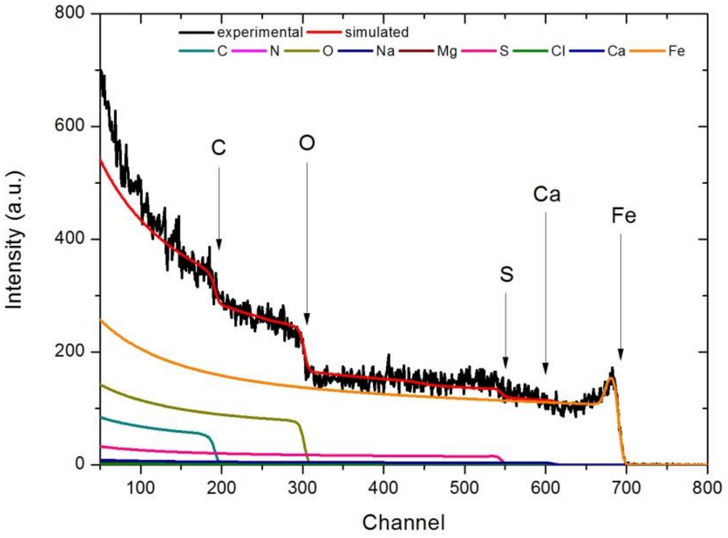

Figure 4. 15. RBS spectrum of ink 3-nuts (recipe 3) in paper support. The simulated curve (red line) was obtained with SIMNRA code assuming two layers.

For the simulation of paper 3 it was assumed only one layer, since we were dealing with only one material (paper). The substrate is composed by cellulose ($C_6H_{10}O_5$) and calcite. Also, elements as Cl, Na, Mg and N in low quantities were incorporated in the analysis to obtain a good fit, considering the elements added to manufacture paper [57] and the PIXE data.

During simulations of ink 3nuts, it was assumed a layered target, being the substrate composed by the elements present in bare paper and a first layer constituted by a mixture between iron ink (simulated as $FeSO_4$) and cellulose+calcite. The major different between the two figures (figure 4.14 and 4.15) is the fact that for bare paper there is not the initial edge correspondent to iron as in the first layer of the ink.

Table 4.4 shows the elemental depth distribution for the fit obtained for this ink. The best layer structure is based on two layers, being the first one (about 500x10^{15} atoms/cm^2 thick) very rich in Fe, S and O (from the ink) and the second layer (considered as infinite) mainly compose by cellulose and calcite as described above, with some elements as Fe, S or Cl as impurities.

Table 4. 4. Concentration (at.%) of the fitted elements in the two simulated layers for ink3 sample.

Depth (10^{15} atoms/cm^2)	C	N	O	Na	Mg	S	Cl	Ca	Fe
500	0,467	0,010	0,395	0,005	0,008	0,020	0,001	0,003	0,080
150000	0,492	0,010	0,392	0,005	0,008	0,018	0,001	0,003	0,050

Table 4.5 shows the values of the first layer thicknesses obtained for the different inks by RBS. The values found by RBS, in atoms/cm^2, have been converted in nm for a better understanding of the depth penetration distance.

Table 4. 5. Estimation of the depth penetration of iron gall inks (considering only the $FeSO_4$ ingredient) in paper. Only the depth of the 1st layer was used for the calculations.

inks	**Depth 1st layer (10^{15} atoms/cm^2)**	**Depth penetration of $FeSO_4$ (nm)**
ink1	1500	41
ink2	900	14
ink3	10000	450
3nut	500	32
3oak	10000	570
ink4	900	42

For conversion, it was considered the density of $FeSO_4$ (1.898 g/cm^3) and the concentrations of iron, sulphur and oxygen obtained with SIMNRA code. As it can be seen, ink penetration is of the order of nanometers. However, from table 4.5 the values obtained differ according to the ink since the depths of the 1st layers were not equal. Thus, the composition of the ink should interfere in its penetration in paper but it can be assumed that the ink stays at the surface, only penetrating few nanometers in the paper support.

For a better analysis of the inks composition, we found interesting to add the discussion of the results obtained using FTIR for KBr pellets of the three types of manufactured ink 3 (which only differ in the tannin source). Figure 4.16 show the FTIR spectra for the three types of ink 3. The broad band at 3700-3000 cm^{-1} appears due to the H_2O molecules. The peak at 2358 cm^{-1} only appears in the ink 3 spectrum which was produced with commercial tannin and in ink 3nut with less expression. It was not possible to identify its provenience since the three inks followed the same recipe and so it was expected to detect its expression also in ink 3oak. Peaks at 1622 cm^{-1}, 1101 cm^{-1} and 610 cm^{-1} may correspond to hydrate iron sulphate [50].

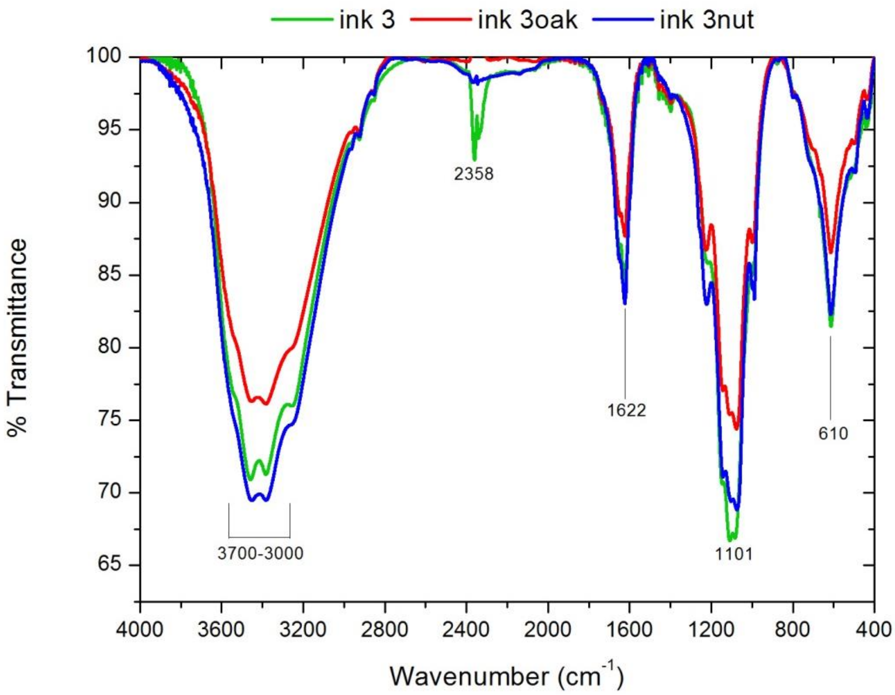

Figure 4. 16. FTIR spectra for the three types of ink 3 produced in laboratory. The marked peaks correspond to iron gall ink composition since it were produced KBr pellets of the inks for this analysis.

4.2. Analysis of old documents from the beginning of the XX century

The documents studied in this work belong to a private collection. We chose five documents dated from the beginning of the 20th century and from the end of the 19th century from Rio de Janeiro, Brazil. The documents are in good state of conservation and in general, they do not show many signs of ink corrosion and paper degradation, although some parts of the documents present holes, stains and foxing problems related to degradation. In Appendix B are shown photographs of the documents and letters were adopted for their identification during this discussion. Documents A and B and E are dated from 1928, document C is dated from 1897 and in document D the date was not specified but considering the documents of the collection it may belong to the end of the 19th century. The title of this chapter was chosen to be “Analysis of documents from the beginning of the XX century” since the documents known to be from the XIX century are already from its end where paper manufacturing and iron gall inks preparation did not vary much from the beginning of the XX century.

Representative X-ray spectra of documents A, B and C are shown in figures 4.17 and 4.18, obtained in uncovered paper and in ink covered regions, respectively.

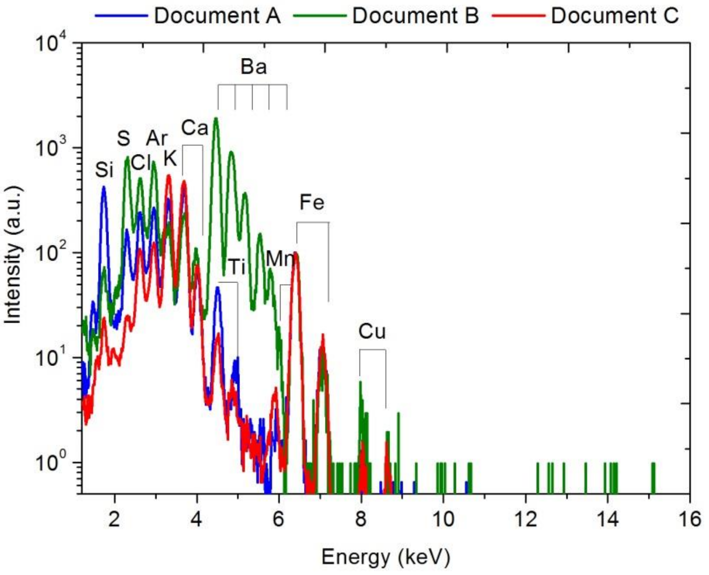

Figure 4. 17. X-ray energy spectra obtained from non-inked areas in documents A, B and C. The signal is normalized to the Fe-Kα line.

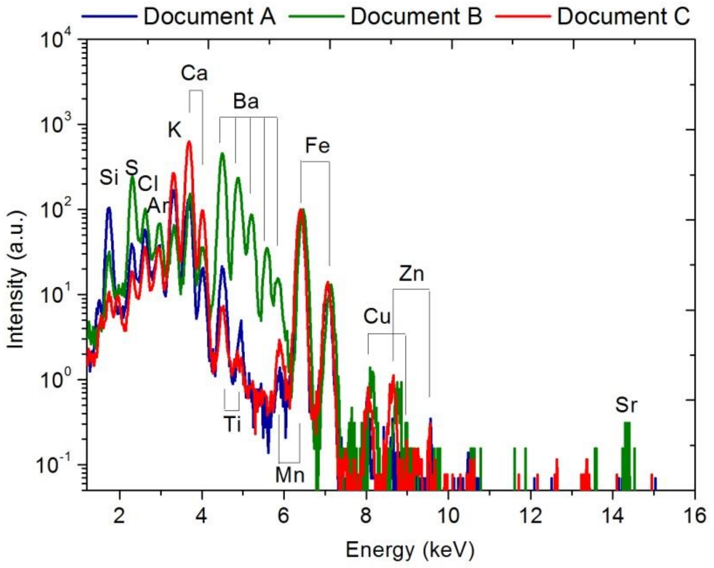

Figure 4. 18. X-ray energy spectra obtained from inked areas in documents A, B and C. The signal is normalized to the Fe-Kα line.

Concerning to the composition of papers analysed (figure 4.17), some differences were detected among them. In all of them Ti was detected which can be attributed to titanium dioxide (TiO_2), widely used as a white pigment or bleaching agent in paper [62]. In document B, the PIXE spectrum in figure 4.17 shows the presence of barium as one of the elements with higher concentration. Barium is an indicator of industrial paper manufacture [63]. All three documents show the presence of manganese in paper composition in low concentration. Additional studies should be done to understand its provenance and discard some kind of contamination, since compounds containing Mn are not among the most used chemicals in pulp and paper manufacturing [57].

Clear differences in paper color and appearance between the documents A,B and C were emphasized by means of UV photography (figure 4.19). In general, the three documents fluoresces faintly whitish, being the document A (the one with the highest amount of Ti) the one with the highest glow signal. The paper from document B appears to be darkish than the other two documents under UV light, fact that probably result from the presence of barium in its composition. It is also possible to recognize foxing and water stains in all the three documents.

Figure 4. 19. UV photography of Document A (right side), Document B (left side) and Document C (down in the picture).

Despite being a characteristic of iron gall inks, sulphur and iron exist in most everything in nature, so it is not surprising to find these elements also in paper. In general, chlorine concentration is invariably smaller in ink spots than adjacent paper. This effect has been observed systematically in the three documents. The concentration of calcium and potassium have to be interpreted with a certain precaution since these elements are expected from the basic ingredients of iron gall inks composition but they can be used as fillers in paper manufacture.

Vitriols, nominally iron sulphates, used in iron gall inks usually contain other metal suphates as impurities, such as manganese, nickel, zinc, copper or lead [6]. However, they may come from deliberate additions to the recipes. In the documents analyzed this conclusion cannot be taken because we do not know the provenience of the ingredients neither the recipes used. PIXE analyses of inked areas in the documents (figure 4.18) detected other elements besides S and Fe in concentrations that might be considered willful added to the inks.

PIXE analysis was performed in different inked areas in Document A which are marked in the photograph of the document in the Appendix B. The S/Fe and Ca/Fe ratios obtained for inked areas and bare paper are shown in figure 4.20. As it was expected, the Ca/Fe ratio is higher for paper but the most significant difference is in S/Fe ratio, that is more or less 3 times higher than the value of the

S/Fe ratio for inked areas. Between inked areas, it can be seen slight differences in the ratio values and it seems to be two distinctive groups of inked areas with similar ratios of S/Fe.

UV and IR illumination of the inks in this document are shown in figure 4.21. These methods confirmed the existence of two different iron gall inks in the written text of the document. Ink 1 used to write the text (spot A3 and spot A4) appears almost transparent to the IR radiation while ink 2 (spot A1 and spot A2) appears legible. UV light reveals some ink migration to the surrounding areas especially in ink 2 due to the degradation processes of the ink [20].

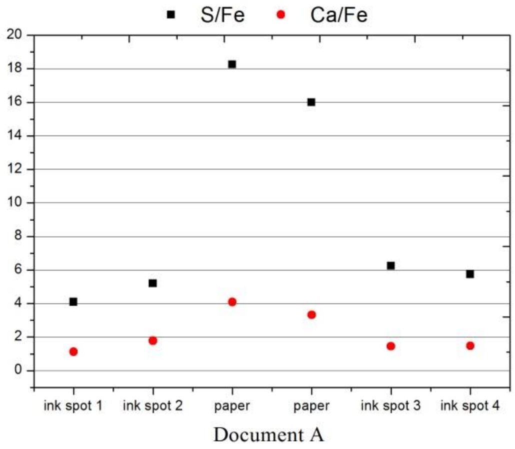

Figure 4. 20. S/Fe and Ca/Fe ratios obtained through PIXE analysis of document A. The amount of sulphur is much higher in non-inked areas while calcium does not differ that much from inked to non-inked areas.

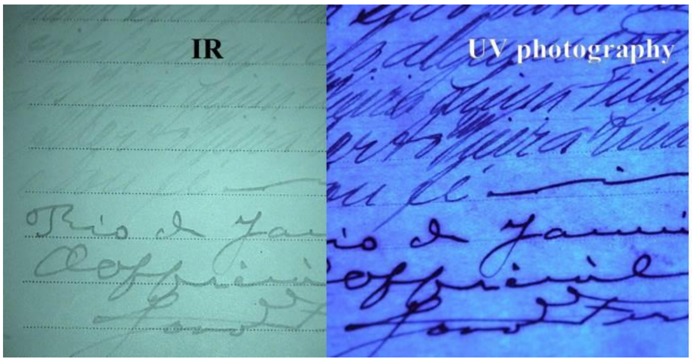

Figure 4. 21. Detail of the IR and UV photography of Document A.

In Document B it were identified copper, zinc and strontium as elements present in inked areas (figure 4.18). Graphic representation of Cu/Fe, Zn/Fe and Sr/Fe ratios for these covered areas are shown in figure 4.22a. Ink spots B1 and B2 (text from the front page of the document) probably correspond to the same ink because they are the only ones where Sr was not detected. Using the same line of though, ink spots B3, B4 and B5 might belong to the same ink since their Cu/Fe, Zn/Fe and Sr/Fe ratios are quite similar and all these spots belong to the main text in the back page of the document. The presence of traces of strontium in four of the six ink spots examined is not fully understood. However, it was also detected the presence of this element in document E. Additionally, ink spot B6 (region of the signature) seems to correspond to a third different ink due to the high amount of copper compared to the other ink spots analyzed. Copper can be associated to vitriol impurities but it appears with relevant ratio in this ink spot and so the possibility of a third ink can be considered. Once again, UV and IR photographs obtained for this document reveal slightly differences between the three types of inks making this assumption not so misplaced.

PIXE elemental maps (figure 4.22b) for Ca, Fe and S were recorded in an area partially inked (spot B4). As it is clear in the images, the iron and calcium signals in inked areas are higher than in non-inked areas while the signal of sulphur is mostly uniform in all map area. The distribution of calcium can be explained if we assume that in non-inked areas, Ca signal may be due to the presence of fillers (for instance calcite) and in the inked areas the Ca signal might come from the Arabic gum (see table 4.1) which is used as binding medium between the iron inks and the paper support [6,18] Although copper and zinc were identified in significant amounts in inked areas, the low statistical data did not allowed the creation of maps with enough contrast.

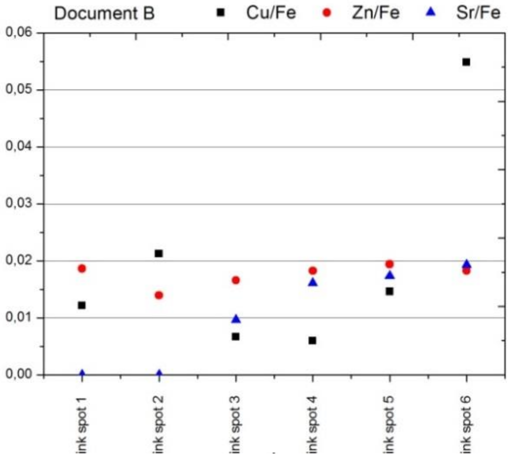

a

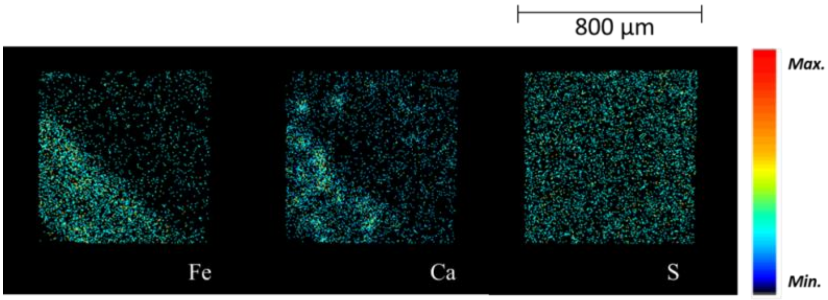

b

Figure 4. 22. Cu/Fe, Zn/Fe and Sr/Fe ratios for the spots analyzed in Document B (a).; 2D elemental maps for Fe and Ca obtained for Document B. (800x800 μm^2) (b).

Document C (dated from 1897) has traces of manganese, zinc and copper in inked areas. Figure 4.23a shows the Cu/Fe, Zn/Fe, Mn/Fe and S/Fe ratios for different marked areas analyzed in the front and back page of this document (see Appendix B). It can be observed that Zn/Fe ratio is higher for ink spots C3 and C4 when compared to the other inked spots analyzed. As in the inked areas in document B, this element could be purposely introduced as an extra compound in the ink or the ingredients used to produce this specific iron gall ink had a different provenience. These suppositions, in addition to the fact that these two ink spots are the only ones that belong to the main text in the back side of the document, indicates that C3 and C4 correspond to on type of ink (ink 1). Inks spots C1 and C2 (main text from the front side of the document) and ink spots C5 to C8 (annotations in the margin and date of the document) appear to have similar ratios of the elements to iron and the assumption of a second type of ink (ink 2) can be made.

Manganese is usually added to inks as a pigment to give a brownish color when incorporated in the form of manganese oxide [28]. However, since its presence was identified in both ink spots and also in bare paper, it is more consistent to assume that this element result from some kind of contamination of paper. Figure 4.23b shows elemental mapping of Fe, Ca and S in ink spot C3, showing higher content in the inked areas, and more specifically in the borders. As in ink spot B4 from document B the profile of the hand-writing is more visible in the Fe and Ca maps.

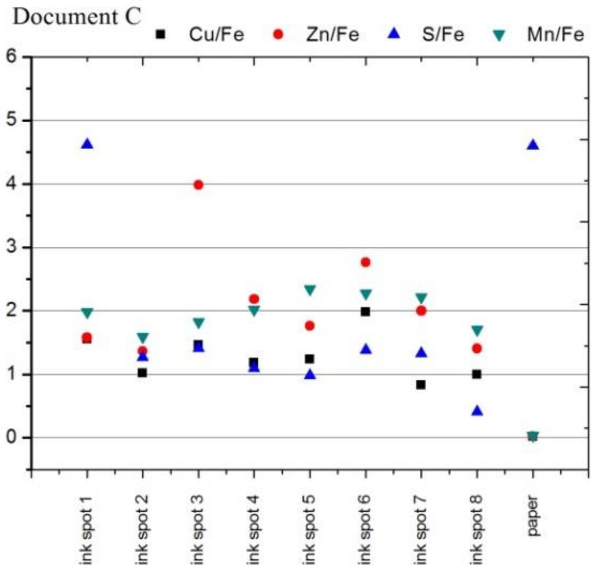

a

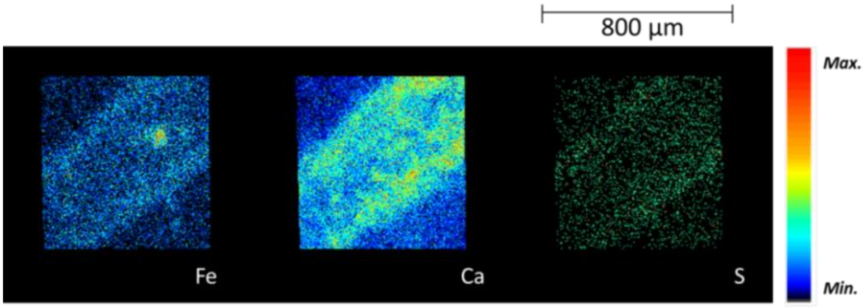

b

Figure 4. 23. Ratios of some elements present in the ink spots analyzed in Document C (Cu/Fe, Zn/Fe and Mn/Fe ratios are multiplied by 100) (a). Elemental maps of ink spot C3 of Document C (800x800 μm^2) (b).

Document D is a testament with two sheets hand-written in their front and back pages. The X-ray energy spectra of inked regions selected from the main text (ink spot D3) and paper are shown in figure 4.24. Paper elemental composition is quite similar to document B considering the identified elements, apart from arsenic that was identified in this paper.

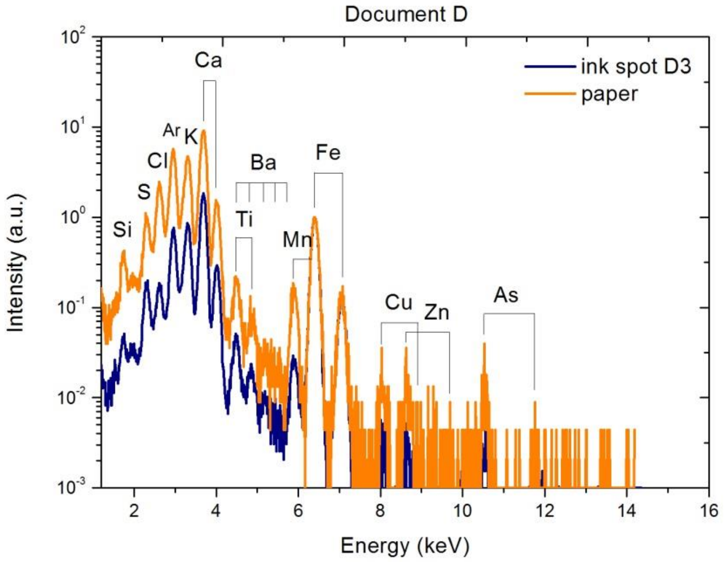

Figure 4. 24. X-ray energy spectra of inked and non-inked areas in document D.

Copper and zinc, despite sulphur and iron, were identified in the analyzed ink spots of this document (Appendix B). The ratios Cu/Fe, Zn/Fe, S/Fe and As/Fe for these ink spots and non-inked area are shown in figure 4.25a.

Despite the variation of S/Fe ratio, the other elements do not show significant differences between them. But, if the S/Fe ratios for ink spots are considered, this document appears to have two different inks. Ink spots D1 and D4 have almost the same S/Fe ratio (ink 1) while ink spot D3 can be a different ink (ink 2). Elemental maps of in spot D3 for S, Fe and Ca are shown in figure 4.25b. In all three maps it is visible the shape of the letter being the Fe map the one showing a more intense signal. This observation is in accordance with the ratios obtained for this spot (figure 4.25a) that reveal that this inks has much higher quantity of Fe than the other ink spots analyzed.

The low As/Fe ratios for all ink spots corroborate the affirmation of this ingredient being part of paper composition.

Another interesting result in the elemental analysis of this document is the case of ink spot D2. As it can be seen in the photograph of the document (see Appendix B) this is an ink stain derived from ink corrosion. In Chapter 2 it was explained the process of iron gall ink corrosion and its influence in paper degradation. Briefly the excess of iron sulphate used in the ink manufacturing allied with the external humidity conditions will cause the conversion of the sulphate ions into sulphuric acid. The S/Fe ratio for ink spot D2 (~5, see the scale on the right side of fig. 4.25a) corroborate this phenomena since the quantity of sulphur in the stain is five times higher than the quantity of iron. Thus, it is not possible to determine if the ink in D2 is of the type of ink 1 or ink 2.

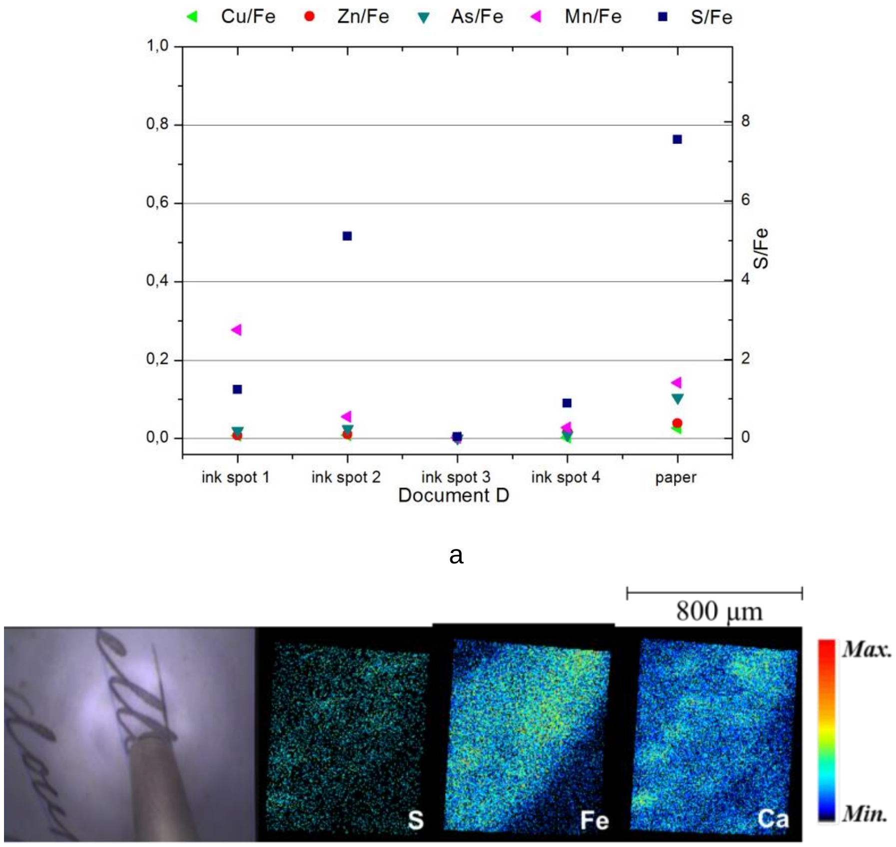

a

b

Figure 4. 25. Ratios of some elements present in the ink spots analyzed in Document D (Cu/Fe, Zn/Fe As/Fe and S/Fe ratios) (a). Elemental maps of ink spot D3 from the main text of Document D (800x800 μm^2) (b); a view from the micro-camera installed in the set-up is also showed.

Figure 4.26 shows photographs under IR and UV illumination of part of the document. UV illumination in ink spot D2 reveals signs of a stain in paper and foxing phenomena in paper. It is clear through IR radiation the difference between the words corresponding to ink 1 and the words from the main text (ink 2) of the document that looks almost transparent.

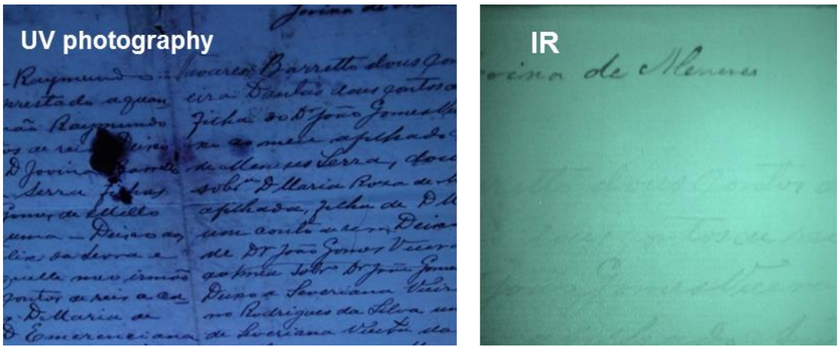

Figure 4. 26. Detail of the IR and UV photography of Document D.

The last document analyzed through PIXE technique is a certificate (document E) dated from 1928 and it consists in one folio written in one side. Figure 4.27 shows the X-ray energy spectra of an inked area (ink spot E3) of the document and bare paper.

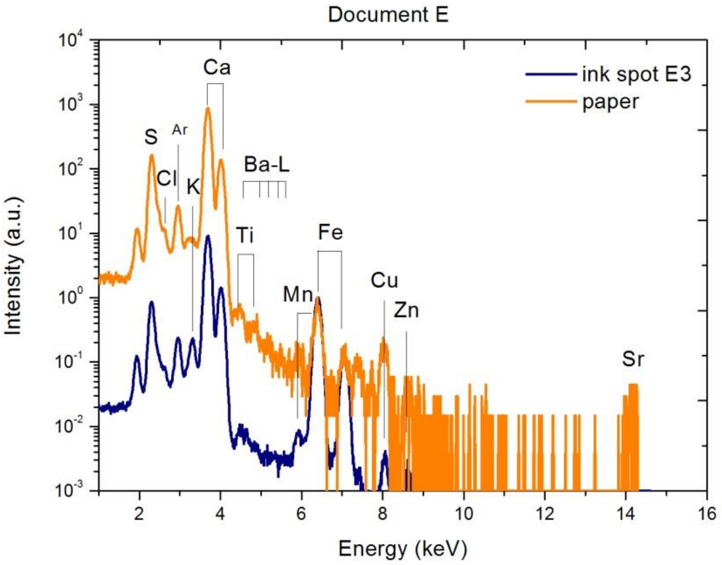

Figure 4. 27. X-ray energy spectra of inked and non-inked areas of document.

Contrary to the other analyzed documents, silicon was not identified neither in inked and non-inked areas. Silicon appears as a constituent of various compounds related to coating sizing in paper manufacturing [60]. The nonexistence of silicon in this document might be an indication that the paper suffered a total different manufacturing process. As in document B, barium was identified in bare paper. Despite iron and sulphur, it were identified copper and zinc and in inked areas. The strontium identified in paper may also be considered a contaminant of paper support [64].

Graphic from figure 4.28a shows the ratios to iron of metallic elements identified in this document E. The Cu/Fe, Zn/Fe and Mn/Fe ratios are almost zero for all ink spots and so it can be considered a contaminant of the iron sulphate [6]. The Sr/Fe ratio (see scale on the right side of the graphic) is also very low which proves the identification of this element as belonging to paper. S/Fe ratio of ink spots is really high in this document (figure 4.28a) as well as the S/Fe ratio for bare paper.

The paper of this document has a huge amount of sulphur that could be one of the reasons why this document presents a considerable level of ink corrosion. UV photography (figure 4.28b) shows signs of ink spreading in paper, a phenomena recurrent in ink corrosion processes. In the UV photograph of the back page of the document it can be seen the text correspondent to the front page that may also be also a sign of corrosion.

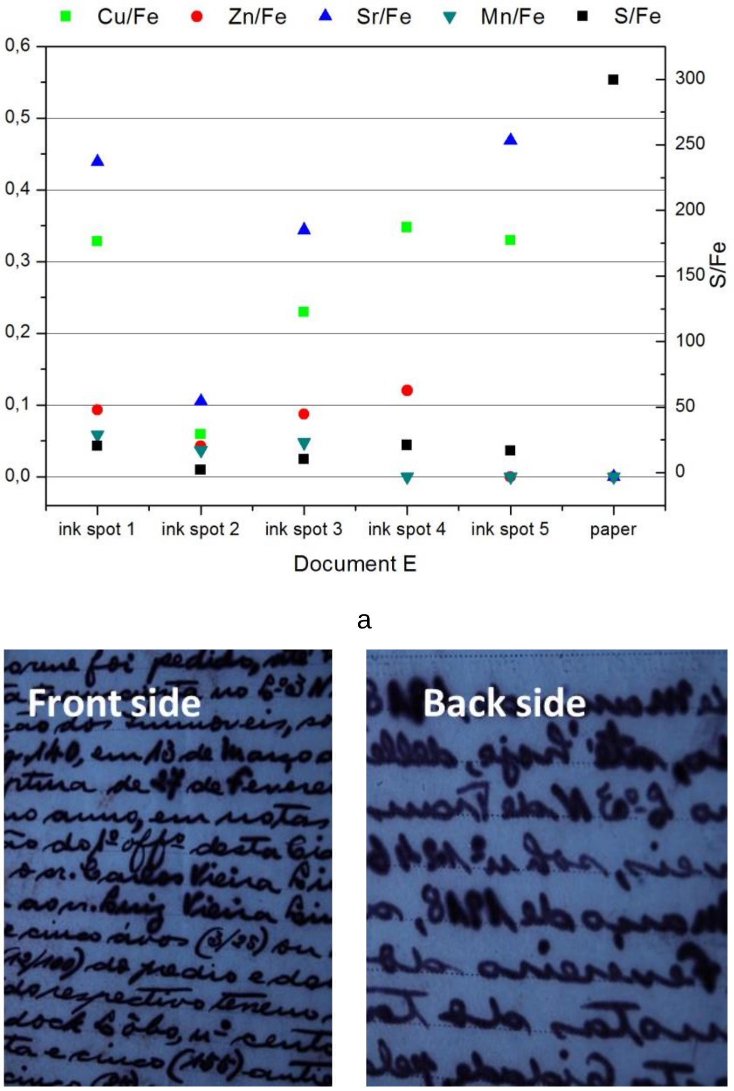

a

b

Figure 4. 28. Cu/Fe, Zn/Fe, Sr/Fe, Mn/ Fe and S/Fe ratios obtained (a). Detail of UV photography of the front page and back page (b) of the document.

In summary, PIXE technique provided the identification of elements in iron gall inks and paper in the five documents. Concerning to the iron gall inks, they were found consistencies with the “new” inks analyzed in the subchapter 4.1.2. In fact, the inks analyzed in the documents have proved to be iron gall inks since it was recognized iron and sulphur in their elemental composition. On the other hand, contrary to the inks produced in the laboratory using commercial iron sulphate, the inks in the documents possess contaminants, such as zinc and strontium probably due to the vitriol used. Copper was identified in documents’ inks but it was not possible to determine its provenience, i.e. if it is a contaminant of the iron sulphate or the Arabic gum, or it was intentionally added.

Elemental composition of paper varies from document to document. Papers from documents B, D and E have barium (found in compounds used for industrial paper manufacturing) which was not identified in documents A and C neither in actual paper. It seems that from the elemental composition, information about the different manufacturing process of paper can be extracted.

For the study of compound composition of paper and iron gall inks, these documents were characterized by XRD technique. Only document C was not studied by XRD because the document was not available. The X-ray diffractograms of document A and B were acquired in D8 Discover while documents D and E were analyzed using the HotBird due to their large dimensions.

Figures 4.29, 4.30, 4.31 and 4.32 show the X-ray diffractograms of inked and non-inked areas for documents A, B, D and E, respectively, and in Table 4.6 a summary of the identified compounds in the four documents analyzed can be found.

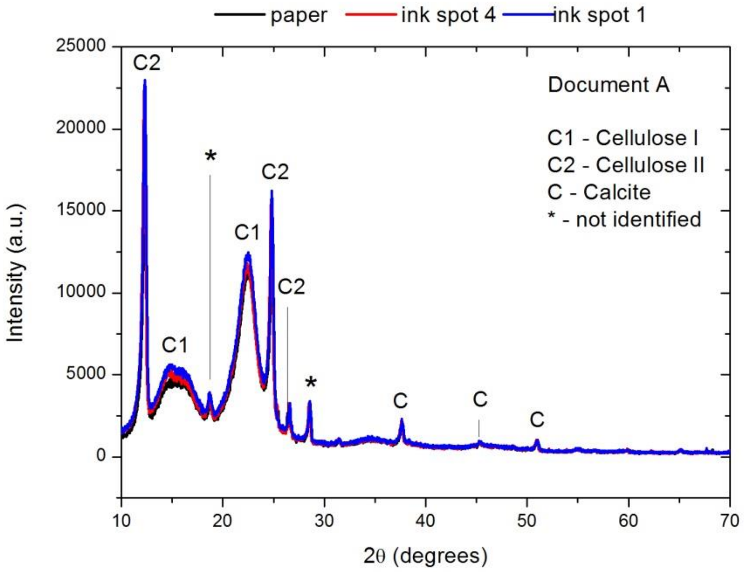

Figure 4. 29. X-ray diffractogram of ink spots and paper of Document A.

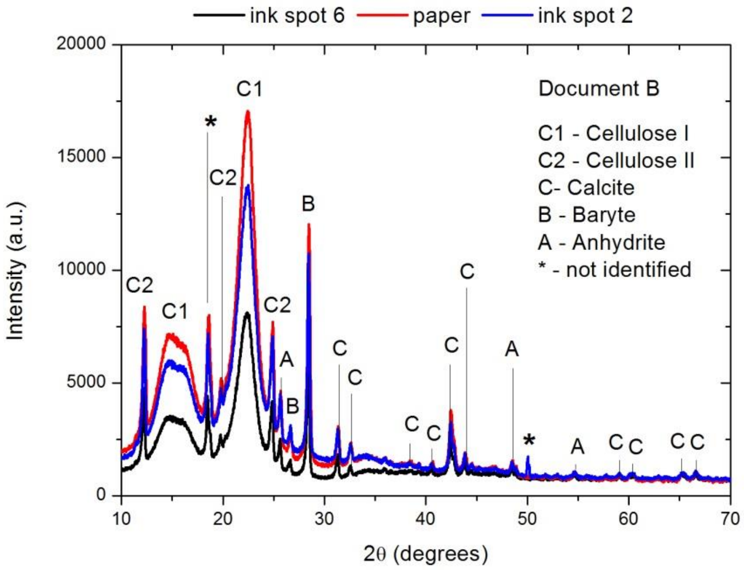

Figure 4. 30. X-ray diffractogram of ink spots and paper of Document B.

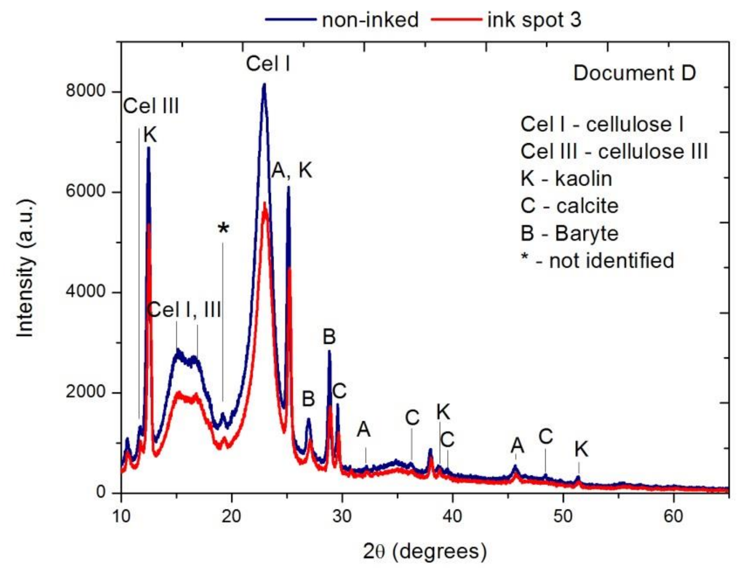

Figure 4. 31. X-ray diffractogram of ink spots and paper of Document D.

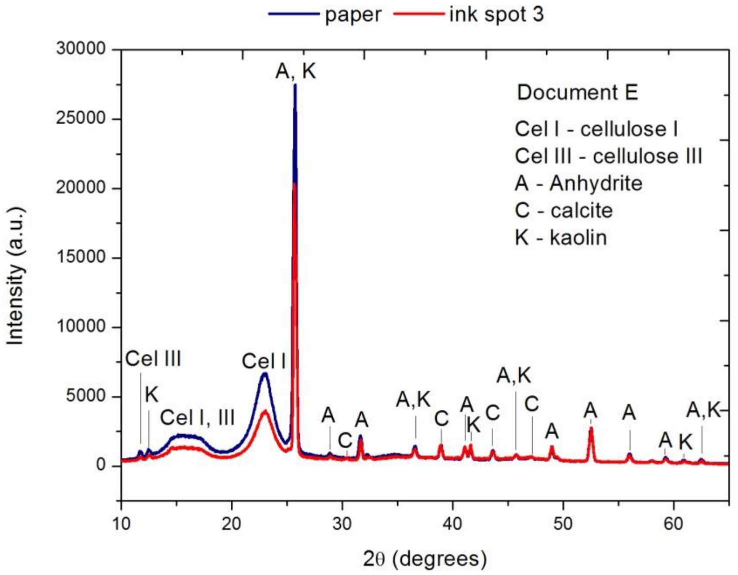

Figure 4. 32. X-ray diffractogram of ink spots and paper of Document E.

Table 4. 6. Summary of the identified compounds in the four documents analyzed.

	Cellulose I	Cellulose II	Cellulose III	Kaolin	Calcite	Anhydrite	Baryte
Document A	•	•			•		
Document B	•	•			•	•	•
Document D	•		•	•	•	•	•
Document E	•		•	•	•	•	

In all documents, cellulose I was identified while cellulose II was identified only in documents A and B and cellulose III was found in documents D and E. As previously explained, cellulose I is the common variety found in nature, cellulose II is the variety found in chemically regenerated celluloses, and cellulose III is produced when chemical treatments are used.

In general, XRD analysis was effective for the identification of compounds belonging to paper. Through PIXE analysis we have identified calcium as one of the main elements in paper elemental composition and by XRD it was possible to link calcium with calcite ($CaCO_3$) or anhydrite ($CaSO_4$), depending on the paper. Other paper compounds were found in the documents. In documents B and D there were identified peaks corresponding to barite ($BaSO_4$). In document E, it were not found any peaks corresponding to this compound even knowing that barium is present in the paper elemental composition of this document.

Another two compounds used in the paper manufacturing that were identified in documents D and E are kaolin ($Al_2Si_2O_5(OH)_4$), used as a filler in paper production, and anhydrite ($CaSO_4$), a sulphate mineral that is transformed in gypsum by the absorption of water [57]. Some peaks were not identified, (marked with * in the figures), and more efforts and literature review should be done in a near future. An extended investigation of compounds composed by Fe, S and O (iron sulphur compounds) was made without any concrete results. The supposition of another inorganic constituent of paper was also considered but no matches were found, however this hypothesis should not be discard.

As in the case of iron gall ink recipes, the Crystallinity Index, CrI, for each document was also calculated in the inked areas and bare paper. In table 4.7 are the CrI values calculated considering the peaks from cellulose I. In all documents it can be concluded that the values for the Crystallinity Index for the samples of paper written with iron gall inks are lower than for bare paper. This fact again may endorse the involvement of the ink in degradation and aging processes of the paper. However, the Crystallinity Index are considerable high, above 80% for documents D and E even for ink+paper. When comparing the values for bare papers with the ones obtained in actual papers (table 4.3), we can assure that we are dealing with old but high quality papers which inherit the high quality of the raw materials used, if we consider the aging and corrosion processes of the documents, for instance the presence of foxing stains.

Table 4. 7. Cristallinity Index (*CrI*) for the documents analyzed on inked and non-inked regions, considering the peaks from cellulose I.

	CrI (%)	
Paper sample	*ink+paper*	*paper*
Document A	77,72	80,33
Document B	76,67	80,33
Document D	84,71	89,45
Document E	84,49	90,60

To study the chemical composition, FTIR analyses were performed in all the documents. Measures were done for all ink spots analyzed by PIXE and bare areas . Figures 4.33 and 4.34 shows the transmittance spectra for non-inked and inked areas, respectively. The spectra are quite similar and we will see that peaks correspondent to paper composition are the ones identified. The lack of information about the ink may results from the low quantity of this material or from overlap of peaks with higher expression correspondent to paper compound.

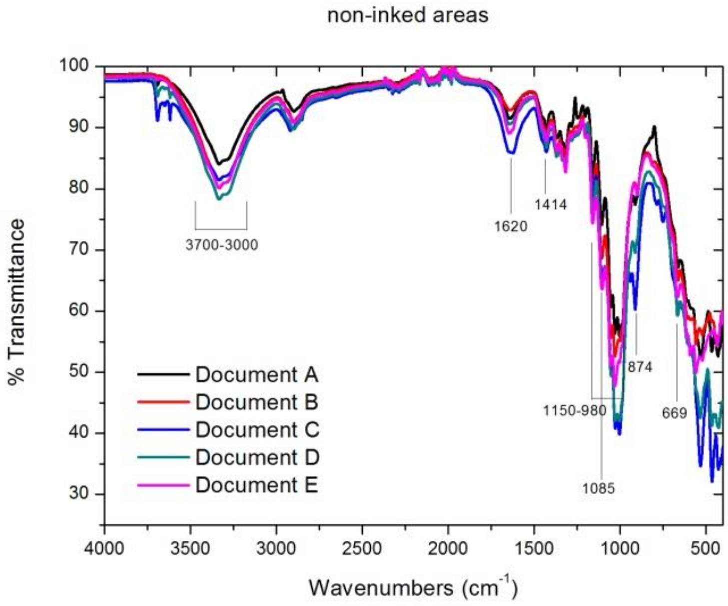

Figure 4. 33. FTIR spectra of non-inked areas in the five documents.

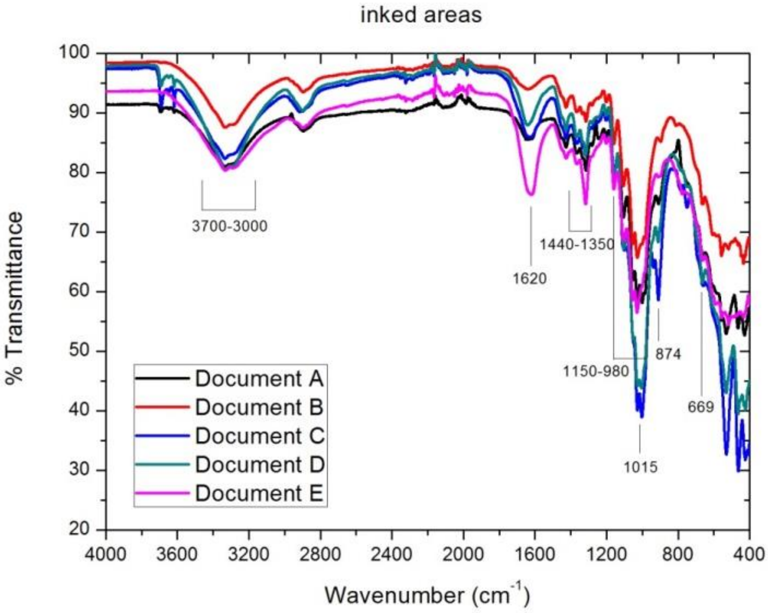

Figure 4. 34. FTIR spectra of inked areas in the five documents.

The analysis of the spectra was done having into account the information obtained from literature (Table 3.1.), although some peaks were not possible to identify due to lack of database information and more literature review is needed. In both figures, the C-OH and C-O-C groups from cellulose exhibit transmittance bands at 3450 cm^{-1} and in the 1150-980 cm^{-1} due to the O-H stretching of intermolecular hydrogen bonded hydroxyl groups and C-O-C stretch, respectively.

The broad 3700-3000 cm^{-1} region and peak 1620 cm^{-1} may represent the stretching vibrations of the H_2O molecules associated to gypsum (remember that anhydrite ($CaSO_4$) is a sulphate mineral that commonly occurs as gypsum by the absorption of water). However, gypsum was not found through XRD analysis, only anhydrite was detected. Having these results into account, the attribution of those peaks to gypsum in the FTIR spectra may be precipitated and we can only assume that these peaks correspond to compounds present in paper. Apart from that, peak 669 cm^{-1} is also characteristic of paper since through comparison of the graphics we see that its expression is higher for non-inked areas. Calcite was identified through XRD in the documents. In the FTIR spectra the peaks at around 1414 cm^{-1} and 1085 cm^{-1} and 874 cm^{-1} are representative of this compound.

Considering only the spectra for inked areas, the chemical bond $S(=O)_2$ exhibit transmittance band at the region between 1440-1350 cm^{-1}. This chemical bond is related to compounds containing sulphur and since this broad band only appears in the inked areas spectra it should be related to iron gall inks composition. The higher absorption value for peak at 1620 cm^{-1} for Document E might be an overlap of the peak correspondent to the vibrations of the H_2O molecules of gypsum, if considered, together with some other compound belonging to ink composition. Some peaks, mainly in the low wavenumber region of the spectra could not be identified.

Chapter 5

The study of elemental and organic compounds composition of iron gall inks by means of nondestructive techniques was well succeeded. Two IBA techniques, PIXE and RBS, were used to identify elemental composition of inks and paper while XRD and FTIR techniques provided the identification of the compounds existent in the samples. IR and UV photography was used to get better perception of corrosion and degradation processes in paper and ink.

PIXE technique using an external proton beam was performed in manuscripts for the first time in Portugal, using the set-up installed at Campus Tecnológico e Nuclear, IST. The optimal experimental conditions are a beam current of 300 pA and an acquisition time of about 15-20 minutes, to assure the pristine conditions of the documents after the measurements.

New inks following six different recipes were produced using contemporary ingredients. Both, ingredients and manufactured inks, were characterized in the scope of this work. XRD analysis allowed the identification of gallic acid and glucose in the three types of tannin sources used and different hydrate iron sulphur compounds (copiapite, rozenite and melanterite) in the vitriol. FTIR analysis allowed the identification of peaks associated to gallic acid in the tannin source and melanterite in the vitriol source.

Regarding the inks which were deposited on paper support, XRD analysis provided the identification of celluloses I and II and calcite as constituents of paper. Ink composition was not possible to identify through XRD technique due to the low quantity of ink. Nevertheless, the results obtained through FTIR for one of the manufactured inks revealed some peaks that can be associated to compounds containing sulphur. By RBS analysis, the penetration depth of the inks was calculated, values in the order of nanometers were found. The influence of the inks in the cellulose fibers of the papers was estimated considering their crystallinity index. In general, it was observed lower values for the inked areas which can be related to corrosion processes.

The characterization of the five documents from the beginning of the XX century, end of the XIX century, by means of their elemental and chemical composition was accomplished. By PIXE it was possible to distinguish between different papers and manufacturing processes, because of the identification of key elements, such as barium, arsenic and strontium. Also, PIXE can differentiate among different inks, even in the same document. Elemental X-ray mapping proved to be helpful in the understanding of the distribution of elements' concentration in the inked regions. By means of UV and IR photography, it was also possible to detect different inks by their signals, as well as to identify stains and ink spreads in paper, related to ink corrosion processes.

The papers from the documents come from good quality materials since their crystallinity index are higher than 80%. By XRD analysis it was possible to identify three types of celluloses: cellulose I, II and III. Calcite, barite, anhydrite and kaolin were also identified. Unfortunately, it was not possible to identify any compound related with the presence of iron gall inks by XRD even when the measurements were done in the inked regions using grazing angles. With FTIR it was not possible to identify other elements than those already identified through XRD in the papers but this technique helped to corroborate the previous results.

The results obtained during this thesis work may be considered a lever for subsequent studies related to the analyses of valuable documents. First, the settlement of the best experimental conditions to use in the external microprobe at CTN/IST is an important acquisition for further studies of documents in an noninvasive way. The other setups used in the laboratory are also able to be used in the study of this kind of artifacts.

This experimental work brought some unsolved questions that can be answered with more studies. In the case of iron gall inks' analysis it may be important to make more studies with different inks from different epochs and regions in order to get a perception of the contaminants that may appear in the inks. A more rigorous study of the crystallinity index may also be made.

References

[1] http://irongallink.org/igi_index8a92.html (March, 2014).

[2] J. C. Dran , J. Salomon, T. Calligaro, P. Walter, Ion beam analysis of art works: 14 years of the use in the Louvre, Nuclear Instruments and Methods in Physics Research B 219–220, 2004,pp 7–15.

[3] F. Lucarrelli and P. A. Mandó in: G Demortier, A. Adriaens, Ion beam study of art and archaeological objects, CGNA19218ENC,2000.

[4] T.A. Cahill, R.N. Schwab, B.H. Kusko, R.A. Eldred, G. Möller, D. Dutschke, D.L. Wick, A.S. Pooley, The Vinland Map, Revisited: New Compositional Evidence on Its Inks and Parchment, Analytical Chemistry, 59, 1987, pp. 829-833.

[5] B.H. Kusko, T.A. Cahill, R.A. Eldred, R.N. Schwab, Proton Milliprobe Analysis of the Gutenberg Bible, Nuclear Instruments and Methods in Physics Research B, 3, 1984, pp. 689-694.

[6] F. Lucarelli, P.A. Mandò, Recent applications to the study of ancient inks with the Florence external-PIXE facility, Nucl. Instr. And Meth. In Phy. Res. B 109/110, 1996, pp. 644-652.

[7] R. Viegas, V. Corregidor, M. T. Peña, E. Alves, L. C. Alves, Preliminary studies on iron gall inks composition using an external ion beam, International Journal of Conservation Science, 4 (Special Issue), 2013, pp. 593-602.

[8] M. Schreiner, M. Grasserbauer, Microanalysis of Art Objects: Objective, Methods and Results, Fresenius Z Anal Chem, 322, 1985, pp. 181-193.

[9] S. Sequeira, Workshop Conservação de Documentos com Tinta Ferrogálica – da Teoria à Práctica, 2013.

[10] R. M. Ion, M. L. Ion, V. I. R. Niculescu, I. Dumitriu, R. C. Fierascu, G. Florea, C. Bercu, S. Serban, Spectral Analysis of Original and Restaurated Ancient Paper from Romanian Gospel, Rom. Journ. Phys. 53, 2008, pp. 781-791.

[11] M. Manso, M. L. Carvalho, Application of spectroscopic techniques for the study of paper documents: A survey, Spectrochimica Acta Part B 64, 2009, pp.482-490.

[12] C. A. Mitchell, T. C. Hepworth, Inks Their Composition and Manufacture, Charles Griffin & Company, LTD., 1904, p. 92.

[13] http://www.alvissaras.50webs.com/eanes.html (March, 2014).

[14] K. Janssens, R Van Grieken, Non-destructive Micro Analysis of Cultural Heritage Materials, Elsevier, 2004.

[15] S. A. E. Johansson, Proton Induced X-ray Emission (PIXE) spectrometry – state of art, Fresenius Z Anal Chem, 324, 1986, pp. 635-641.

[16] T.A. Cahill, R.N. Schwab, B.H. Kusko, R.A. Eldred, G. Möller, D. Dutschke, D.L. Wick, A.S. Pooley, The Vinland Map, Revisited: New Compositional Evidence on Its Inks and Parchment, Analytical Chemistry, 59, 1987, pp. 829-833.

[17] B. Kusko, R. Schwab, Historical Analysis by Pixe, Nuc. Inst. And Meth. In Phys. Res. B22, 1987, pp. 401-406.

[18] C. Remazeilles, V. Quillet, T. Calligaro, J. C. Dran, L. Pichon, J. Salomon, PIXE elemental mapping on original manuscripts with an external microbeam. Application to manuscripts damaged by iron-gall ink corrosion, Nuc. Inst. And Meth. In Phys. Res. B 181, 2001, pp. 681-687.

[19] G. Verhoeven, Imaging the invisible using modified digital still cameras for straightforward and low-cost archaeological near-infrared photography, Journal of Archaeological Science 35, 2008, pp. 3087-3100.

[20] I. Montani, E. Sapin, A. Pahud, P. Margot, Enhancement of writings on a damaged medieval manuscript using ultraviolet imaging, Journal of Cultural Heritage 13, 2012, pp. 226-228.

[21] P. Ballirano, G. Caracciolo, C. Sadun, R. Caminiti, The use of energy dispersive X-ray diffraction (EDXD) for the investigation of the structural and compositional features of old and modern papers, Microchemical Journal 88, 2008, pp. 107-112.

[22] C. Burgaud, V. Rouchon, P. Refait, A. Wattiaux, Mössbauer spectrometry applied to the study of laboratory samples made of iron gall ink, Appl. Phys. A 92, 2008, pp. 257-262.

[23] J. J. Workman, Infrared and Raman spectroscopy in paper and pulp analysis, Appl. Spectrosc. Rev. 36, 2001, pp. 139-169.

[24] G. Bitossi, R. Giorgi, M. Mauro, B. Salvadori, L. Dei, Spectroscopic techniques in cultural heritage conservation: A survey, Appl. Spectrosc. Rev. 40, 2005, pp.187-228.

[25] A. Gorassini, P. Calvini, A. Baldin, Fourier Transformed Infrared Spectroscopy (FTIR) Analysis of Historic Paper Documents as a Preliminary Step for Chemometrical Analysis, CMA4CH 2008, Mediterraneum Meeting.

[26] A. Gambaro, R. Ganzerla, M. Fantin, E. Cappelletto, R. Piazza, W.R.L. Cairns, Study of 19th century inks from archives in the Palazzo Ducale (Venice, Italy) using various analytical techniques, Microchemical Journal 91, 2009, pp. 202-208.

[27] L. Moura, M. J. Melo, C. Casanova, A. Claro, A study on Portuguese manuscript illumination: The Charter of Vila Flor (Flower town), 1512, Journal of Cultural Heritage 8, 2007, pp. 299-306.

[28] M. Manso, A. Le Gac, S. Longelin, S. Pessanha, J. C. Frade, M. Guerra, A. J. Candeias, M. L. Carvalho, Spectroscopic characterization of a masterpiece: The Manueline foral charter of Sintra, Spect. Acta Part A: Molecular and Biomolecular Spectroscopy 105, 2013, pp. 288-296.

[29] M. B. H. Breese D. N. Jamieson, P. J.C. King., Materials Analysis Using a Nuclear Microprobe, John Wiley & Sons Inc., (1996), p. 141.

[30] S. Johansson, J. Campbell, PIXE: A Novel Technique for Elemental Analysis, John Wiley & Sons Inc., (1988), p. 13.

[31] The GUPIXWIN manual and user-guide, version 2.1, p.17.

[32] T. Calligaro, J.C. Dran, J. Salomon, P. Walter, Review of accelerator gadgets for art and archaeology, Nuclear Instruments and Methods in Physics Research B, 226, 2004, pp. 29-37.

[33] V. Corregidor, L.C. Alves, P.A. Rodrigues, M. Vilarigues, R.C. Silva, The External Ion Beam Facility in Portugal for Studying Cultural Heritage, e-Conservation Magazine, 22, 2011, pp. 40-52.

[34] G.W. Grime, M. Dawson, Recent developments in data-acquisition and processing on the Oxford scanning proton microprobe, Nucl. Instrum. Methods B 104, 1995, p. 107.

[35] J.A. Maxwell, W.J. Teesdale, J.L. Campbell, The Guelph PIXE software package II, Nuclear Instruments and Methods in Physics Research, B, 95, 1995, p. 407.

[36] V. Corregidor, R. Viegas, T. Peña, e. Alves, L.C. Alves, Preliminary Studies on Inks composition using an External Ion Beam, http://www.itn.pt/projs/microfex/posters/INART2013_Inks.jpg (March, 2014).

[37] S. Rubin, T.O. Passell, E. Bailey, Analytical Chemistry 29 (1957), p.736.

[38] B. Schmidt, K. Wetzig, Ion Beams in materials processing and analysis, Springer (2012), p. 317.

[39] J. W. Mayer, E. Rimini, Ion Beam Handbook for Material Analysis, Academic Press Inc. (1977), p. 42.

[40] http://www.srim.org/SRIM/SRIMLEGL.htm (March, 2014)

[41] http://home.rzg.mpg.de/~mam/ (March, 2014)

[42]https://fys.kuleuven.be/iks/nvsf/experimental-facilities/X-ray-diffraction-2013-bruker-d8-discover (March, 2014)

[43] N. Franco, Desenvolvimento das Capacidades de Análise do Difractómetro Hotbird e a sua aplicação ao Estudo de Heterojunções de Si-Ge, IST, 2001.

[44] http://www.itn.pt/facilities/uk_hotbird.htm (March, 2014)

[45] J. Coates, Interpretation of Infrared Spectra, A Practical Approach, Encyclopedia of Analytical Chemistry, John Wiley & Sons Ltd.

[46] S. Duckett, B. Gilbert, Foundations of Spectroscopy, Oxford Science Publications, Oxford University Press.

[47] N. Rangelova, L. Radev, S. Nenkova, I. M. Miranda Salvado, M. H. Vas Fernandes, M. Herzog, Methylcellulose/SiO_2 hybrids: sol-gel preparation and characterization by XRD, FTIR and AFM, Cent. Eur. J. Chem. 9(1) (2011), pp. 112-118.

[48] Sadtler, The Infrared Spectra Atlas of monomers and polymers, Sadtler Research Laboratories, 1980.

[49] H. Böke, S. Akkurt, S. Özdemir, E. Hale Göktürk, E. N. Caner Saltik, Quantification of $CaCO_3$-$CaSO_3.0.5H_2O$-$CaSO_4.2H_2O$ mixtures by FTIR analysis and its ANN model, Materials Letters 58 (2004), pp. 723-726.

[50] M. Ursescu, T. Măluţan, S. Ciovică, Iron gall inks influence on papers' thermal degradation, European Journal of Science and Theology , 2009, Vol.5, No.3, pp. 71-84.

[51] http://www.thermoscientific.com/en/product/omnic-series-software.html (March, 2014)

[52] R. V. Shoute, H. Verougstraete-Marcq, Art History and Laboratory Scientific Examination of Easel Paintins, PACT 13, 1986.

[53]http://www.realscience.breckschool.org/upper/fruen/files/Enrichmentarticles/files/IronGallInk/IronGallInk.html, (April, 2014).

[54] K. C. S. Andrade; C. W. P. de Carvalho; C. Y. Takeiti; H. M. C. de Azeredo; J. da S. Corrêa; C. M. Caldas, Goma de cajueiro (Anacardium occidentale): Avaliação das modificações químicas e físicas por extrusão termoplástica, Polímeros vol.23 no.5 São Carlos, 2013.

[55] S. Caruso, Caratterizzatione ed invecchiamento di leganti pittorici a base di gomme vegetali, Tesi di Laurea, Universita' degli Studi di Torino, Torino, 2006.

[56] S. Anguera MC, STRUCTURE OF PAPER FIBERS IN ANCIENT MANUSCRIPTS - ACIDIC DECOMPOSITION AND DEACIDIFICATION, Restaurator 17, 1996, pp. 117-129.

[57] http://www.paperonweb.com/chemical.html (March, 2014)

[58] H. A. Foner, N. Adan, The characterization of Papers by X-Ray Diffraction (XRD): Measurement of Cellulose Crystallinity and Determination of Mineral Composition, Journal of the Forensic Science Society 23, 1983, pp. 313-321.

[59] L. Segal, C.M. Conrad, The characterization of cellulose derivatives by means of the X-ray diffractometer, American Dyestuff Reporter, 1957, pp. 637-642.

[60] L. Segal, J. J. Creely, A. E. Martin, Jr., C. M. Conrad, An empirical method for estimating the degree of crystallinity of native cellulose using the X-ray diffractometer, Textile Research Journal 29, 1959, pp. 786-794.

[61] N. Terinte, R. Ibbett, K. C. Schuster, Overview on native cellulose and microcrystalline cellulose I structure studied by X-ray diffraction,(WAXD): comparison between measurement techniques, Lenzinger Berichte 89, 2011, pp. 118-131.

[62] http://minerals.usgs.gov/minerals/pubs/commodity/titanium/ (March, 2014)

[63] R. Kresse, U. Baudis, P. Jäger, H.H. Riechers, H. Wagner, J. Winkler, H.U. Wolf, Barium and Barium Compounds, Ullmann's Encyclopedia of Industrial Chemistry, Wiley Blackwell (John Wiley & Sons), 2000, p. 629.

[64] W. Faubel, S. Staub, R. Simon, S. Heissler, R. Nüesch, A. Pataki, G. Banik, Non-destructive analysis for the investigation of decomeposition phenomena of historical manuscripts and prints, Spectrochimica ActaPart B 62, 2007, pp. 669-676.

Appendix A

Recipes

Recipe 1

Ingredients:

- 11,7 g of tannic acid
- 5 g of Arabic gum
- 15 g of iron (II) sulphate
- 500 ml of water

Recipe 2

Ingredients:

- 17,5 g of tannic acid
- 8,25 g of Arabic gum
- 36,75 g of iron (II) sulphate
- 250 ml of water

Recipe 3

(Recipes 3, 3oak and 3nuts follow this recipe with the only difference being the tannin source used)

Ingredients:

- 1 g of tannic acid (or oak galls or nut galls)
- 4 g of Arabic gum

- 24 g of iron (II) sulphate
- 200 ml of water

Recipe 4

Ingredients:

- 9 g of oak galls
- 9 g of Arabic gum
- 3 g of iron (II) sulphate
- 300 ml of water

Method of preparation

First, it is necessary to weigh the gall nuts and crush them (if you are dealing with commercial tannin, ignore this step).

Put the tannin powder in a glass container with water and heat, until the solution is boiling. It is important that you let the solution rest (in our recipes we wait few minutes for recipes 1,2 and 3 and an hour and a half for recipe 4) so it ferment.

Carefully, add the iron (II) sulphate and the Arabic gum to the mixture in the heated water and mix everything until you get an homogeneous solution.

Appendix B

Photographs of the documents

Document A

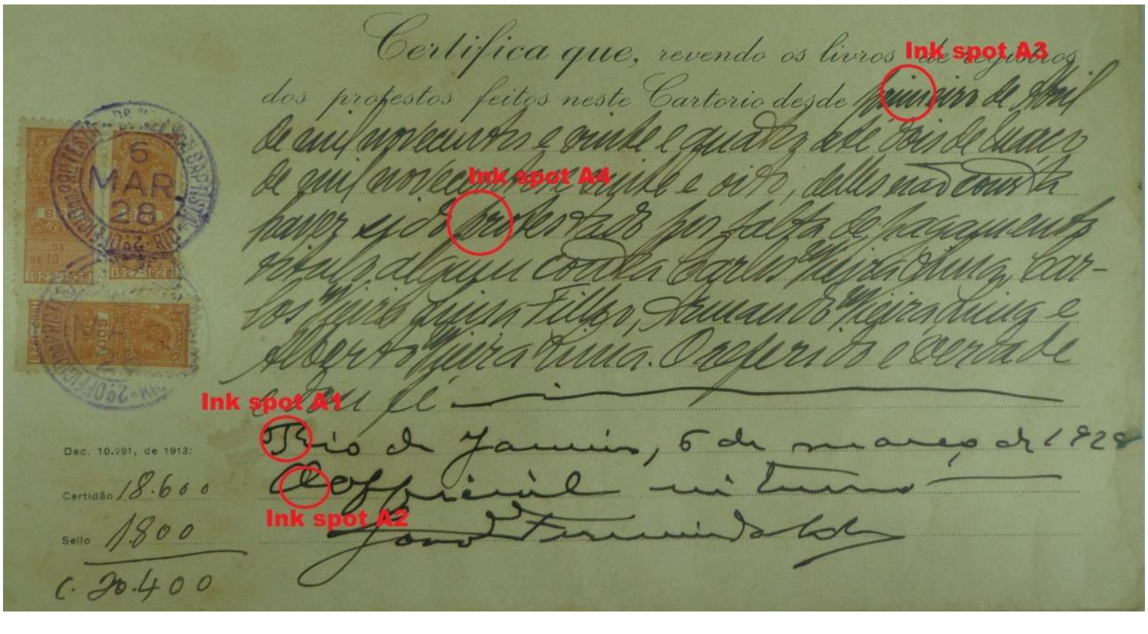

Certifica que, revendo os livros de registros dos protestos feitos neste Cartorio desde primeiro de Abril de mil novecentos e vinte e quatro até hoje dois de março de mil novecentos e vinte e oito, delles não consta haver sido protestado por falta de pagamento titulo algum contra Carlos Nogueira Lima, Carlos Nogueira Lima Filho, Armando Nogueira Lima e Alberto Nogueira Lima. O referido é verdade e dou fé.

Rio de Janeiro, 6 de março de 1928

O official interino

João Fernandes

6 MAR 28

Dec. 10.291, de 1913:

Certidão 18.600

Sello 1.800

C. 20.400

Document B

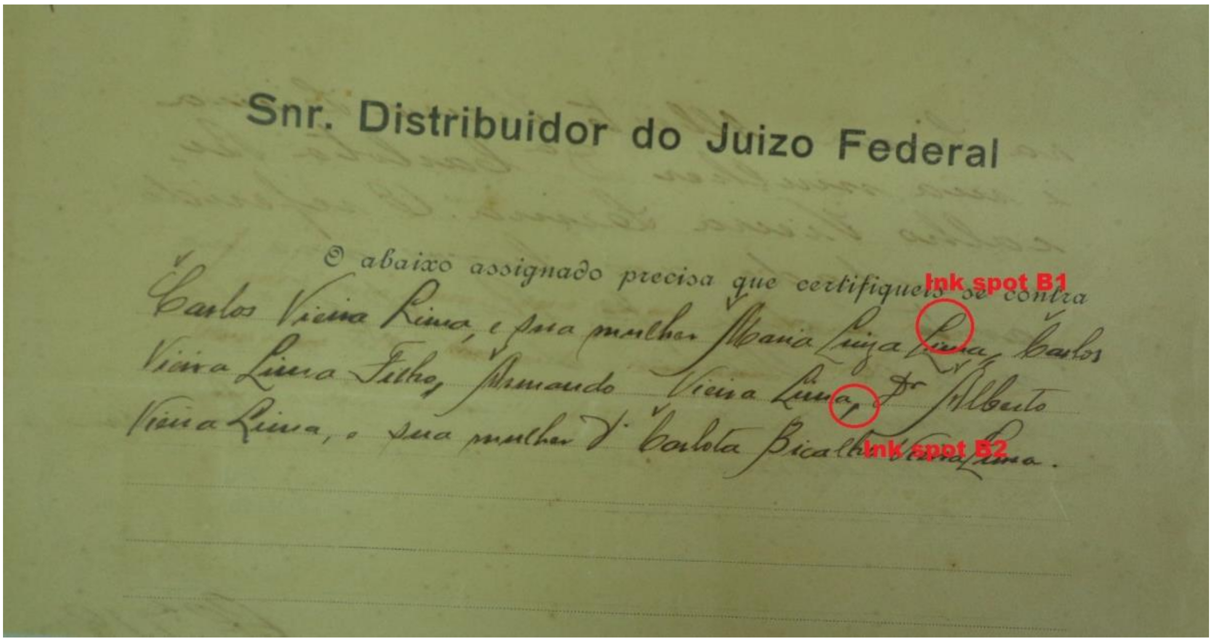

Snr. Distribuidor do Juizo Federal

O abaixo assignado precisa que certifiqueis se contra Carlos Vieira Lima, e sua mulher Maria Luiza Lima, Carlos Vieira Lima Filho, Armando Vieira Lima, Dr Alberto Vieira Lima, e sua mulher D. Carlota Bicalho Vieira Lima.

Front page

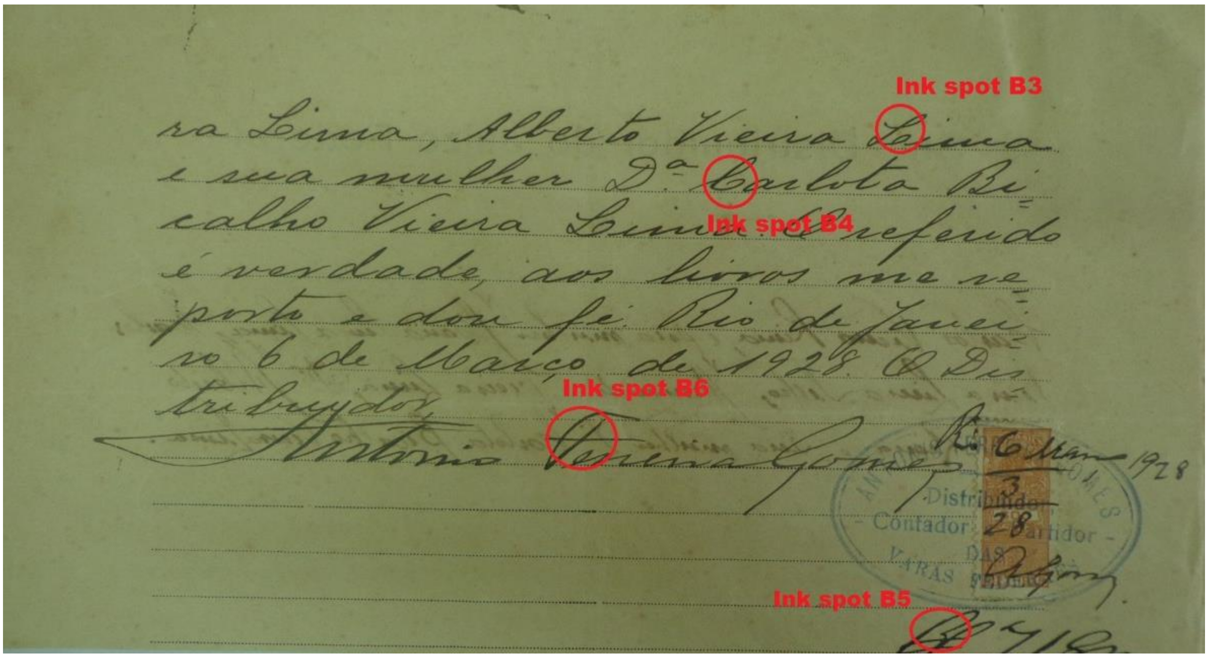

ra Lima, Alberto Vieira Lima e sua mulher Dª Carlota Bicalho Vieira Lima. O referido é verdade, aos livros me reporto e dou fé. Rio de Janeiro 6 de Março de 1928. O Distribuidor,

Antonio Ferreira Gomes

R. 6 Mar 1928

3/28

Distribuidor
Contador Partidor
DAS VARAS FEDERAES

Back page

Document C

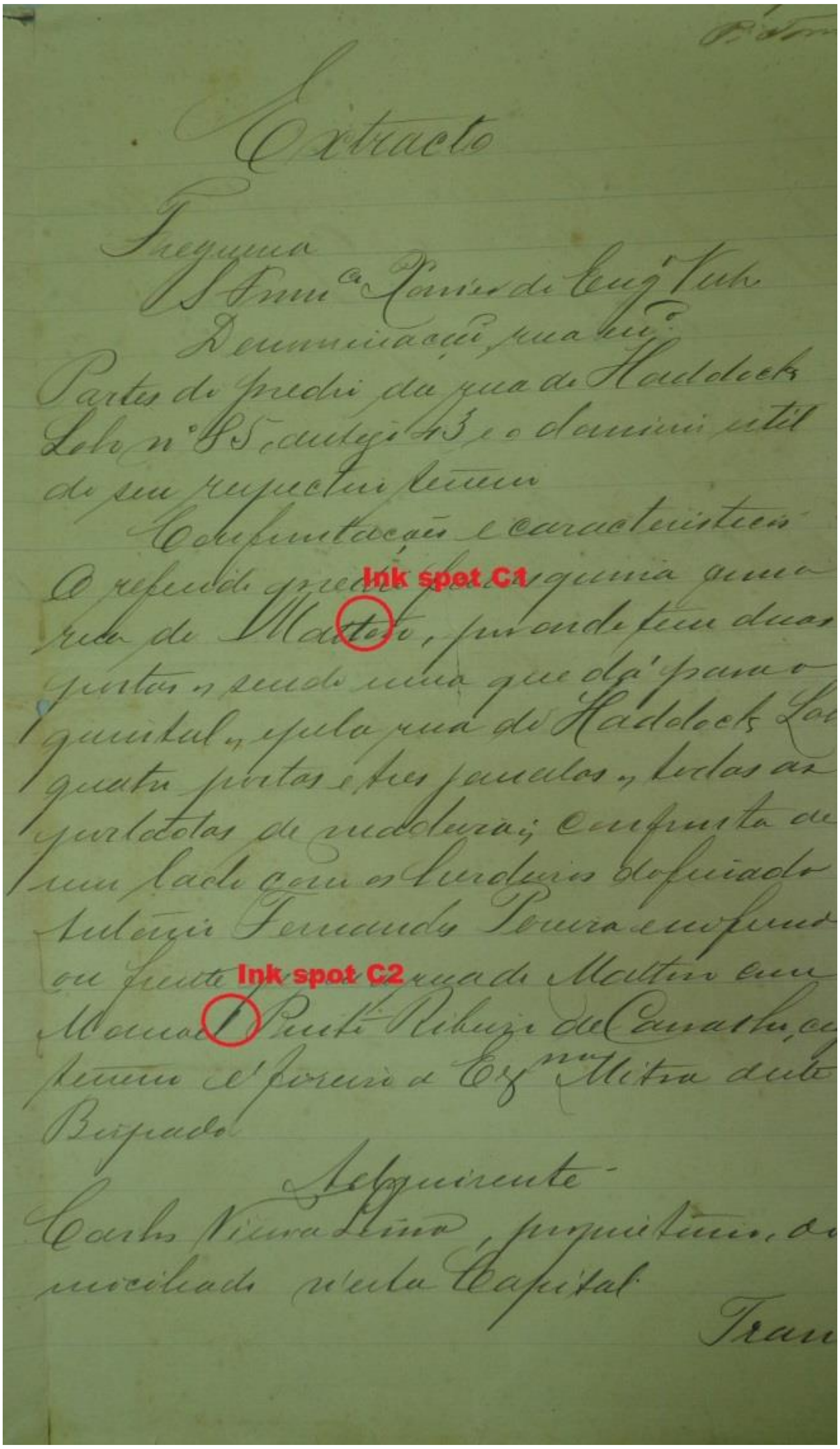
P. Tom

Extracto

Freguezia

S. Fran.co Xavier do Eng.o Velho

Denominação, rua e n.o

Partes do predio da rua de Haddock Lobo n.o 85, antigo 43, e o dominio util do seu respectivo terreno

Confrontação e caracteristicos

O referido predio faz esquina para a rua de Mattos, por onde tem duas portas, sendo uma que dá para o quintal, e pela rua de Haddock Lobo quatro portas e tres janellas, todas as guarnecidas de madeira; confronta de um lado com os herdeiros do finado Antonio Fernandes Pereira e no fundo ou frente para a rua de Mattos com Manoel Pinto Ribeiro de Carvalho, cujo terreno é foreiro á Exma Mitra deste Bispado

Adquirente

Carlos Vieira Lima, proprietario, domiciliado nesta Capital

Tran

Front page

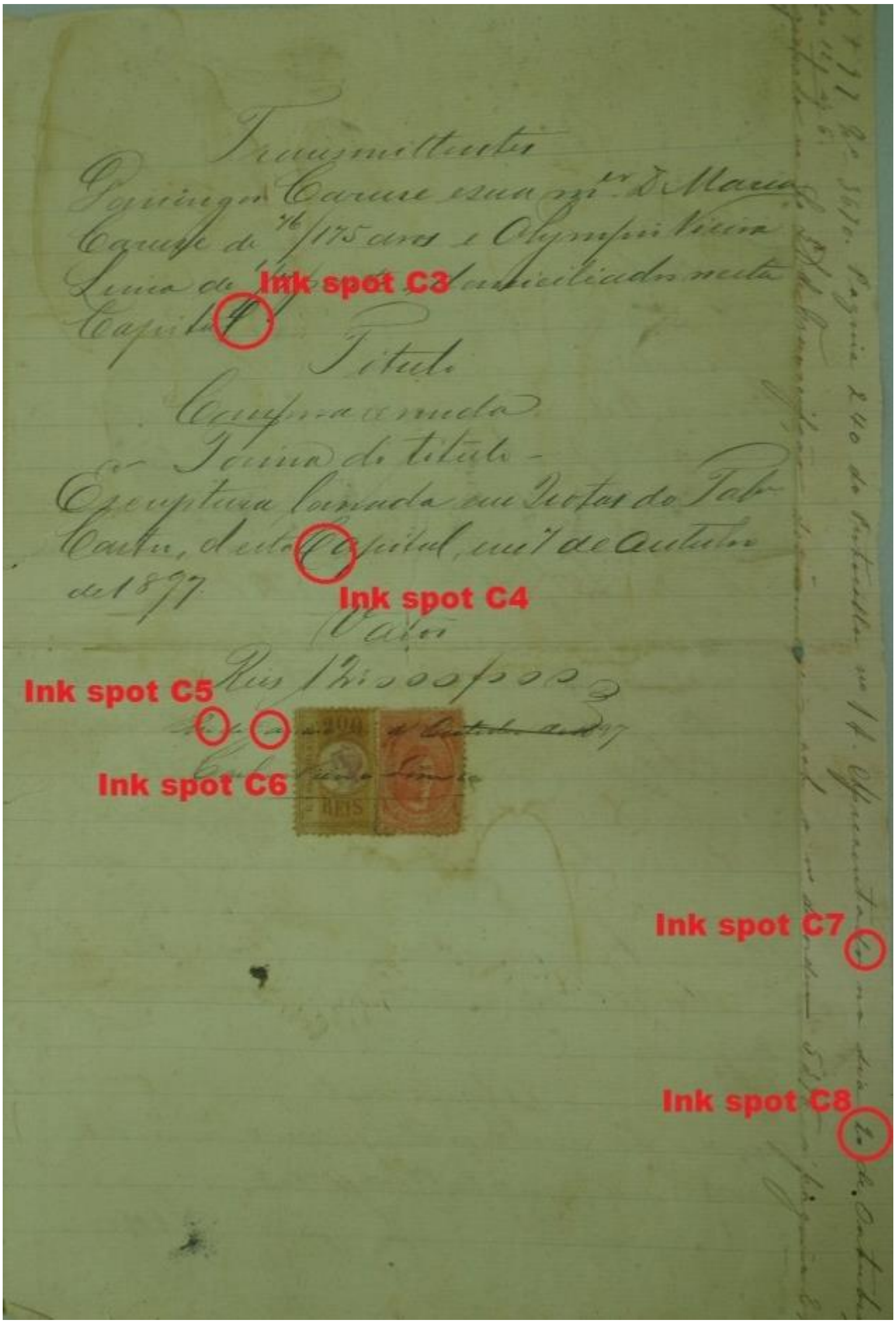

Transmittente
Domingos Carneiro e sua mulher D. Maria Carneiro de 76/175 avos e Olympio Vieira Lima de [illegible] domiciliados nesta Capital

Titulo
Compra e venda

Forma do titulo -
Escriptura lavrada em Notas do Tab. Castro, desta Capital, em 7 de Outubro de 1877

Valor
Reis 12:000$000

Back page

Document D

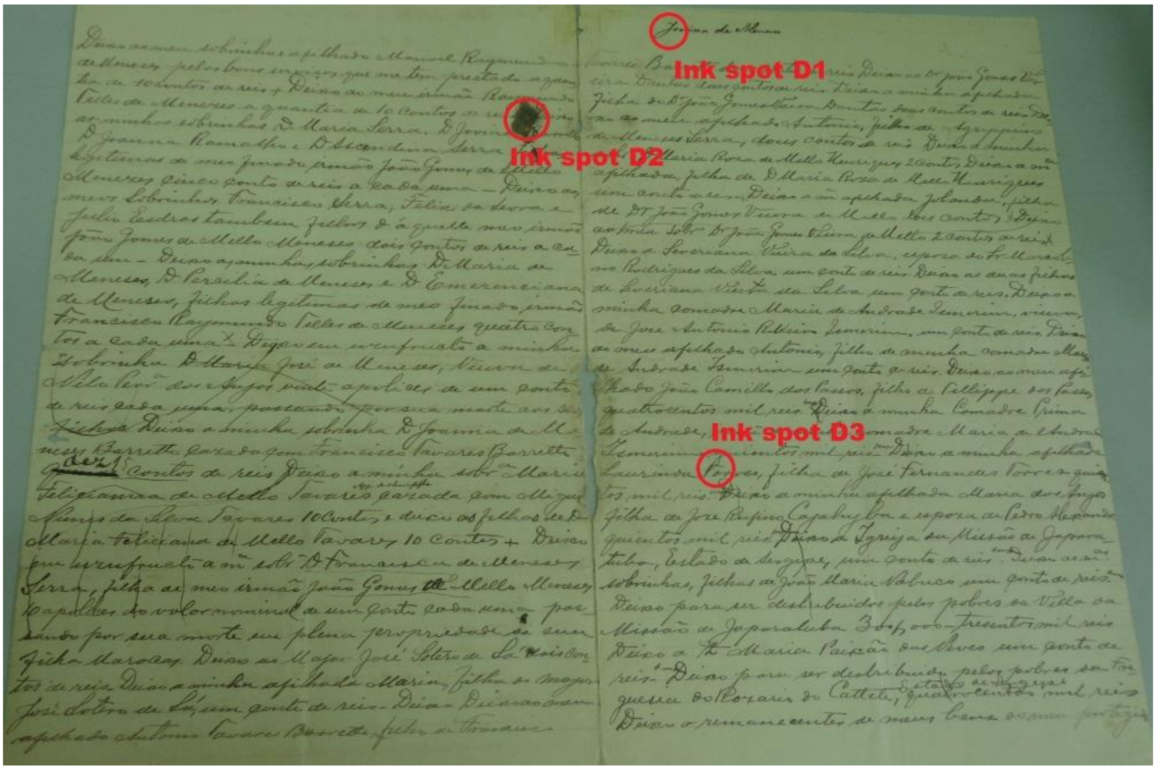

Front page

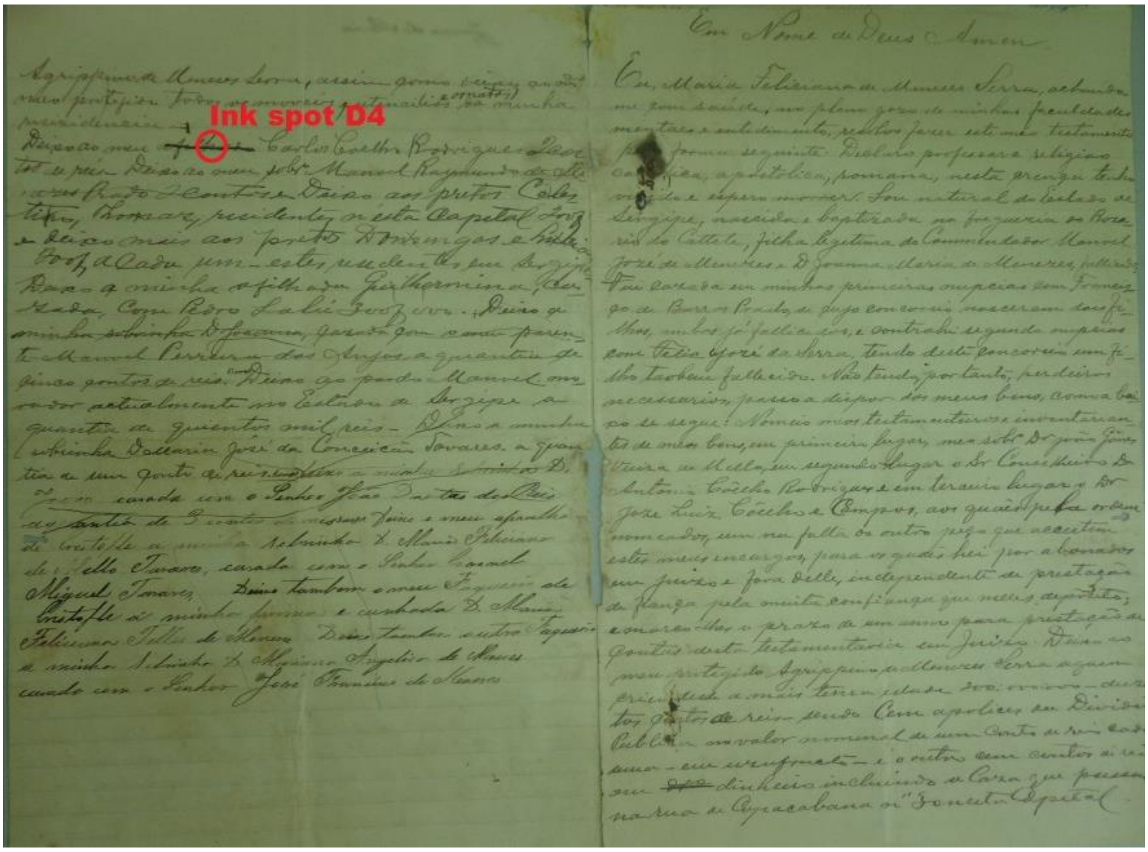

Back page

Document E

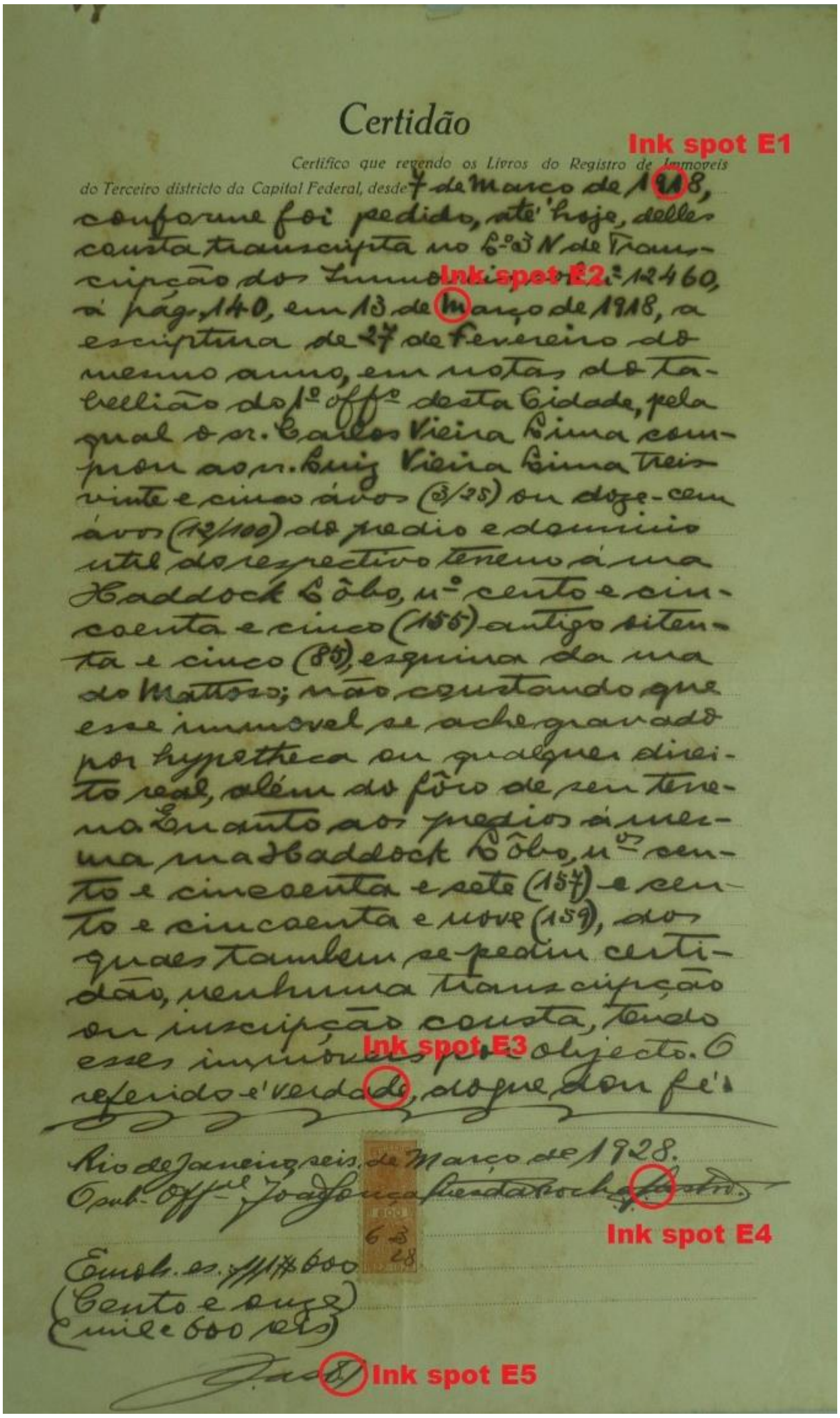

Certidão

Certifico que revendo os Livros do Registro de Immoveis do Terceiro districto da Capital Federal, desde 7 de Março de 1918, conforme foi pedido, até hoje, delles consta transcripta no L.º 3 N de Transcripção dos Immo[illegible].º 12460, á pág. 140, em 13 de Março de 1918, a escriptura de 27 de Fevereiro do mesmo anno, em notas do tabellião do 1º offº desta Cidade, pela qual o sr. Carlos Vieira Lima comprou ao sr. Luiz Vieira Lima treis vinte e cinco ávos (3/25) ou doze-cem ávos (12/100) do predio e dominio util do respectivo terreno á rua Haddock Lôbo, n.º cento e cincoenta e cinco (155) antigo sitenta e cinco (85), esquina da rua do Mattoso; não constando que esse immovel se ache gravado por hypotheca ou qualquer direito real, além do fôro de seu terreno. Quanto aos predios á mesma rua Haddock Lôbo, n.os cento e cincoenta e sete (157) e cento e cincoenta e nove (159), dos quaes tambem se pedem certidão, nenhuma transcripção ou inscripção consta, tendo esses immoveis por objecto. O referido é verdade, do que dou fé.

Rio de Janeiro, seis de Março de 1928.
O sub-Offl. João Gonçalves da Rocha Castro.

600
6-3
28

Emol. es. 111$600
(Cento e onze
mil e 600 reis)

Appendix C

Powder diffraction charts

Reference: PhasanX Version 2.00 – Powder Diffraction Phase Analysis

- Glucose ($C_6H_{12}O_6$)

2θ	Int.	h k l	2θ	Int.	h k l	2θ	Int.	h k l	2θ	Int.	h k l
11,8059	20	1 1 0	28,4013	60	1 0 2	44,2102	30	1 2 3			
16,3110	70	1 0 1	31,8550	60	3 0 1	49,6995	20	5 1 0			
16,9392	70	1 2 0	32,8279	30	1 4 1	51,3467	40	1 7 0			
17,7604	20	1 1 1	36,0860	30	3 3 0	53,0452	10	5 2 1			
19,2799	80	0 2 1	37,0892	40	2 4 1	54,5471	20	2 7 0			
20,3522	70	2 1 0	39,4740	30	2 3 2	56,7448	10	0 2 4			
21,5516	50	1 2 1	40,0409	30	3 1 2	59,0541	10	2 1 4			
23,5165	100	2 2 0	40,5675	30	2 5 0						
24,3667	60	2 1 1	41,7653	20	4 1 1						
26,7498	50	1 3 1	43,3414	40	4 2 1						

- Copiapite ($Fe_{14}O_3(SO_4)_{18}.63H_2O$)

2θ	Int.	h k l	2θ	Int.	h k l	2θ	Int.	h k l	2θ	Int.	h k l
8,4142	100		18,0152	20	-1 2 1	27,5072	10	-1 2 2	36,3430	20	0 -7 1
9,9304	10	0 2 0	18,4694	10	0 -3 1	28,2178	10	0 -3 2	37,2807	30	1 -7 1
11,0370	10		19,3649	20	1 0 1	29,1601	40	-2 4 0	39,3124	10	3 1 0
12,3176	10	0 0 1	20,2117	10	1 -2 1	29,6555	10	-1 -3 2	41,3845	10	-3 2 2
12,8757	30	0 -1 1	21,3939	30	-1 4 0	30,5915	10	1 -2 2	43,2542	10	-1 4 3
13,8257	10	0 1 1	22,9621	10	1 2 1	31,7043	10	2 1 1	44,1421	20	-3 4 2
14,8519	20	0 3 0	23,7074	10		32,9024	40	1 -6 1	45,4982	20	0 7 2
16,1909	10	-1 1 1	24,2991	30	0 4 1	33,9291	10	0 -5 2	47,2279	20	2 6 1
16,6506	10	0 2 1	24,7804	10	-2 1 0	34,8825	20	2 4 0	48,5687	10	0 9 1
17,3059	20	1 2 0	25,9560	40	0 1 2	35,3080	10	-1 7 0	50,2264	10	-1 0 4

- Rozenite ($FeSO_4.4H_2O$)

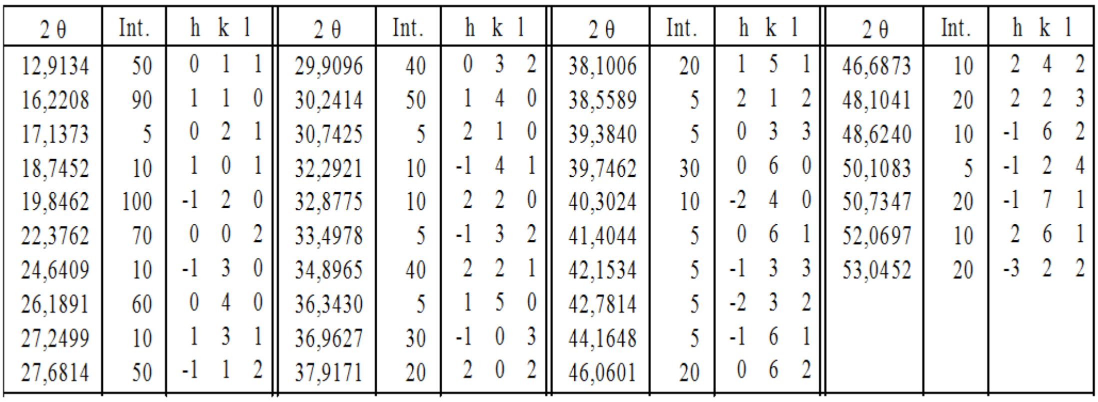

2θ	Int.	h k l	2θ	Int.	h k l	2θ	Int.	h k l	2θ	Int.	h k l
12,9134	50	0 1 1	29,9096	40	0 3 2	38,1006	20	1 5 1	46,6873	10	2 4 2
16,2208	90	1 1 0	30,2414	50	1 4 0	38,5589	5	2 1 2	48,1041	20	2 2 3
17,1373	5	0 2 1	30,7425	5	2 1 0	39,3840	5	0 3 3	48,6240	10	-1 6 2
18,7452	10	1 0 1	32,2921	10	-1 4 1	39,7462	30	0 6 0	50,1083	5	-1 2 4
19,8462	100	-1 2 0	32,8775	10	2 2 0	40,3024	10	-2 4 0	50,7347	20	-1 7 1
22,3762	70	0 0 2	33,4978	5	-1 3 2	41,4044	5	0 6 1	52,0697	10	2 6 1
24,6409	10	-1 3 0	34,8965	40	2 2 1	42,1534	5	-1 3 3	53,0452	20	-3 2 2
26,1891	60	0 4 0	36,3430	5	1 5 0	42,7814	5	-2 3 2			
27,2499	10	1 3 1	36,9627	30	-1 0 3	44,1648	5	-1 6 1			
27,6814	50	-1 1 2	37,9171	20	2 0 2	46,0601	20	0 6 2			

- Melanterite ($FeSO_4 \cdot 7H_2O$)

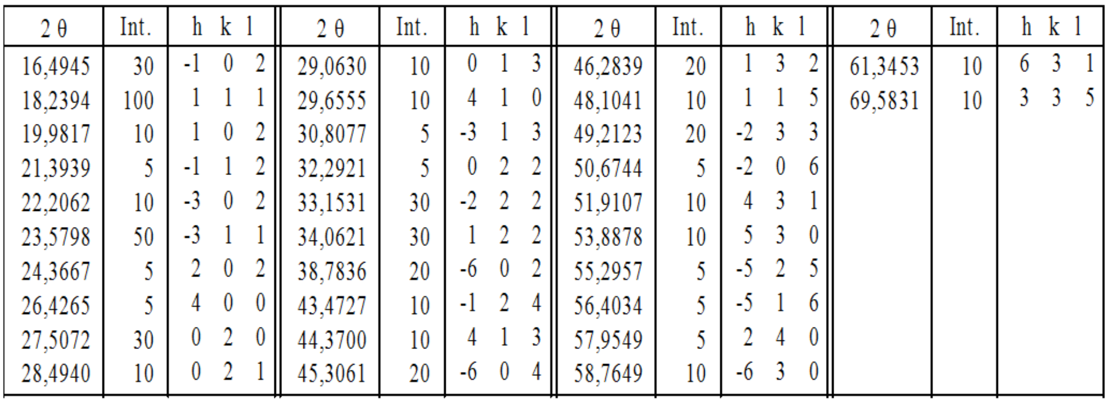

2θ	Int.	h k l	2θ	Int.	h k l	2θ	Int.	h k l	2θ	Int.	h k l
16,4945	30	-1 0 2	29,0630	10	0 1 3	46,2839	20	1 3 2	61,3453	10	6 3 1
18,2394	100	1 1 1	29,6555	10	4 1 0	48,1041	10	1 1 5	69,5831	10	3 3 5
19,9817	10	1 0 2	30,8077	5	-3 1 3	49,2123	20	-2 3 3			
21,3939	5	-1 1 2	32,2921	5	0 2 2	50,6744	5	-2 0 6			
22,2062	10	-3 0 2	33,1531	30	-2 2 2	51,9107	10	4 3 1			
23,5798	50	-3 1 1	34,0621	30	1 2 2	53,8878	10	5 3 0			
24,3667	5	2 0 2	38,7836	20	-6 0 2	55,2957	5	-5 2 5			
26,4265	5	4 0 0	43,4727	10	-1 2 4	56,4034	5	-5 1 6			
27,5072	30	0 2 0	44,3700	10	4 1 3	57,9549	5	2 4 0			
28,4940	10	0 2 1	45,3061	20	-6 0 4	58,7649	10	-6 3 0			

- Calcite ($CaCO_3$)

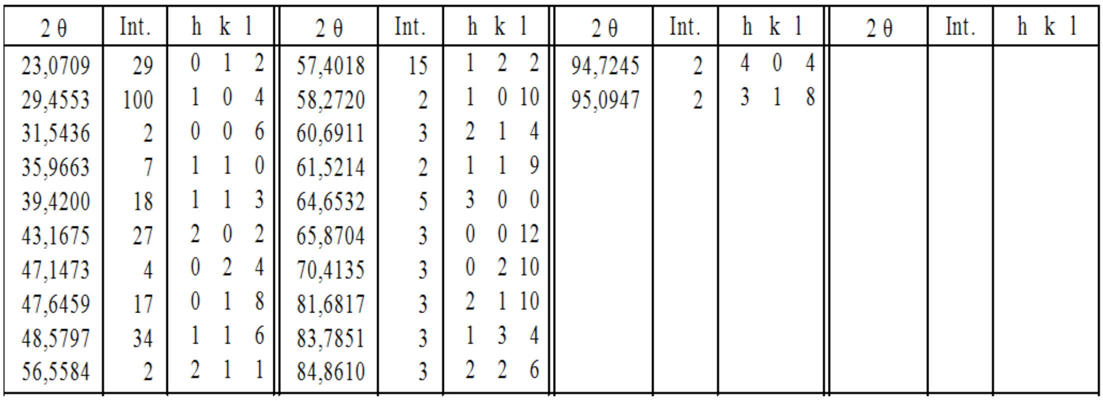

2θ	Int.	h k l	2θ	Int.	h k l	2θ	Int.	h k l	2θ	Int.	h k l
23,0709	29	0 1 2	57,4018	15	1 2 2	94,7245	2	4 0 4			
29,4553	100	1 0 4	58,2720	2	1 0 10	95,0947	2	3 1 8			
31,5436	2	0 0 6	60,6911	3	2 1 4						
35,9663	7	1 1 0	61,5214	2	1 1 9						
39,4200	18	1 1 3	64,6532	5	3 0 0						
43,1675	27	2 0 2	65,8704	3	0 0 12						
47,1473	4	0 2 4	70,4135	3	0 2 10						
47,6459	17	0 1 8	81,6817	3	2 1 10						
48,5797	34	1 1 6	83,7851	3	1 3 4						
56,5584	2	2 1 1	84,8610	3	2 2 6						

- Barite ($BaSO_4$)

2 θ	Int.	h	k	l	2 θ	Int.	h	k	l	2 θ	Int.	h	k	l	2 θ	Int.	h	k	l
19,9817	17	2	0	0	32,8279	47	0	2	0	46,6111	1	2	2	2	54,9723	10	1	1	4
20,4470	36	0	1	1	36,1763	14	2	1	2	47,0463	7	3	2	1	56,1781	8	2	3	1
22,7831	57	1	1	1	36,7434	2	3	1	1	49,0146	16	3	0	3	57,8354	8	1	3	2
23,5798	12	2	0	1	38,7488	15	2	2	0	51,0694	3	0	0	4	57,9549	7	5	0	2
24,8790	31	0	0	2	39,0814	6	1	0	3	51,9107	9	0	3	1	60,2849	18	3	2	3
25,8640	100	2	1	0	39,4740	7	3	0	2	52,1016	9	1	0	4	60,6340	11	5	1	2
26,8565	67	1	0	2	40,8168	27	2	2	1	53,0121	5	1	3	1	62,0284	3	0	2	4
28,7661	97	2	1	1	42,6120	80	4	0	1	53,1116	6	5	0	1	63,0125	10	1	2	4
31,5436	53	1	1	2	42,9521	76	3	1	2	54,5471	7	2	3	0	63,8338	3	5	2	1
32,7292	16	3	0	1	44,0065	23	4	1	0	54,8298	14	4	2	1	65,3921	8	1	3	3

- Anhydrite ($CaSO_4$)

2 θ	Int.	h	k	l	2 θ	Int.	h	k	l	2 θ	Int.	h	k	l	2 θ	Int.	h	k	l
22,9110	5	1	1	1	46,8199	3	2	2	2	61,0850	1	1	3	3	78,5971	3	2	3	4
25,4370	100	0	2	0	47,3700	1	1	1	3	62,2379	5	4	1	2	79,8674	2	2	5	2
28,5800	2	0	0	2	48,6749	16	0	3	2	65,4432	2	0	2	4	81,6481	1	5	3	1
31,3680	29	0	1	2	49,1361	3	3	2	1	65,7673	1	3	2	3	82,6145	4	0	6	0
31,9710	3	1	2	1	52,2309	11	0	4	0	66,8282	3	2	4	2	82,7511	5	6	0	0
36,2901	7	2	2	0	52,2901	10	4	0	0	66,9750	3	2	1	4	82,8691	5	4	0	4
38,6410	20	2	0	2	52,7981	1	1	2	3	68,6600	1	3	4	1	84,1172	1	4	4	2
40,8161	20	2	1	2	55,7222	15	2	3	2	71,4190	4	2	2	4	84,2433	1	4	1	4
41,3130	8	3	0	1	57,7783	2	3	3	1	72,8652	1	0	3	4	84,5413	1	5	1	3
43,3311	8	1	3	1	58,9819	4	2	4	0	74,1970	6	4	3	2	88,3087	7	6	2	0
45,4491	4	1	0	3	60,6670	3	4	0	2	77,0221	1	4	4	0					

- Kaolin ($Al_2Si_2O_5(OH)_4$)

2 θ	Int.	h	k	l	2 θ	Int.	h	k	l	2 θ	Int.	h	k	l	2 θ	Int.	h	k	l
12,3694	50				32,7046	4	0	-3	1	45,6921	12	-1	2	3	58,1954	4	-2	0	4
19,8912	75	0	2	0	35,1223	85	-1	2	2	46,8917	6	-2	3	1	60,1550	8	-1	5	2
20,4470	85	1	1	0	35,5829	50	-1	-3	1	47,9961	6	1	3	2	62,5867	100	-3	-3	1
21,3419	65	-1	-1	1	36,1311	85	2	0	0	48,5963	8	1	4	1					
21,6046	40				37,8012	25	1	1	2	49,6417	6	1	-1	3					
23,2052	50	0	-2	1	38,5761	95	1	-3	1	51,1922	4	0	5	0					
23,9014	20				39,4200	65	-2	0	2	53,9564	8	-1	-1	4					
24,9926	50	1	0	1	40,1712	20	0	4	0	54,4419	20	-1	5	0					
26,4265	12	1	-1	1	41,3251	12	-2	2	0	55,2235	25	-3	0	2					
28,3276	4	0	-1	2	42,6965	6	2	-1	1	56,9364	16	1	-5	1					

- Native cellulose ($c_6H_{10}O_5$)

2θ	Int.	h k l	2θ	Int.	h k l	2θ	Int.	h k l	2θ	Int.	h k l
14,0912	20	-1 0 1	34,0621	60	3 1 0						
14,9022	80		34,6046	40	-2 3 1						
16,4945	70	-1 1 1	34,8825	80	0 4 0						
17,3400	20	1 0 1	38,6105	40	-2 3 2						
20,6393	60	0 2 1	41,5841	60	2 4 0						
22,8425	100	0 0 2	42,6120	20	1 2 3						
28,2178	40	1 3 0	44,3700	20	3 0 2						
29,0630	40	-1 2 2	46,5351	40	-4 1 2						
30,3783	40										
31,2495	40	1 3 1									

Appendix D

Activity during the Master thesis

R. Viegas, V. Corregidor, M. T. Peña, E. Alves, L. C. Alves, Preliminary Studies on Iron Gall Inks Composition using an External Ion Beam, Internation Journal of Conservation and Science 4 (2013) 593.

Poster publication entitled “Preliminary Studies on Inks composition using an External Ion Beam” at the 1st International Conference on Innovation in Art Research and Technology (INART), Évora, 10-13 July, 2013.

Poster publication entitled “Compositional characterization of iron gall inks in manuscripts – From ingredients until the document” at the Congress Microscopy in Research, Monte da Caparica, 9-10 December, 2013.

A poster entitled "Application of nondestructive analytical techniques to the study of Iron Gall inks" will be presented this July in the 14th International Conference on Nuclear Microprobe Technology and Applications, in Padova, Italy.

Workshop

During this thesis work, I did a workshop entitled “Conservação de documentos com tinta ferrogálica – da teoria à prática.” (Conservation of iron gall ink documents - from theory to practice.).

This was organized by the Direcção Geral do Património Cultural; Instituto de Investigação Científica e Tropical; Associação Profissional de Conservadores-Restauradores de Portugal (ARP).

It took place at the Arquivo Histórico do Ultramar, in Lisbon, from 6-8 November, 2013.

This workshop was certificated by the Associação Profissional de Conservadores-Restauradores de Portugal (ARP).

Preliminary Studies on Inks composition using an External Ion Beam

Victoria Corregidor[1,2], Rita Viegas[1,3], Teresa Peña[3], Eduardo Alves[1,2] and Luís C. Alves[1,2]

[1] Campus Tecnológico e Nuclear, Instituto Superior Técnico, Universidade Técnica de Lisboa, E.N. 10 (ao Km 139,7), 2686-953 Sacavém, Portugal
[2] CFNUL, Av. Prof. Gama Pinto, 2, 1649-003 Lisboa, Portugal
[3] Instituto Superior Técnico, Universidade Técnica de Lisboa, Portugal

Objectives

The knowledge of paper making techniques and inks is of great importance for dating , restoration processes and knowledge of our culture heritage . The need to find a non destructive method that can provide compositional information of the documents makes the use of Ion Beam Analytical (IBA) techniques such as Particle Induced X-ray Emission (PIXE) , a great solution for this kind of studies.

Although the IBA techniques are usually considered as non-destructive, experimental working conditions should be carefully determined, in order to avoid damages as residual stains caused by the beam.

The aim of this preliminary studies is to find the best experimental conditions for documents analysis without damaging the sample and to identify the elements present in paper and inks.

Choosing the experimental conditions…

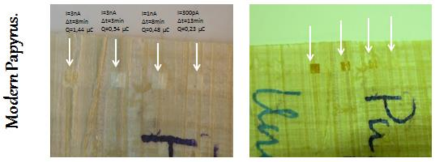

Day of exposure

Two weeks after the exposure

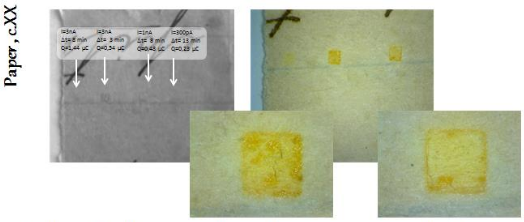

Each paper has different composition and needs its own experimental conditions. High currents modify the structural properties of paper and recovery is not longer possible.

Conclusions

- Beam intensity should be in the order of pA to avoid structural changes. Low currents can produce stains, depending on the paper, which disappear after few days. On the other hand, time has to be increased to obtain good statistical results.
- High currents produce structural changes in paper, which need further studies.
- By PIXE it is possible to identify elemental differences between papers and inks.
- It is possible also to obtain elemental maps distribution and correlate with ink. In future, RBS measurements will help to study the ink diffusion on paper.
- Other complementary techniques, such as XRF, Raman Spectroscopy, Optical Microscopy, U.V. or I.R. Photography will be used.

References

F. Lucarelli, P. A. Mandò, IBA techniques for the study of ancient manuscripts (2000).
L. Guintini., F. Lucarelli, P.A. Mandò, W. Hooper, P.H. Barker, Nucl. Instr. & Meth .B95 (1995) 389.
C. Remazeilles, V. Quillet, T. Calligaro, J.C. Dran, L. Pichon, J. Salomon, Nucl. Instr. and Meth. B 181 (2001) 681-687.
A.E. Sven, E. Johansson, Proton-induced X-ray emission (PIXE) spectrometry – state of art.

Experimental Conditions

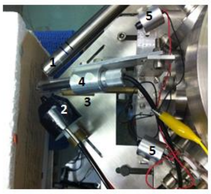

2 MeV proton beam, external beam

1. X-ray detector
2. Particle detector with He flow
3. Exit nozzle, 100 nm Si_3N_4
4. micro-camara
5. laser

The use of **external beam** :

- Avoids problems of dehydration of the paper,
- Reduces local heating effects at the point of incidence of the beam,
- Avoids sampling.

For these preliminary studies different type of supports were used: modern paper and papyrus, paper from beginning of XX century, recent and ferrogalic inks… all of them without valuable importance.

From photography…

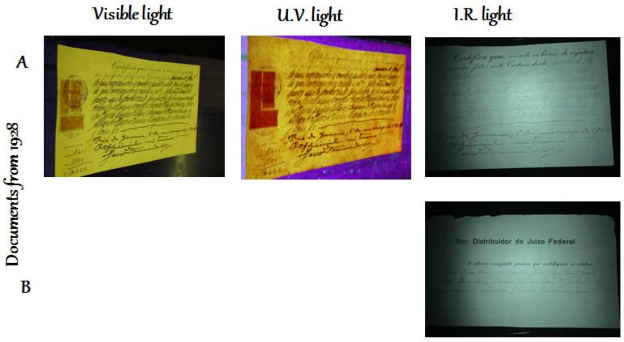

In both cases, U.V. light reveals paper degradation such as foxing or stains. I.R. light often can differentiate between dyes and pigments that look indistinguishable to the naked eye.

From PIXE…

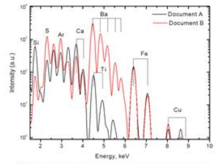

Elemental composition of papers is different.
The presence of Ba indicates industrial production.

By PIXE it is possible to identify differences between inks and also the distribution. Elemental changes are mainly due to S/Fe, , Ca/Fe , Cu/Fe and Zn/Fe alterations.

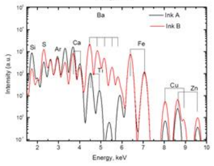

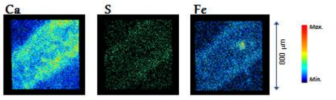

Acknowledgments

V. Corregidor acknowledges the funding support from the FCT - Ciência 2008 program.
V. Corregidor acknowledges Banco Santander-Becas Iberoamérica and Physics Institute from Universidad Nacional Autónoma de México.
Special thanks to Prof. J.L. Ruvalcaba and his group for offering their resources and discussions.
The authors also thanks the work of M. Almeida, I. Costa, T. Matias and I. Silvestre from Ciência Viva program.
Special thanks to R. Winstanley for sharing with us his collection.

Compositional characterization of iron gall inks in manuscripts

From ingredients until the document

V. Corregidor[1,2]
R. Viegas[1,3]
N. Franco[1]
M. T. Peña[3]
E. Alves[1]
L.C. Alves[2,4]

1 IPFN, Instituto de Plasmas e Fusão Nuclear, Instituto Superior Técnico, Universidade de Lisboa, 2686-953 Sacavém, Portugal
2 CFNUL, Centro de Física Nuclear da Universidade de Lisboa, Av. Prof. Gama Pinto, 2, 1649-003 Lisboa, Portugal
3 CFTP, Centro de Física Teórica de Partículas, e Departamento de Física - IST., Instituto Superior Técnico, Universidade de Lisboa, Lisboa, Portugal
4 Campus Tecnológico e Nuclear, Instituto Superior Técnico, Universidade de Lisboa, 2686-953 Sacavém, Portugal

Motivation

Writing is one of the most efficient ways of making history subsist. In XII century paper was widespread in Europe and until this time carbon inks were mostly used to write manuscripts.

The iron gall inks, originating from the Roman period, were recurrently used until mid-20th century in Europe, mostly because of its indelibility and easy access to the ingredients.

Although there are many recipes, the basic recipe consists of water, arabic gum, tannin acid extracted from gall nuts and vitriol (iron sulfate). In some cases, depending on the recipe, additives as wine or vinegar were introduced.

Thanks to the differences in the ink composition and to the presence of trace elements, it is possible to distinguish between different inks/recipes.

The aim of this study is to apply PIXE technique to the study of elemental composition of:

- The starting ingredients used in iron gall ink manufacturing,
- Iron gall inks made in the lab and also in different handwritten documents from the XX century.

Experimental

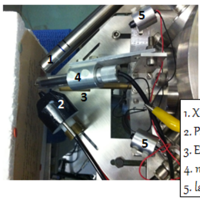

2 MeV proton beam, external beam

1. X-ray detector
2. Particle detector with He flow
3. Exit nozzle, 100 nm Si3N4
4. micro-camara
5. laser

The use of **external proton beam**:

- Avoids problems of dehydration of the paper,
- Reduces local heating effects at the point of incidence of the beam,
- Avoids sampling.

HRXRD measurements

- D8 Discover system from Bruker-AXS
- Cu Kα1 monochromated radiation used
- 2-bounce Ge(220) monochromator.

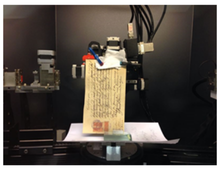

Composition analysis

1. The ingredients

PIXE spectra of the starting compounds and the iron gall ink (drop)

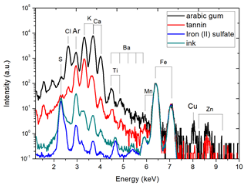

Arabic Gum: Ba, Ti, Ca, Fe...

Tannin acid: Fe, S, K...

Iron(II) sulphate: Fe, S, Zn...

Ink drop: Fe, S, K...

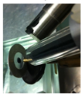

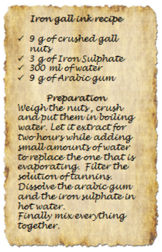

Iron gall ink recipe

- ✓ *9 g of crushed gall nuts*
- ✓ *3 g of Iron Sulphate*
- ✓ *300 ml of water*
- ✓ *9 g of Arabic gum*

Preparation

Weigh the nuts, crush and put them in boiling water. Let it extract for two hours while adding small amounts of water to replace the one that is evaporating. Filter the solution of tannins. Dissolve the arabic gum and the iron sulphate in hot water.

Finally mix everything together.

2. Different recipes

PIXE spectra of inks using different sources of tannin acid.

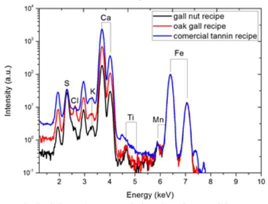

Inks made in laboratory contains low impurities Concentration. It was not possible to detect Zn or Cu.

HR-XRD diffractograms of inked areas and paper support

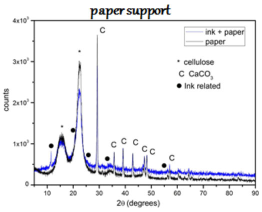

XRD results show the presence of crystalline cellulose and calcite. Slightly differences between inked and not inked areas are found.

3. Handwritten document from XX century

PIXE spectra of inked and not inked area in a handwritten document.

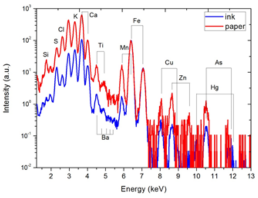

Cu, Zn and As are present in both: ink and paper. These metals can be found as contaminants of vitriol, which could be obtained from different sources.

Traces of Ba and Hg were found in the ink composition.

Barium is usually used in paper production but, as shown earlier, it can also be detected in Arabic gum.

The presence of Hg could be related with the origin of vitriol, also known as vitriol of mercury, although further studies are needed.

2 D PIXE maps of inked area in a handwritten document.

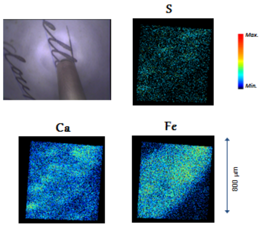

Fe, S and Ca signals in inked area are higher than in non-inked area.

References

http://www.ink-corrosion.org
M. Manso et al. Spectrochimica Acta A: Mol. & Biomol. Spectroscopy 105, (2013), pp. 288–296
F. Lucarelli et al. Nuc. Inst. & Meth. B 109/110, (1996), pp. 644-652
C. Remazeilles et al. Nuc. Inst. & Meth. B 181, (2001), pp. 681-687.

Acknowledgments

V. Corregidor acknowledges the funding support from the FCT - Ciência 2008 program.
Special thanks to R. Winstanley for sharing with us his collection.

Conclusions

Although the starting materials have trace elements as Ba, Zn or Ti , it was not possible to detect them when the manufactured ink is applied in a paper support.

Nevertheless, in a handwritten document from the XX century, it was possible to detect the presence of Zn, Ba or even Hg in the ink. Their presence could be related with the use of intentionally additional constituents or contamination of the starting ingredients, depending in the concentration.

From the HRXRD diffractograms it is not possible to distinguish between inked and not inked areas, because the high signal from the paper support and the small amount of ink under study.

Microscopy in Research 2013
December 9-10, Egas Moniz - Cooperativa de Ensino Superior CRL, Monte da Caparica